7. SOURCE TERMS AND SOURCE TERM PROBABILITIES

7.1 Truck and Train Accident Scenarios

7.1.1 Event Trees

To estimate accident source terms, the mechanical and thermal environments that a cask might experience during truck and train accidents must be estimated. Because all of the variations of all of the accidents in the historic record plus all plausible accidents not yet observed constitutes far too many accidents to examine individually, a smaller representative set of accidents is formulated and the frequencies of occurrence of each representative accident are estimated.

Representative sets of accidents can be developed by constructing accident event trees. Event trees for truck and train accidents were developed during the course of the Modal Study [7-1]. Figures 7.1 and 7.2 present these event trees. Inspection of these figures shows that an event tree depicts an accident scenario as a sequence of events and also gives the probability of each event in the sequence. Thus, a path on the event tree constitutes a unique sequence of events and the product of all of the probabilities of the events on a path (branch point probabilities) gives the probability of that accident scenario. For example, in the truck accident event tree shown in Figure 7.1, a truck accident that leads to a collision with a pedestrian is depicted by the uppermost branches of the tree, specifically the branches labeled “Collision,” “Non-fixed object,” and “Cones, animals, pedestrians.” Because the probabilities of these branches are 0.7412, 0.8805, and 0.0521, the chance that this accident scenario occurs (expressed as a percent), given that any truck accident has been initiated, is 3.4002 = 100 [(0.7412)(0.8805)(0.0521)], where 3.4002 is called the path (scenario) probability and gives the fraction of all truck accidents that follow this path. Because the probability of any accident occurring is not included in this product, the resulting fraction is a conditional probability, that is conditional on the occurrence of an accident of any severity and type. Further, because of the way the tree is constructed, each probability on the tree is conditional on the branch point probabilities that precede it and many branch point probabilities are represented by far more significant figures than is warranted by the underlying data because the sum of the branch point probabilities for any single branch of the tree must sum exactly to one.

Because each event tree path (accident scenario) defines a set of accident conditions (mechanical and/or thermal environments), the impact of each scenario on a radioactive material transportation cask can be estimated by hypothetically subjecting the cask to the conditions that characterize the end point of the path. The Modal Study performed such an analysis for each path on their truck and train accident trees. On these trees, paths that seemed capable of failing a Type B spent fuel cask are indicated by placing an asterisk (*) after the path number (path Accident Index). Thus, the Modal Study analyses found, for example, that collisions of a truck with a train might generate mechanical loads large enough to fail a Type B spent fuel cask thereby allowing radioactivity to be released from the cask to the environment. Accordingly, the truck accident scenario, denoted by the Accident Index 5, which has a conditional chance of occurring of 0.7701 percent (conditional on the occurrence of some truck accident), is tagged with an asterisk.

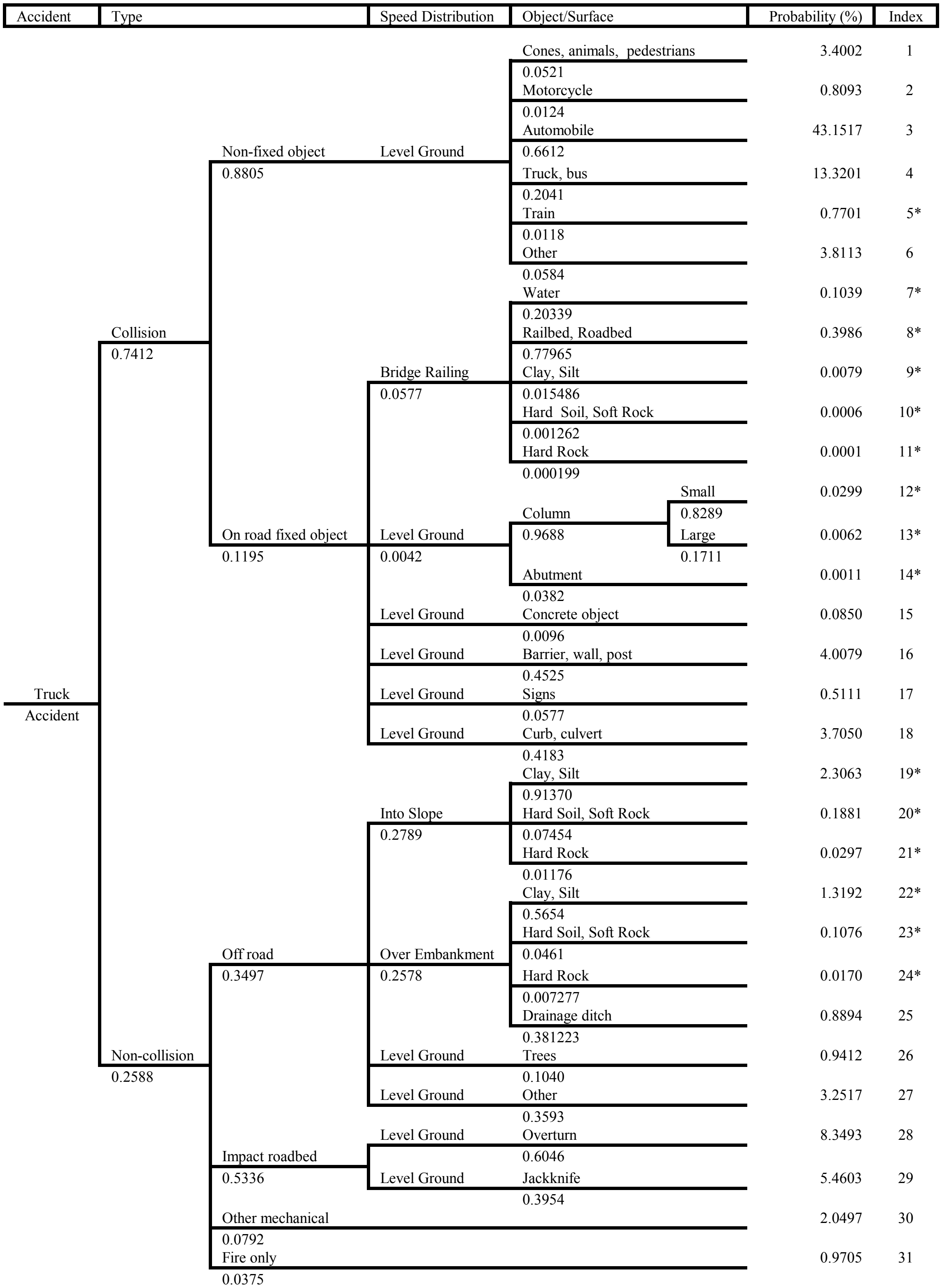

Figure 7.1 Modal Study truck accident event tree.

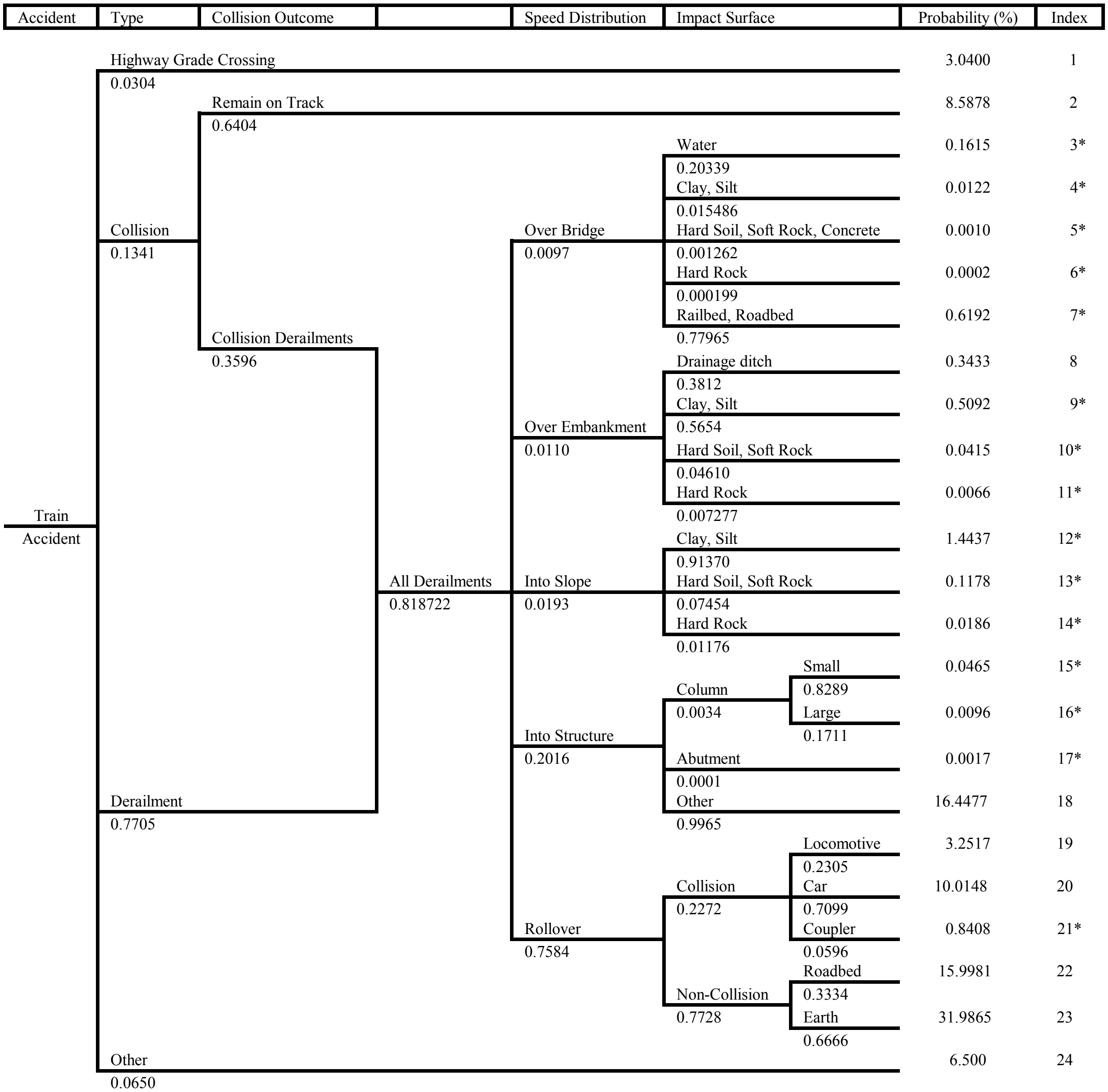

Figure 7.2 Modal Study train accident event tree.

The suitability of an event tree depends on whether it depicts a suitable representative set of accidents and on the whether the data used to estimate the event tree branch point probabilities, and thus the probability of occurrence of each accident scenario, are still current. Inspection of Figures 7.1 and 7.2 shows that early branches on these event trees define accident conditions (e.g., on the truck event tree, a collision with a non-fixed object) while later branches provide information that specifies the accident speed distribution (e.g., the branch labeled "Over Embankment" on the train event tree) and the object (e.g., column or abutment on both trees) or surface (e.g., hard rock, clay/silt on both trees) that is struck. Inspection of these trees suggests that each tree depicts a comprehensive set of credible accidents (i.e., all probable accident scenarios appear to have been included and no unusually severe but credible accident scenarios appear to have been omitted). Accordingly, the structures of both trees seem appropriate. Therefore, the suitability of these trees for use in this study depends principally on the currency of the branch point probabilities. For each tree, this was investigated by comparing tree branch point probabilities to similar but more recent data.

7.1.2 Route Wayside Surface Characteristics

The occurrence frequencies of route wayside surfaces (clay/silt, hard soil/soft rock, hard rock), presented in the Modal Study were developed by performing visual surveys of two segments of California interstate highways (Interstate 80 from Davis, California, to the Nevada border and Interstate 5 from the San Diego County/Orange County line to the Los Angeles County/Kern County line). Each survey classified visible wayside surfaces as hard rock, untilled soil (which was equated to hard soil/soft rock), and tilled soil (which was equated to clay/silt). After comparing the results of these visual surveys to data available from agricultural soil surveys and geological highway maps, Modal Study analysts chose the following values for wayside route surface frequencies of occurrence: clay/silt, 0.9137; hard soil/soft rock, 0.07454, and hard rock, 0.01176. Moreover, although developed by survey of interstate highway wayside surfaces, because rail wayside surface data was not available, as the "Into Slope" branches on Figures 7.1 and 7.2 show, these surface occurrence frequencies were used for both the truck and the train event trees.

Because the finite element cask impact calculations described in Section 5 showed that only impact at a high speed onto an essentially unyielding surface (e.g., a large monolithic chunk of rock that doesn't fragment easily) was likely to cause the seal of a Type B spent fuel cask to leak, the frequency of occurrence of wayside hard rock becomes an unusually important branch point probability. But for high-speed impacts, shallow layers of soft soil will easily be penetrated without significant expenditure of kinetic energy. Therefore, if only high-speed impacts onto hard rock are likely to cause a spent fuel cask seal to leak, then not only is visible hard rock of concern, but so is hard rock that lies beneath but close to the soil surface.

7.1.2.1 U.S. Geologic Survey Data

The amount of hard rock (expressed as a percent of the route length) traversed by the two segments of I-80 and I-5 surveyed for the Modal Study was reestimated using data developed by the U.S. Geologic Survey (USGS) [7-2]. To do this, a digital (electronic) USGS map of the surface geology of the continental United States was analyzed using a Geographic Information System (GIS). The analysis identified the number of kilometers of each interstate segment that traverse plutonic and intrusive rock formations, the two hardest rock-types depicted on the USGS map. Table 7.1 compares the Modal Study visual estimates of the percentage of each route segment length that is hard rock to the results developed by GIS analysis of the USGS data.

The USGS data in the table suggest that substantially larger portions of the two interstate segments traverse hard rock than was found by the Modal Study visual surveys of these two route segments. However, because the USGS map does not indicate the depth of the soil layers that lie over these hard rock layers, it is not possible to decide whether a cask impacting the overlying soil would penetrate to and be damaged by impacting the underlying hard rock layer.

Table 7.1 Wayside Hard Rock on Modal Study Segments of I-5 and I-80

Route Segment	Hard Rock (%)
Interstate 5	
Modal Study Visual Survey	0.0
GIS Analysis of USGS Data	5.7
Interstate 80	
Modal Study Visual Survey	2.4
GIS Analysis of USGS Data	22.9

7.1.2.2 U.S. Agricultural Department Data

Because the USGS data could not identify overlying soil layers thick enough to absorb most of the cask impact energy before the layer was penetrated, the GIS analysis performed using the USGS data was repeated using a digitized U.S. Agricultural Department map [7-3] that showed the locations of coherent, monolithic rock formations in the continental United States that must be removed by blasting (i.e., hard rock) and rock that can be removed by a backhoe because it fragments relatively easily (i.e., soft rock), and also specified the amount of dirt that lies above each type of rock. In addition, the map showed the locations of surface soil layers of various depths (thicknesses) that contained rocks with average diameters (d_{rock}) larger than some reference diameters (e.g., $d_{rock} \geq 3$ inches, $d_{rock} \geq 10$ inches). Given the information about the character of near-surface soil and rock layers provided by the Agricultural Department map, the following definitions were adopted for hard rock, soft rock, hard soil, and soft soil.

Hard Rock: Rock that must be removed by blasting that lies on average within 24 inches of the route wayside surface (minimum distance to the rock layer ≤ 12 inches; maximum distance to the rock layer ≤ 36 inches).

Soft Rock: Rock that can be removed by a backhoe that lies on average within 24 inches of the route wayside surface (minimum distance to the rock layer ≤ 12 inches; maximum distance to the rock layer ≤ 36 inches).

Hard Soil: Soil that contains ≥ 10 percent rocks with average diameters ≥ 3 inches.

Soft Soil: Everything else.

Four observations about these definitions are in order. First, rock layers that lie more than three feet below the surface are not of concern because penetration by the cask of three feet of surface soil will consume so much of the cask's impact energy that impact onto a rock layer that lies below this soil will be unlikely to cause the cask seal to leak. Second, a layer of soil that contains rocks of a significant size (e.g., diameters ≥ 3 inches) that occupy a significant fraction (e.g., ≥ 10 percent) of the volume of the layer will significantly increase the effective hardness of the layer. Third, the preceding definitions mean that any wayside surface that isn't hard or soft rock will be hard soil if the surface soil layer contains ≥ 10 percent rocks with average diameters

≥ 3 inches; if it does not, it will be soft soil. And fourth, implicit in the definition of hard soil is the assumption that a thin layer of surface soil that contains rocks is unlikely to lie over a thick layer of rock-free soil. Thus, if the surface soil layer is thin, then the wayside surface character will be determined by the near-surface underlying rock layer, and if the surface layer is not thin, then its characteristics will be determined by the characteristics of the rocks that it contains.

The wayside surface characteristics of the two interstate highway segments surveyed for the Modal Study were reanalyzed using GIS techniques to interrogate the digitized U.S. Agricultural Department map. Table 7.2 presents the results (expressed as percentages) obtained for the two California interstate segments and compares them to the results obtained by the visual surveys conducted for the Modal Study. Inspection of Table 7.2 again suggests that the Modal Study visual survey of wayside interstate highway surfaces significantly underestimated the presence of hard rock, soft rock, and hard soil layers that lie close enough to the surface of the ground so that cask penetration to and/or impact onto these layers will determine the extent of cask damage during collision accident scenarios.

Table 7.2 Wayside Surfaces on Modal Study Segments of I-5 and I-80

Route Segment	I-80		I-5	
	Modal Study	US Ag. Data	Modal Study	US Ag. Data
Hard Rock	2.4	17.4	0.0	0.0
Hard Soil/Soft Rock	7.4		7.2	
Soft Rock		13.4		20.3
Hard (rocky) Soil		21.0		0.0
Soft Soil	90.2	48.2	92.9	79.7

7.1.2.3 New Route Wayside Surface Occurrence Frequencies

Because of the importance of impacts onto hard rock and because the visual surveys of interstate wayside surfaces conducted for the Modal Study appeared to significantly underestimate surface or near-surface hard rock layers, new wayside surface occurrence frequencies were developed for the four illustrative real truck and rail routes described in Section 8.3 (Crystal River to Hanford, Maine Yankee to Skull Valley, Maine Yankee to the Savannah River Site, and Kewaunee to the Savannah River Site) by GIS interrogation of the digitized U.S. Agricultural Department map. Table 7.3 presents the results of these GIS analyses.

Finally, in order to be somewhat conservative with respect to the wayside occurrence of hard rock and soft rock/hard soil, the average fractional frequencies of occurrence of hard rock and soft rock/hard soil presented in Table 7.3, rounded up to the next integer, were chosen for use in this study, and the frequency of occurrence of soft soil was calculated by subtraction of the sum of these two occurrence frequencies from 1.0. Table 7.4 presents the frequencies of occurrence obtained by this procedure.

Table 7.3 Wayside Surface Characteristics for Three Illustrative Shipping Routes

Route	Hard Rock	Soft Rock	Hard (Rocky) Soil
Truck			
Crystal River to Hanford	2.1%	4.0%	2.9%
Maine Yankee to Savannah River Site	5.4%	0.0%	6.9%
Kewaunee to Savannah River Site	2.7%	0.0%	0.9%
Rail			
Crystal River to Hanford	2.5%	1.9%	3.9%
Maine Yankee to Savannah River Site	2.8%	0.0%	2.5%
Kewaunee to Savannah River Site	0.3%	0.0%	1.4%

Table 7.4 Fractional Occurrence Frequencies for Route Wayside Surfaces Selected for Use in This Study

Mode	Clay/Silt	Hard Soil/Soft Rock	Hard Rock
Truck	0.91	0.05	0.04
Rail	0.91	0.06	0.03

7.1.3 Truck Accident Data

The Modal Study truck accident event tree was constructed using Bureau of Motor Carrier Safety (BMCS) accident data for the years 1973 through 1983 for all trucks (no accidents were discarded based on truck size) and all types of roads (i.e., city streets, county roads, state highways, interstate highways) [7-4]. The frequency with which various roadside structures (e.g., bridge railings, columns, abutments, barriers, and signs) are struck during collisions was developed from California Department of Transportation reports for the years 1975 through 1983. The sizes of columns and abutments next to highways, a distribution of highway bridge heights and of the surfaces below highway bridges were all developed during the Modal Study by counting these features while conducting the two surveys of segments of Interstate Highways 5 and 80.

Because the Modal Study truck event tree is based on data that is now more than 15 years old, that data was compared to more recent accident data developed by Clauss, et al. [7-5]. The data developed by Clauss, et al. was drawn from two databases, the TIFA (Trucks Involved in Fatal Accidents) file maintained by the University of Michigan Transportation Research Institute, and the GES (General Estimates System) file maintained by the National Highway Traffic Safety Administration. TIFA file entries report data for medium and heavy duty truck accidents that occurred on U.S. highways and caused fatalities. GES file entries report data extracted from police reports for fatal and non-fatal accidents. Clauss, et al. used TIFA file data for the years 1980 through 1990, and GES file data for the years 1988 through 1990.

Table 7.5 compares the conditional probabilities of occurrence of Modal Study truck accident scenarios to estimates of the probabilities of occurrence of the same type of accident drawn from the study of Clauss, et al. Inspection of Table 7.5 shows that Modal Study conditional accident probabilities are similar to TIFA and GES accident probabilities, usually differing from the TIFA or GES result by about a factor of two. As the Modal Study examined all truck accidents (both fatal and non-fatal) without any restriction on truck size, while the TIFA and GES data excludes small truck accidents, the fact that the probabilities agree to about a factor of two suggests that truck accidents that occurred during the 1980s are not substantially different in character from those that occurred during the late 1970s and early 1980s. Thus, the Modal Study conditional probabilities would seem to still be representative of current truck accidents. Accordingly, it was concluded that the structure of the tree (set of scenarios embedded in the tree) reasonably depicted the variety of possible truck accidents and did not omit important accident branches.

Table 7.5 Conditional Probabilities of Occurrence of Various Truck Accident Scenarios (%)

Scenario/Accident	Modal Study	TIFA (fatal)	GES (all)	GES (fatal)
Collision Scenarios				
Truck + Bus Truck + Tanker	13.32	 6.13	 6.65	 7.90
Car	43.15	68.83	66.05	74.88
Train	0.77	0.57	0.18	0.42
Water Immersion	0.10	 0.20		
Hard Object[a]	0.81	2.04	1.94	0.51
Soft Object[b]	4.93	2.59	7.46	0.43
Non-Fixed Object	7.21	9.67	6.57	4.94
Non-Collision Scenarios				
Overturn Rollover	8.35	 8.17	 4.48	 10.03
Fire	0.97	1.80	0.46	0.39

a. For Modal Study, sum of Hard Soil, Soft Rock, Hard Rock, and Columns and Abutments.
b. For Modal Study, sum of Clay, Silt, Railbed, Roadbed, and Drainage Ditch.

Both the Modal Study and the study of Clauss, et al. developed estimates of the probability that a truck collision would initiate a fire. The Modal Study developed estimates of the fractions (expressed as percentages) of various types of truck collisions (e.g., collision with a car) that initiated fires. The study of Clauss, et al. developed estimates of the fractions (expressed as percentages) of all truck accidents that were collisions with trucks, cars, tankers, or other objects that also caused both fires and a fatality. Clauss, et al. also found that 1.7 percent of all fatal truck collisions led to fires. Therefore, multiplication of the results of Clauss, et al. for fatal collisions with cars, or trucks and tankers, or other objects that initiate fires and cause a fatality by 1.7 percent (e.g., for truck collisions with cars, $37.5 \times 0.017 = 0.6$) yields a result directly comparable with the results given in the Modal Study. Table 7.6 presents and compares these estimates. Inspection of Table 7.6 shows that the Modal Study results and those of Clauss, et al. differ by factors of two, which suggests that the Modal Study results are most likely still representative.

Table 7.6 Truck Accidents that Initiate Fires (Percentages)

	Clauss, et al.		Modal Study
	Fraction All Fatal Collisions that Initiate Fires that Impact Listed Object (%)	**Fraction Accidents of this Type that Initiate Fires (%)**	**Fraction Accidents of this Type that Initiate Fires (%)**
Collision with			
Car	37.5	0.6	0.3
Truck, Tankers	24.0	0.4	0.8
Truck	22.1	0.37	
Tanker	1.9	0.03	
Other Objects	38.6	0.7	1.3
Non-Collisions			
Ran off road			1.1
Overturns			1.2
Other			13.0

Finally, weighted summation of the Modal Study results in Table 7.6 using the probabilities of occurrence of each accident type as given in Figure 7.1 shows that, in agreement with Clauss, et al., 1.8 percent of all of the truck accidents examined by the Modal Study initiate fires, where

$$1.8 = 0.432(0.3) + 0.132(0.8) + 0.177(1.3) + 0.091(1.1) + 0.083(1.2) + 0.085(13.0)$$

Accordingly, as Figure 7.3 shows, the Modal Study truck accident event tree was used in this study with only one modification, replacement of the Modal Study wayside route surface frequencies of occurrence, that were developed by visual surveys of interstate highway segments, by the frequencies developed by GIS analysis of three representative real spent fuel highway transportation routes using U.S. Agricultural Department data.

7.1.4 Train Accident Data

The Modal Study train accidents event tree was constructed using data published in Federal Railroad Administration Accident/Incident Bulletins for the years 1975 through 1982 [7-6]. Because no rail line wayside surface data were available and because rail and highway routes were believed to traverse similar terrain [7-7], the Modal Study used the results of the survey of California Interstates 5 and 80 to specify the branch point probabilities for the train derailment accident branches labeled "Over Bridge," "Over Embankment," and "Into Slope," and also for the occurrence frequencies of the impact surfaces "Water," "Clay, Silt," "Hard Soil, Soft Rock, Concrete," "Hard Rock," "Railbed, Roadbed," and "Drainage Ditch." In addition, although train accident experts stated [7-8] that most train derailments leave the derailed cars upright or tipped

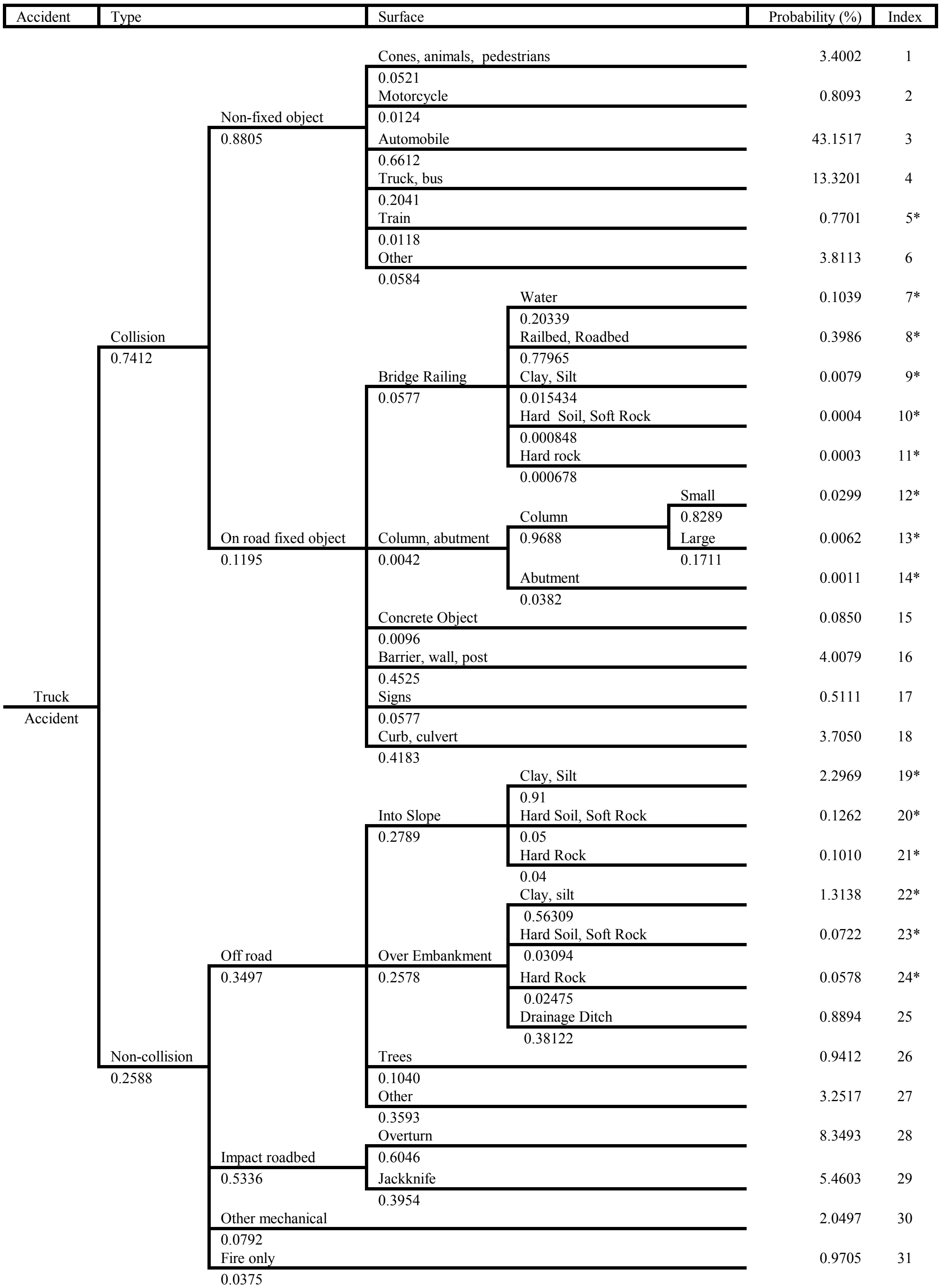

Figure 7.3 Modified Modal Study truck accident event tree.

over but only slightly damaged, the Modal Study train accident event tree does not divide derailment accidents into minor derailments (those where the derailed cars remain upright or simply tip over) and major derailments (those where at least some of the derailed cars are severely damaged). Lastly, the Modal Study train accident event tree does not contain a branch for fire-only accidents (i.e., fires not initiated by collisions or derailments).

Rail accident data for the years 1988 through 1995 were reviewed for this study by Department of Transportation (DOT) Volpe Center staff. Table 7.7 compares the conditional occurrence probabilities developed by the Modal Study for train accidents to those developed by the DOT Volpe Center. Inspection of Table 7.7 shows that train accident scenario probabilities constructed from recent data generally differ from the probabilities constructed during the Modal Study by factors of two or less. Inspection of the Modal Study train accident event tree suggests that the following three derailment paths probably lead only to minor damage: (1) derailments that lead to impacts into structures other than columns or abutments, (2) rollover derailments that do not lead to additional collisions, and (3) rollover derailments where the cars that roll over bump into other cars or locomotives and that the fraction of all derailments that these paths account for is 0.9490, where

$$0.9490 = (0.2016)(0.9965) + (0.7584)(0.2272)(0.2305+0.7095) + (0.7584)(0.7728)$$

Now, because (1) this fraction agrees well with the Volpe Center estimate of 0.9782 for the frequency of occurrence of minor derailments, (2) the paths that contribute to this fraction were all judged in the Modal Study to generate minor accidents, and (3) Table 7.7 shows that recent train accident data are consistent with the data developed by the Modal Study, as Figure 7.4 shows, the Modal Study train accident tree is used with only two modifications. First, the Modal Study wayside route surface frequencies of occurrence, that were developed by visual surveys of Interstate Highway segments, were replaced by the frequencies developed by GIS analysis of

Table 7.7 Conditional Probabilities of Occurrence of Various Train Accident Scenarios (%)

Scenario/Accident	Modal Study	DOT Volpe Center
Grade Crossing	0.0304	0.1298
Collision	0.1341	0.0875
Remain on Track	0.6404	0.4429
Collision Derailment	0.3596	0.5162
Derailment	0.7705	0.6511
Minor Damage		0.9782
Severe Damage		0.0218
Other	0.0650	0.1315
Fire/Explosion		0.0147
Obstruction/Other		0.1168

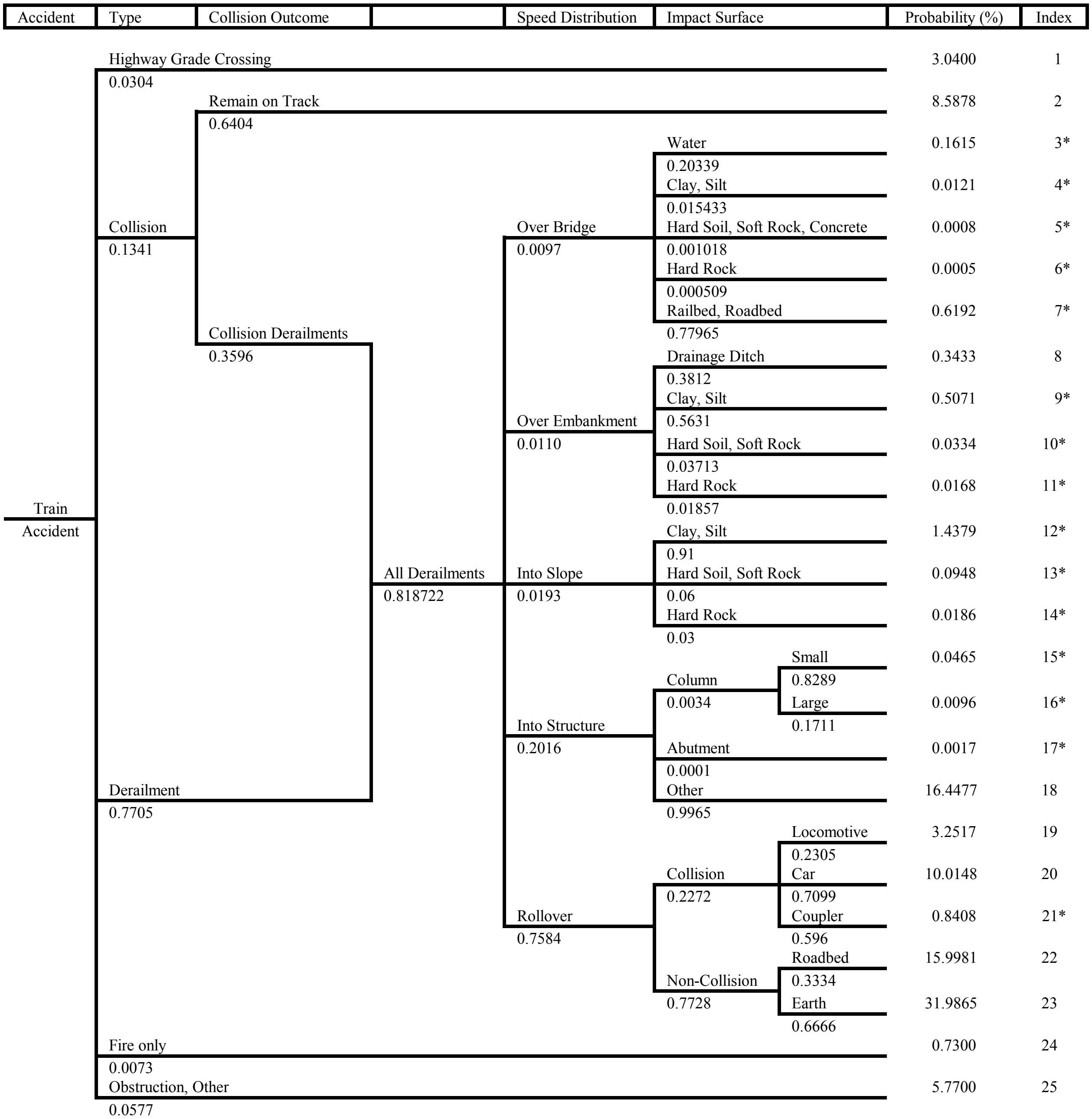

Figure 7.4 Modified Modal Study train accident event tree.

three representative real spent fuel rail transportation routes using U.S. Agricultural Department data; and second, consistent with Volpe Center results, the first-level branch on the Modal Study train event designated “Other” that has an occurrence probability of 0.0650, is split into a “Fire only” branch and an “Obstruction, Other” branch that have respectively the following occurrence probabilities:

Fire only	0.0073 = (0.0650)(0.0147/0.1315)
Obstruction, Other	0.0577 = (0.0650)(0.1168/0.1315)

7.2 Source Term and Source Term Probability Expressions

Type B spent fuel transportation casks are massive, extremely strong structures deliberately designed to withstand large mechanical and/or thermal loads without losing containment integrity. Nevertheless, although unlikely, it is possible that a truck or a train that is carrying a Type B spent fuel cask could be involved in an accident so severe that both the cask and at least some of the spent fuel rods in the cask may fail. Were this to happen, radioactive species would be released from the spent fuel into the cask interior and some of these species could be transported from the cask interior through the cask leak to the environment.

To estimate the risks associated with accidents that might occur during the transport of spent fuel by truck or train, estimates of the magnitude of the radioactive releases that might be caused by severe transportation accidents and of the probability of occurrence of these releases must be developed for three broad classes of transportation accidents: fires without collisions, collisions without fires, and collisions that lead to fires.

7.2.1 RADTRAN Risk Equations

By definition, risk is the product of the magnitude (M) of an undesirable accident consequence and its probability of occurrence (P). Thus, risk = $P \cdot M$ where M is calculated using a transportation consequence code, for example RADTRAN [7-9, 7-10], and is a strong function of the accident source term, the prevailing meteorology at the time of the hypothesized accident, the population that might be exposed to radiation as a result of the accident, and the effectiveness of any actions taken to avoid radiation exposures, for example, evacuation and/or relocation of population, and decontamination, temporary interdiction, and/or condemnation of contaminated property. The meteorological, population, and emergency response input required by the RADTRAN code are discussed in Sections 3.4.3.3, 3.4.1.4, and 3.4.3.2. This section derives expressions for accident source terms and for their probabilities of occurrence. Values for the parameters in these expressions are developed in subsequent sections.

7.2.2 Accident Source Terms

Accident source terms (ST_{jk}) depend on the accident scenario (j) and on the cask (k) involved in the accident. Here they are calculated as the product of the inventory of each radionuclide (i) in the spent fuel being carried in the transportation cask and two release fractions, the fraction of that inventory that is released from each failed rod to the cask interior, and the fraction of the inventory that is released to the cask interior that is transported through the cask leak to the environment. Thus,

$$ST_{jk} = \sum_i ST_{ijk} = \sum_i I_{ik} f_{release,ijk} = f_{rod,jk} \sum_i I_{ik} f_{RCijk} f_{CEijk}$$

where ST_{ijk} is the amount of radionuclide i released from cask k during accident scenario j, I_{ik} is the number of curies of nuclide i in the inventory of cask k, $f_{release,ijk}$ is the fraction of the inventory of radionuclide i in cask k that is released to the environment during accident scenario j, $f_{rod,jk}$ is the fraction of the rods in cask k that fail during accident scenario j, f_{RCijk} is the fraction of nuclide i that is released during scenario j to the interior of cask k from each failed rod, and f_{CEijk} is the fraction of the amount of each radionuclide released to the cask interior that is transported to the environment through the cask leak.

7.2.3 Cask Inventories

Spent fuel assemblies contain radionuclides that were produced by fissioning of uranium and by activation of assembly hardware and of materials in deposits on assembly surfaces. For this study, the ORIGEN code [7-11, 7-12] was used to calculate inventories for a generic pressurized water reactor (PWR) assembly that contained 289 fuel rods and for a generic boiling water reactor (BWR) assembly that contained 64 rods. As is described below, after dropping radionuclides that do not contribute significantly to radiation doses and adding important radionuclides formed by activation of deposits on assembly surfaces (e.g., Co-60), cask inventories were calculated by multiplying the modified single assembly inventories by the number of assemblies transported in each of the four generic casks defined in Tables 4.1 through 4.4.

7.2.3.1 Fuel Burnup

Because inventory size depends on fuel burnup, which is an ORIGEN input, and the length of the fuel cooling time after fuel discharge from the reactor, which is an ORIGEN output, initially a DOE report [7-13] was consulted to identify average and maximum BWR and PWR fuel burnups, and then, for each burnup, an ORIGEN calculation was performed that depicted the variation of inventory size with fuel cooling time. The DOE report contains data on spent fuel that has been discharged from commercial power reactors located in the United States. Table 7 in that report presents a tabulation by fuel burnup ranges of the number of metric tons of uranium in BWR and PWR spent fuel discharged during the years 1968 through 1994. This table showed that the maximum burnups reported were about 45 to 50 GWDt/MTU (gigawatt-days thermal per metric ton of uranium) for BWR spent fuel and about 55 to 60 GWDt/MTU for PWR spent fuel; and that the most probable burnups were approximately 30 GWDt/MTU for BWR spent fuel and 35 GWDt/MTU for PWR spent fuel. In addition, extrapolation to 1998 of data in Table 5 in that report showed that ten years was the quantity-weighted (weight in MTU) average age of all of the tabulated spent fuel.

7.2.3.2 ORIGEN Calculations

ORIGEN calculations were performed for the most probable and the maximum PWR and BWR fuel burnup levels, where these levels are 30 and 50 GWDt/MTU for BWR spent fuel and 35 and 60 GWDt/MTU for PWR spent fuel. Full descriptions of these calculations are presented in Appendix C. Table 7.8 summarizes the results of these calculations. Table 7.8 shows that—for both BWR and PWR spent fuel and for any fuel cooling time—the total number of curies in high (maximum) burnup spent fuel is less than a factor of two greater than the number in spent fuel having the most probable burnup. The table also shows that, due to decay, the number of curies decreases rapidly during the first three years after discharge and rather slowly after five years of cooling, and also that the number of curies at three years after discharge is approximately a factor of two greater than the number of curies at ten years, which is the quantity-weighted average age of the fuel. Nevertheless, even though most of the spent fuel that will eventually be shipped is likely to be average burnup fuel that has cooled for about ten years, in order to be conservative, the ORIGEN results for maximum burnup fuel after three years of cooling were chosen for use in this study. This choice means that the total curie content of the inventories used in the RADTRAN risk calculations described in Section 8 are most likely conservative by about a factor of four.

Table 7.8 Summary of ORIGEN Calculations, Total Curies per Assembly for All Radionuclides

Burnup (GWDt/MTU)	Fuel Cooling Time (years)						
	At Discharge	0.5	1.0	3.0	5.0	10.0	30.0
BWR							
Most probable, 30	2.87E+07	5.66E+05	3.38E+05	1.40E+05	9.38E+04	6.60E+04	3.55E+04
Maximum, 50	2.99E+07	7.04E+05	4.52E+05	2.06E+05	1.44E+05	1.03E+05	5.61E+04
PWR							
Most probable, 35	1.30E+08	2.29E+06	1.28E+06	4.60E+05	2.85E+05	1.93E+05	1.04E+05
Maximum, 60	1.07E+08	2.34E+06	1.47E+06	6.34E+05	4.32E+05	3.05E+05	1.68E+05

7.2.3.3 Elimination of Unimportant Radionuclides

An ORIGEN inventory contains approximately 800 radionuclides. This large set of radionuclides was reduced to a much smaller set that contained only radionuclides that together accounted for 99.9 percent of the health hazard posed by the total inventory using radionuclide A_2 values [7-14, 7-15] as a measure of radiation health hazard. The RADSEL code [7-16] was used to perform this reduction. For each radionuclide in the total inventory, RADSEL computes the ratio of the nuclide's number of curies and its A_2 value, sums and normalizes these ratios, sorts the ratios according to magnitude, and then retains the smallest set of radionuclides whose ratios sum to 0.999.

7.2.3.4 Radioactive Gases

Although tritium gas and tritiated water are very active biologically, the quantities per assembly calculated by ORIGEN for three-year cooled PWR (482 Ci) and BWR (168 Ci) fuel are so small compared to the A_2 value for tritium (1080 Ci) that they contribute less than 0.1% to the health hazard of the total inventory. Therefore, tritium was not included in the reduced, maximum burnup, three-year cooled, BWR or the PWR inventories. However, although the relative contribution to total health hazard of Kr-85 is also less than 0.1% for the three-year cooled fuel, because Kr is the most important member of the non-condensible gas chemical element group, it was retained in the reduced BWR and PWR assembly inventories despite its minor contribution to health hazard. Accordingly, the following quantities per assembly of Kr-85 were added back into the reduced BWR and PWR inventories generated by RADSEL: 5.87E3 Ci to the PWR assembly inventory, and 1.74E3 Ci to the BWR assembly inventory.

7.2.3.5 CRUD

During reactor operation, corrosion products formed in the reactor's primary cooling system deposit on fuel assembly surfaces where elements in these deposits are activated by neutron bombardment. The resulting radioactive deposits are called CRUD [7-17]. Due to vibratory loads during incident free transportation, impact loads during collision accidents, and thermal loads during accidents that lead to fires, portions of these radioactive deposits may spall from the rods. Then, if some of these spalled materials become airborne during an accident, their release to the atmosphere could contribute to the radiation exposures caused by the accident. Although CRUD contains a number of radionuclides, only Co-60 would contribute significantly to these radiation exposures. Since the CRUD deposits on typical PWR and BWR spent fuel rods contain respectively 0.2 and 1.0 Ci of Co-60 per rod [7-17] and the generic PWR and BWR assemblies for which ORIGEN inventories were calculated contain respectively 289 and 64 spent fuel rods, the amounts of Co-60 produced by activation of deposits on assembly surfaces is 57.8 Ci for the generic PWR assembly and 64 Ci for the generic BWR assembly.

7.2.3.6 Inventories for Generic PWR and BWR Assemblies

The final generic PWR and BWR assembly inventories were now constructed by adding the amounts per assembly of Kr-85 and of the Co-60 in CRUD to the reduced generic assembly inventories that were generated by eliminating all radionuclides shown by the RADSEL calculation to contribute negligibly to radiation exposures from the full assembly inventories calculated by ORIGEN. Table 7.9 presents these reduced modified generic assembly inventories.

7.2.4 Chemical Element Classes

To simplify the development of accident source terms, fission products are assigned to chemical element classes that have similar physical and chemical properties and therefore are expected to have similar transport characteristics. Each group is called a chemical element class and for convenience each is denoted by one of the elements assigned to the class. After assignment to classes, rod-to-cask and cask-to-environment release fractions are developed for each chemical element class.

Fission products are usually assigned to one of three general chemical element classes: non-condensible gases, condensible gases, and particulates. Each class may be further subdivided if the transport properties of its member elements differ widely. For example, because the volatile forms of cesium and iodine, Cs, CsOH, CsI, I_2, have very different volatilities and chemical properties, Cs and I are usually assigned to different classes of condensible gasses. In addition, elements with unique chemistries are placed in special chemical element classes. For transportation accident analysis, Co and Ru are usually placed in special classes. Co is placed in a special element class because it is the major constituent of the radioactive deposits called CRUD that form on the outside of spent fuel rods during reactor operation. Ru is placed in a special element class because, if exposed to oxygen while at elevated temperatures, involatile RuO_2 can be converted to RuO_3 and RuO_4, which are much more easily vaporized, thereby greatly increasing the rate of release of Ru from fuel pellets.

Table 7.9 Generic High Burnup, Three-Year Cooled, Fuel Assembly Inventories for RADTRAN Calculations (Ci/assembly)

Generic BWR Assembly	
Nuclide	**Amount (Ci)**
Co-60	6.40e+01
Kr-85	1.74e+03
Sr-90	1.59e+04
Y-90	1.59e+04
Ru-106	1.42e+04
Cs-134	2.15e+04
Cs-137	2.59e+04
Ce-144	1.03e+04
Pm-147	8.49e+03
Pu-238	1.67e+03
Pu-239	7.44e+01
Pu-240	1.36e+02
Pu-241	2.91e+04
Am-241	2.05e+02
Am-242M	8.09e+00
Am-243	1.22e+01
Cm-242	1.82e+02
Cm-243	1.42e+01
Cm-244	2.95e+03

Generic PWR Assembly	
Nuclide	**Amount (Ci)**
Co-60	5.78e+01
Kr-85	1.74e+03
Sr-90	5.36e+04
Y-90	5.36e+04
Ru-106	4.43e+04
Cs-134	6.99e+04
Cs-137	7.90e+04
Ce-144	3.87e+04
Pm-147	2.58e+04
Eu-154	8.42e+03
Pu-238	4.81e+03
Pu-239	2.14e+02
Pu-240	4.28e+02
Pu-241	6.52e+04
Am-241	4.36e+02
Am-242M	1.33e+01
Am-243	2.51e+01
Cm-242	3.76e+02
Cm-243	2.88e+01
Cm-244	5.62e+03

For this study, fission products are assigned to five chemical element classes. The five classes and the representative element that denotes each class are:

Representative Element	**Description**
Xe	Noble (non-condensible) gases
Cs	Condensible gases
Ru	Single element group
Co	Fission products found in CRUD
Part	All other fission products

Condensible gases are not subdivided into a cesium (Cs) and an iodine (I) class because, by the time spent fuel is removed from a reactor's spent fuel pool and released for transport to an interim or a permanent repository, almost all iodine nuclides except I-129 will have decayed away and the remaining I-129 will have reacted with Cs to form CsI. Thus, an iodine chemical element class is not needed. Finally, the class denoted by Part represents all fission products that exist in chemical forms (usually refractory hydroxides and oxides, e.g., Sr which transports as $Sr(OH)_2$, Pu which transports as PuO_2) that transport only as particles.

7.2.5 Release Fractions

This section develops expressions for accident release fractions. Expressions are developed for four broad classes of accidents: collision accidents that do not initiate fires (Collision only), collision accidents that initiate fires and generate mechanical or thermal loads that cause the cask seal to leak (Collision + Fire, 1 leakage path), collision accidents that initiate fires and generate mechanical or thermal loads that cause the cask seal to leak and also lead to failure of the cask shell by puncture or shear (Collision + Fire, 2 leakage paths), and fire accidents that do not involve collisions (Fire only). The first three of these four accident categories correspond to accident categories 4, 5, and 6 in the six-category accident severity scheme that is frequently used when performing RADTRAN calculations [7-18]. The last accident category, fires not initiated by collisions, leads to accidents that have severities that are similar to those of Category 5 accidents, but release fraction expressions that are different than those used to calculate release for accidents initiated by collisions that lead to fires. Because their release fraction expressions are unique, they are here not lumped into Category 5, but are placed in a separate fire-only category. Collisions that lead both to double cask failures and to fires are separated from collisions that lead to fires, but only a single cask failure, because differential thermal heating of a cask with a double failure may cause combustion gases, including some air, to flow through the cask. Flow of gas through the cask could sweep most fission products released to the cask interior out of the cask to the environment, thereby minimizing fission product retention in the cask. Flow of air into the cask could also lead to the oxidation of UO_2 to UO_3 and of RuO_2 to RuO_3 and RuO_4 [7-19]. Because Cs diffuses though UO_3 more easily than through UO_2, oxidation of fuel enhances Cs release rates. Because RuO_3 and RuO_4 are much more volatile than RuO_2, conversion of RuO_2 to RuO_3 and RuO_4 substantially increases release of Ru.

7.2.5.1 Mechanical Failure of Cask Seals and Spent Fuel Rods.

The response of four generic Type B spent fuel casks—two truck casks and two rail casks—and of the spent fuel rods carried in the casks, to high-speed impacts onto yielding real-world surfaces (clay/silt, hard soil/soft rock, hard rock, water, railbed/roadbed) and objects (small columns, large columns, abutments) is discussed in Section 5. Puncture and shear failures of rail tank cars during collision accidents were also analyzed in that section.

The analysis of puncture and failures presented in Section 5.3 suggests that formation of a puncture or shear probe during a collision accident depends only weakly on accident speed. Therefore, probe formation is possible during any collision accident. But a probe, if formed (or already present at the accident site), can puncture a cask only if the probe (a) is sharp enough and so oriented upon impact with the cask that it initiates a puncture or tear in the cask shell (does not glance off of the cask surface) and (b) has a stem that is sufficiently robust so that it does not break before the cask shell is completely penetrated by the probe. Since these two conditions are both improbable, the analysis concluded that failure of a cask by puncture or shear was possible during any collision accident but also was most unlikely.

The finite element calculations described in Section 5 and their extrapolation to real-world yielding surfaces strongly suggest that only extremely high-speed impacts onto slightly yielding surfaces (e.g., hard rock) are likely to cause the seals of Type B steel-lead-steel and steel-DU-steel spent fuel truck casks to leak. Specifically, the calculations show so little distortion of the cask closures of the generic steel-lead-steel and steel-DU-steel spent fuel truck casks following 120 mph impacts onto an unyielding surface that seal leakage cannot be predicted with certainty even for impacts this severe. Nevertheless, even though not large enough to predict that seal leakage is certain to occur, because distortion of the cask closure is clearly discernable, 120 mph impacts onto an unyielding surface are assumed to cause the seal of truck casks to leak and that leak path is arbitrarily assumed to have a cross-sectional area of 1 mm^2. Thus, if v_{seal} is the speed that produces a seal leak, then by definition v_{seal} = 120 mph for impacts of truck casks onto an unyielding surface at any orientation and $v_{seal} = v_{120}$ for impacts of truck casks at any orientation onto real world yielding surfaces, where v_{120} is the impact speed for the specified impact orientation onto the real yielding surface that causes the same damage to the truck cask and its contents as is caused by a 120 mph impact at the same impact orientation onto an unyielding surface.

For rail casks, the finite element calculations indicate that seal leakage occurs for impacts onto an unyielding surface at some impact orientations at speeds as low as 60 mph. Specifically, for both the steel-lead-steel and the monolithic steel generic rail casks, closure region distortions are sufficiently large for 60 mph impacts onto an unyielding surface in the center of gravity over corner impact orientation to allow seal leakage to be predicted (i.e., the predicted separation of the lid well from the cask lid is larger than the compliance of the O-ring seal, which means that sealing function should be lost). Closure region distortion also appears to be large enough to predict seal leakage for side impacts of the monolithic steel generic rail cask onto an unyielding surface at 60 mph.

The finite element calculations also show that, for some yielding surfaces, many impact accidents, that do not cause the cask seal to leak, will cause slumping of cask contents or inward collapse of the cask shell that is sufficiently severe so that fuel rods would be expected to fail either by buckling or tearing and also that the impact speed that produces failure of some fraction of the rods in the cask will be different for end, corner, and side impacts. Thus, the impact speeds that cause rod to fail or seals to leak depend on both the nature of the impact surface and the cask orientation at the time of impact.

Although failure of some fuel rods is expected for most severe collision accidents, the finite element analyses described in Section 5.1 do not predict the fraction of rods failed. They did, however, provide estimates of the peak rigid body accelerations that the fuel rods would experience as a result of cask impacts onto unyielding surfaces. This allowed results from an analysis of the strains generated in PWR and BWR fuel rods carried in a typical PWR or BWR assembly [7-20] for regulatory impacts to be scaled to match the accelerations produced by impacts onto unyielding surfaces at 60, 90, and 120 mph. Comparison of the scaled rod strains to the rod failure criterion developed for the analysis of regulatory impacts [7-21] then allowed the fraction of the rods in a typical PWR or BWR assembly failed by 30, 60, 90, and 120 mph impacts onto an unyielding surface to be estimated.

Accordingly, for each impact orientation examined in Section 5.1 and each class of real-world yielding surfaces, four speeds were determined, v_{30}, v_{60}, v_{90}, and v_{120}, where v_{30}, v_{60}, v_{90}, and v_{120} are the impact speeds for the stated impact orientation (end, corner, or side) onto the real yielding surface that inflict damage onto the cask and its contents equivalent to the damage caused by 30, 60, 90, and 120 mph impacts onto an unyielding surface. These four speeds define four speed ranges, $v_{30} \leq v < v_{60}$, $v_{60} \leq v < v_{90}$, $v_{90} \leq v < v_{120}$ and $v_{120} \leq v$, where v is the cask impact speed onto the real yielding surface or object at the stated impact orientation.

7.2.5.2 Thermal Failure of Cask Seals and Spent Fuel Rods

During normal transport under ambient conditions, the peak temperature of spent fuel in a Type B spent fuel cask is about 300°C [7-22]. Because the average temperature of free burning hydrocarbon fuel fires is about 1000°C [7-23], elastomeric cask seals and spent fuel rods can both fail if the cask that contains them is heated long enough by a hot fire.

Type B spent fuel casks are usually equipped with elastomer seals (e.g., Viton O-rings). When heated to temperatures above 350°C at rates comparable to the heating rates of engulfing hydrocarbon fuel fires, these seal materials degrade thermally losing about 5 percent of their mass if heated to 380°C, 10 percent if heated to 400°C, and 70 percent if heated to 450°C [7-24]. Elastomeric O-rings lose sealing function, as measured by helium leak detection, if heated to about 400°C, but can be repeatedly cycled from ambient temperatures to temperatures approaching 380°C without loss of sealing function [7-25]. Loss of mass without loss of sealing function upon heating to 380°C occurs because elastomeric O-rings usually contain or are coated with volatile organics (e.g., oils). Thus, the mass loss that occurs first upon heating is due to the vaporization of these volatile organics and not to thermal decomposition of rubber matrix materials, which causes the O-ring to shrink and, when shrinkage is appreciable, sealing function to be lost. Accordingly, heating of elastomeric cask seals to temperatures above 400°C is probably required, if loss of sealing function is to be large enough to allow significant quantities of gasborne aerosols to escape from the cask through the failed seal. Nevertheless, it is here assumed that elastomeric cask seals begin to leak when heated to 350°C and, in order to be consistent with the treatment of seal failures caused by impacts, it is also assumed that the seal leak produced by heating to 350°C has a cross-sectional leak area of about 1 mm^2 (because no credit is taken for vapor and particle deposition during most of the 60 to 80 minutes that is required for an engulfing fire to heat a cask to seal failure temperatures, source term magnitudes and thus accident consequences are relatively insensitive to seal failure temperatures). Finally, the substantial mass loss that is caused by heating to 450°C is assumed to cause O-ring sealing function to be lost around the entire circumference of the cask closure producing a leak area that is determined by the roughness of the surfaces of the cask lid and lid well where they contact each other and the length of the closure circumference.

When heated to elevated temperatures, spent fuel rods fail by burst rupture. During the experiments of Lorenz, et al. [7-26], sections of spent fuel rods that had been heated to 900°C failed by burst rupture when rod pressures reached 275 psig. Wilmot's analysis of release of fission products from spent fuel rods during transportation accidents assumes rod failure by burst rupture occurs at 850°C [7-27]. The critical review of spent fuel transportation accident conditions by Sanders, et al. [7-28] indicates that rod burst rupture is expected to occur at temperatures near 725 to 750°C. And, after correcting for differences in burnup and internal pressure, data in the Cask Designers Guide suggest that spent fuel rods may fail due to creep rupture occurs at 850°C [7-27]. The critical review of spent fuel transportation accident conditions by Sanders, et al. [7-28] indicates that rod burst rupture is expected to occur at temperatures near 725 to 750°C. And, after correcting for differences in burnup and internal pressure, data in the Cask Designers Guide suggest that spent fuel rods may fail due to creep rupture at temperatures as low as 700°C [7-29]. Because the release of Cs vapors will be greater when rods fail at higher rather than lower temperatures, the temperature at which rods fail by thermal burst rupture is assumed to be 750°C, the middle of this range, rather than 700°C, the bottom of the range.

Let the internal temperature of a Type B spent fuel cask during normal transport under ambient conditions be T_a = 300°C, the temperature where elastomeric spent fuel cask seals begin to leak through a leak path with a cross-sectional area of 1 mm^2 be T_s = 350°C, the temperature where spent fuel rods fail by burst rupture be T_b = 750°C, and the average temperature of hydrocarbon fuel fires be T_f = 1000°C. These four temperatures define three temperature ranges, $T_a \leq T_{cask} \leq T_s$, $T_s < T_{cask} < T_b$, and $T_b \leq T_{cask} \leq T_f$, where T_{cask} is the internal temperature of the cask.

7.2.5.3 Collision-Only Scenarios

Collisions that do not initiate fires must be unusually severe if seal leakage is to caused by impact. For impacts onto an unyielding surface at 60 mph by a Type B rail cask and at 120 mph by a Type B truck cask, the finite element cask impact calculations described in Section 5 indicate that, even though slumping of cask internal structures is so great that many of the rods in the cask are likely to fail, distortion of the cask seal region is not great enough to conclude that seal leakage definitely occurs. Despite this, here it is assumed that (a) leakage of the cask's elastomeric seals is produced by all collisions that lead to impact of a Type B spent fuel cask onto a yielding surface at a velocity that subjects the cask to mechanical loads equal to those generated by impacts onto an unyielding surface at 60 mph for rail casks and at 120 mph for truck casks, (b) the leakage area produced by these impacts is about 1 mm^2, and (c) such impacts cause at least some of the rods in the cask to fail.

MELCOR calculations [7-30] indicate that, when cask leak path cross-sectional areas are small (~ 1 mm^2), the mass deposition rate of vapors and particles onto cask interior surfaces is rapid compared to the mass rate of their release from the cask to the environment. Thus, unless cask depressurization is rapid, deposition of vapors and large particles onto cask interior surfaces will be efficient which means that deposition of radioactive materials will also be efficient. Therefore, for collision accidents that do not initiate fires, deposition of particles and vapors onto cask interior surfaces during rod depressurization is assumed to be appreciable whenever cask seal leakage areas are small. Thus, for Collision-Only scenarios (Category 4 accidents), $f_{release}$, the total release fraction for release of fission products from failed rods to the environment, is given by

$$f_{release} = f_{rod,impact} f_{RC} \left(1 - f_{deposition}\right)\left(1 - \frac{p_{atm}}{p_{Imp}}\right) \tag{1}$$

where $f_{rod,impact} = 1.0$ is the fraction of the rods in the cask that are failed by the collision impact, f_{RC} is the fraction of the materials in a spent fuel rod that is released to the cask interior upon rod failure, $f_{deposition}$ is the fraction of those materials that rapidly deposit onto cask interior surfaces upon release from the failed spent fuel rods, p_{atm} is atmospheric pressure, and p_{Imp} is the cask internal pressure after depressurization of the fuel rods that failed as a result of the collision impact. Note that although the values of f_{RC} and $f_{deposition}$ will depend on the physical and chemical properties of the materials (radionuclide species) being released from the failed fuel rods, for simplicity in this and subsequent equations, they are written without attachment of the radionuclide species subscript i (e.g., as f_{RC} rather than f_{RCi}).

7.2.5.4 Collision Plus Fire Scenarios

Consider a collision accident that is severe enough to fail some of the rods in the spent fuel cask, but not the cask seal, and that also initiates a fire that heats the cask to the temperature T_s where the cask seal fails due to thermal degradation causing the cask to depressurize. Now let p_{atm} be atmospheric pressure, p_{Imp} be the cask internal pressure after depressurization of the fuel rods that failed as a result of the collision impact, T_a be the cask internal temperature during normal transport under ambient conditions, V_{cask} be the internal free volume of the cask, $V_{expansion}$ be the volume that the gases initially in the cask plus the gases released to the cask by rod failure would occupy at T_s and atmospheric pressure, and f_{CE} be the fraction of the gasborne radioactive materials that escape from the cask to the environment when the cask seal fails due to thermal degradation. But

$$f_{CE} = 1 - \frac{V_{cask}}{V_{expansion}} \quad \text{and} \quad \frac{p_{Imp} V_{cask}}{T_a} = \frac{p_{atm} V_{expansion}}{T_s} \quad \text{and therefore} \quad \frac{V_{cask}}{V_{expansion}} = \frac{p_{atm} T_a}{p_{Imp} T_s}$$

So, if deposition of particles and vapors is neglected during the time required for the fire to heat the cask from T_a to T_s,

$$f_{CE} = 1 - \frac{V_{cask}}{V_{expansion}} = 1 - \frac{p_{atm} T_a}{p_{Imp} T_s}$$

By extending this approach, a conservative expression can now be developed for release due to failure of some rods by an impact that does not fail the cask seal followed by heating of the cask in a fire first to the temperature T_s where the cask seal begins to leak, then to the temperature T_b where the remaining rods fail by burst rupture, and finally to the temperature of the fire T_f. As before, let p_{Imp} be the cask pressure after rod failure due to impact and p_{atm} be atmospheric pressure. In addition, let f_{imp} be the fraction of the rods failed by impact, f_{bur} be the fraction of rods failed by thermal burst rupture, p_b be the cask pressure after rod failure due to burst rupture, f_{RCimp} be the release fraction for fission products to the cask interior from a rod failed by impact, f_{RCf} be the release fraction for fission products to the cask interior from a rod failed by thermal burst rupture due to a fire, and f_{dep} be the fraction of the materials released from failed rods to the cask interior that deposits rapidly onto cask internal surfaces. Then, the total release fraction f_{rel}

for release of fission products from failed rods to the environment during Category 5 accidents is given by

$$\begin{aligned} f_{rel} = {} & f_{imp} f_{RCimp}\left(1-f_{dep}\right)\left\{\left[1-\frac{p_{atm}}{p_{imp}}\frac{T_a}{T_s}\right]+\left[\frac{p_{atm}}{p_{imp}}\frac{T_a}{T_s}\right]\left[1-\frac{T_s}{T_b}\right]+\left[\frac{p_{atm}}{p_{imp}}\frac{T_a}{T_b}\right]\left[1-\frac{p_{atm}}{p_b}\frac{T_b}{T_f}\right]\right\} \\ & + f_{bur} f_{RCf}\left(1-f_{dep}\right)\left\{\left[1-\frac{p_{atm}}{p_b}\frac{T_b}{T_f}\right]\right\} \end{aligned} \tag{2}$$

where $f_{bur} = 1 - f_{imp}$, because all rods not failed by impact are assumed to fail when the rod burst rupture temperature is reached, and the expression is conservative because deposition of particles and vapors is assumed to occur only immediately following rod failure and not during the time periods during which the cask is heated by the fire to elevated temperatures.

Inspection of Equation 2 shows that the first term in the equation gives the release fraction for materials released due to rod failure caused by collision impacts and the second term gives the release fraction for materials released due to rod failure caused by thermal burst. In addition, the three parts of the first term respectively reflect the effect on release of (1) cask pressurization due to rod depressurization upon impact failure followed by heating of cask gases to the temperature where seal leakage begins, (2) heating of cask gases from the temperature of seal leakage almost to the temperature of rod burst rupture, and (3) cask pressurization due to burst rupture of the remaining unfailed rods followed by heating of cask gases from the burst rupture temperature to the temperature of the engulfing fire.

Equation 2 also is used to calculate the release fraction for Category 6 accidents, collisions that initiate fires and fail not only the cask seal by impact but also the cask body by puncture or shear. For these accidents, f_{dep} in the last term of the equation is set to zero, because the flow of gases through the cask during these accidents is assumed to transport all materials released to the cask interior from the failed rods through the cask failures to the environment.

Finally, for Category 5 and Category 6 accidents that heat the cask to temperatures $\geq T_b$, all Cs in particles deposited on cask internal surfaces is assumed to volatilize. Volatilization of all Ru in particles deposited on cask internal surfaces is also assumed to occur during all Category 6 accidents since, during these accidents, air is assumed to be flowing through the failed cask which would cause involatile RuO_2 to be oxidized to volatile RuO_4.

7.2.5.5 Fire-only Scenarios

For fires not initiated by collisions (Category Fire-only accidents), when the inner wall of the cask shell reaches a temperature of 350°C = T_s, thermal degradation of the cask's elastomeric seal is assumed to cause the cask seal to begin to leak through a leak path that has a cross-sectional area of 1 mm^2. In addition, whenever the cask shell temperature exceeds 450°C, decomposition of the elastomeric seal is assumed to be so extensive that the effective leak path has a cross-sectional area equal to the product of the closure circumference and the roughness height of the lid and the lid well where they contact inside of the closure. In addition, all of the rods in the cask are assumed to fail by burst rupture when the cask inner shell temperature reaches 750°C = T_b, and, whenever rod failure occurs, the fire is assumed to burn long enough to heat the cask to T_f = 1000°C, the average temperature T_f of a hydrocarbon fuel fire which is here assumed to be 1000°C. Therefore, for Category Fire-only accidents,

$$f_{rel} = f_{bur} f_{RCf} \left(1 - f_{dep}\right) \left[1 - \frac{p_{atm}}{p_b} \frac{T_b}{T_f}\right] \tag{3}$$

where f_{bur} = 1.0 is the fraction of rods in the cask that fail when the cask internal temperature reaches the rod burst temperature T_b.

7.2.5.6 Expansion Factor Ratios

Now let $f_{e1} = (p_{atm}/p_{imp})(T_a/T_s)$, $f_{e2} = T_s/T_b$, $f_{e3} = (p_{atm}/p_{imp})(T_a/T_b)$, $f_{e4} = (p_{atm}/p_b)(T_b/T_f)$, and $f_{e5} = (p_{atm}/p_{Imp})$. After substitution of these expansion factor symbols, the equations for release caused by collisions that do not initiate fires, by collisions that do initiate fires, and fires not initiated by collisions reduce to:

Accident Category	**Term**	**Part**	**Failure Mode**	**Temperature Range**
Collisions that do not initiate Fires				
$f_{rel} = f_{imp} f_{RCimp} (1-f_{dep})(1-f_{e5})$	1		Impact	T_a
Collisions that initiate Fires				
$f_{rel} = f_{,imp} f_{RCimp} (1-f_{dep})(1-f_{e1})$	1	1	Impact	$T_a \le T_{cask} \le T_s$
$+ f_{imp} f_{RCimp} (1-f_{dep})(f_{e1})(1-f_{e2})$	1	2		$T_s < T_{cask} < T_b$
$+ f_{imp} f_{RCimp} (1-f_{dep})(f_{e3})(1-f_{e4})$	1	3		$T_b \le T_{cask} \le T_f$
$+ (1-f_{imp}) f_{RCfire} (1\text{-}f_{dep})(1-f_{e4})$	2		Rupture	$T_b \le T_{cask} \le T_f$
Fires without Collisions				
$f_{rel} = (1-f_{imp}) f_{RCfire} (1-f_{dep})(1-f_{e4})$	1		Rupture	$T_b \le T_{cask} \le T_f$

7.2.6 Accident Cases

The four accident categories, the four velocity ranges, and the three temperature ranges defined above allow 18 truck accident cases and 20 train accident cases that lead to release of radionuclides to be defined (because RADTRAN requires that the probabilities of the cases supplied as input sum to one, before being input to RADTRAN, these accident cases are augmented by one case that includes shipments not subject to accidents and shipments that involve accidents that do not lead to a release of radionuclides, i.e., 19 total truck cask and 21 total train cases). For truck accidents, the 18 accident cases consist of one Category 4 case, twelve Category 5 cases, four Category 6 cases, and one Category Fire-only case. Table 7.10

presents the characteristics (cask failure mechanism, impact velocity range, and temperature range) of each truck accident case.

In Table 7.10, the single Category 4 accident case represents collisions that do not initiate fires but are so severe that the impact forces cause the cask seal to leak and all of the rods in the truck cask to fail. The twelve Category 5 accident cases occur in four groups of three accident cases. The first three groups represent collisions that are not severe enough to cause seal leakage but initiate fires that heat the cask to temperatures greater than the temperature where the cask seal begins to leak due to thermal degradation. The fourth group of three Category 5 accident cases represents collisions that both initiate fires and are also so severe that the impact causes the cask seal to leak. Because for these three cases $v_{seal} \geq v_{120}$, the initial impact also fails all of the rods in the cask. Cases 14 through 17, the Category 6 accident cases, are the same as Cases 4, 7, 10, and 13 except that a second failure of the cask by puncture or shear is assumed. Because of the

Table 7.10 Truck Accident Cases

Category	Case	Cask Seal Failure by		Velocity Range				Temperature Range		
		Impact	Fire	v_{30}-v_{60}	v_{60}-v_{90}	v_{90}-v_{120}	$\geq v_{120}$	T_a-T_s	T_a-T_b	T_a-T_f
4	1	X					X			
5	2		X	X				X		
	3		X	X					X	
	4		X	X						X
	5		X		X			X		
	6		X		X				X	
	7		X		X					X
	8		X			X		X		
	9		X			X			X	
	10		X			X				X
	11	X					X	X		
	12	X					X		X	
	13	X					X			X
6	14		X	X						X
	15		X		X					X
	16		X			X				X
	17	X					X			X
Fire Only	18		X							X
No Release	19									

double failure of the cask, it is also assumed first that flow of combustion gases or air through the cask carries out to the environment all fission products released from the rods to the cask interior while the cask is hot, and second that oxidation of fuel and of RuO_2 enhances the releases of Cs and Ru compared to the releases that characterize Case 4, 7, 10, and 13 accidents. Finally, the single case in the Fire Only category represents fires not initiated by collisions that heat the cask to temperatures high enough to fail all of the spent fuel rods by burst rupture and also the cask seal by thermal degradation.

If a term for the deposition of particles and vapors, while a fire is heating the cask to elevated temperatures, were added to Equation 2, then Category 5 accident Cases 8, 9, and 10 would have slightly smaller release fractions than Category 5 accident Cases 11, 12, and 13. Because particle and vapor deposition during periods of cask heating by a fire is neglected, the release fractions calculated for accident Cases 11, 12, and 13 will be the same as those calculated for accident Cases 8, 9, and 10. Finally, because the rod failure fractions ($f_{rod,impact}$) for the four Category 6 accident cases (Cases 14, 15, 16, and 17) are ordered as follows,

$$f_{rod,impact,Case\ 14} < f_{rod,impact,Case\ 15} < f_{rod,impact,Case\ 16} = f_{rod,impact,Case\ 17}$$

the release fractions for these four accident cases have the following order:

$$f_{release,Case\ 14} > f_{release,Case\ 15} > f_{release,Case\ 16} = f_{release,Case\ 17}$$

Increasing the fraction of rods failed by impact decreases the release fraction for Category 6 accidents because for this accident category, deposition processes are assumed to be effective for materials released to the cask interior when rods are failed by impact but is neglected when rods fail by burst rupture. Deposition is neglected following burst rupture because the combustion gases that are assumed to be flowing through the cask during Category 6 accidents are also assumed to carry all materials released to the cask interior out to the environment without significant depletion by deposition to cask interior surfaces.

For train accidents, because rail cask seals may leak after impacts onto an unyielding surface at some orientations at speeds as low as 60 mph, the train accident matrix consists of 20 accident cases, three Category 4 cases, twelve Category 5 cases, four Category 6 cases, and one Category Fire-only case. Table 7.11 presents the characteristics (cask failure mechanism, impact velocity range, and temperature range) of each train accident case.

Table 7.11 Train Accident Cases

Category	Case	Cask Seal Failure by		Velocity Range				Temperature Range		
		Impact	Fire	v_{30}-v_{60}	v_{60}-v_{90}	v_{90}-v_{120}	$\geq v_{120}$	T_a-T_s	T_a-T_b	T_a-T_f
4	1	X			X					
	2	X				X				
	3	X					X			
5	4		X	X				X		
	5		X	X					X	
	6		X	X						X
	7	X			X			X		
	8	X			X				X	
	9	X			X					X
	10	X				X		X		
	11	X				X			X	
	12	X				X				X
	13	X					X	X		
	14	X					X		X	
	15	X					X			X
6	16		X	X						X
	17	X			X					X
	18	X				X				X
	19	X					X			X
Fire Only	20		X							X
No Release	21									

7.2.7 Source Term Probabilities

For transportation accidents, the probability P that an accident is so severe that it generates a source term that leads to consequences with magnitude M is expressed as the product of the probability that any accident occurs ($P_{accident}$), the probability that the truck or rail car carrying the cask is involved in the accident ($P_{vehicle}$), and the fraction of all possible accidents ($F_{severity}$) that lead to releases of radioactivity that cause consequences of magnitude M. Therefore,

$$P = P_{accident} P_{vehicle} F_{severity} \tag{4}$$

7.2.7.1 Accident Probabilities

The probability that a truck or train is involved in an accident of any severity while traveling a route of length L is usually expressed as the sum of the chances that an accident occurs on the urban, suburban, and rural portions of the route. Thus,

$$P_{accident} = \sum_{m=1}^{3} Lf_m Rate_{accident,m}$$

where m is a link index, which is here used to denote the urban, suburban, and rural portions of the route, $Rate_{accident,m}$ is the accident frequency, without regard to severity, per unit distance traveled on the urban, suburban, and rural portions of the route, and f_m is the fraction of the route length that is urban, suburban, or rural. Values for L, f_m, and $Rate_{accident,m}$ were developed in Sections 3.3.1 and 3.3.2.

7.2.7.2 Vehicle Involvement

Values for $P_{vehicle}$, the probability that the vehicle carrying the spent fuel cask is involved in the accident, are developed in Section 7.4.2 directly from accident data. Thus, $P_{vehicle}$ is not formulated as an algebraic combination of other variables.

7.2.8 Accident Severities

The massive nature and robust construction of Type B spent fuel casks mean that only an extremely severe collision and/or a hot, long-duration fire can cause both the cask and a significant fraction of the spent fuel rods being transported in the cask to fail. The severity of a collision accident depends on accident type, accident speed, cask impact angle, the hardness of the impact surface, the fraction of the accident energy that is consumed damaging structures other than the cask, the size of the cask leak, and the fraction of the rods in the cask that are failed by the impact loads. Because only a hot, long duration fire can heat a spent fuel cask to temperatures that are high enough to cause both the cask seal and spent fuel rods to fail, the severity of fire accidents depends on fuel type (combustion characteristics), the amount of fuel available to be burned, the effects of fuel runoff and of adsorption of fuel by the ground, fuel availability and rate of combustion, the stand-off distance of the fire from the cask, and the size of the cask leak.

7.2.8.1 Severity Fraction Expressions

Let $P_{scenario,j}$ be the probability that an accident follows accident scenario j (the probability of path j on the truck or rail accident event trees depicted in Figures 7.3 and 7.4). For collision accidents, let $P_{puncture/shear}$ be the conditional probability that during the collision the cask shell is failed by puncture or shear and $P_{speed,j}$ be the probability that the cask impact speed v for collision accident scenario j is large enough to cause consequences of magnitude M by itself for collision-only accidents or in conjunction with the effects of any ensuing fires for collision accidents that initiate fires. For accidents that involve fires (collisions that initiate fires and fire-only accidents), let $P_{fire/scenario,j}$ be the probability that accident scenario j initiates a fire and $P_{severe\ fire,k}$ be the probability that the fire raises the temperature of cask k high enough to cause the additional damage (seal leakage due to thermal degradation and rod failure by burst rupture) required to produce consequences of magnitude M.

Given these definitions and assuming that these probabilities are largely independent, for collisions that don't initiate fires (Category 4 accidents),

$$F_{severity,j} = P_{scenario,j}\, P_{speed,j} \tag{5}$$

where $P_{scenario,j}$ is the probability of accident scenario j and $P_{speed,j}$ is the probability that the cask impact speed for accident scenario j is large enough to cause consequences of magnitude M, and all of the probabilities are conditional probabilities that are conditional on the occurrence of an accident and each probability in this and subsequent expressions is also conditional on the probabilities in the expression that precede it.

For Category 5 accidents that involve collisions that initiate fires,

$$F_{severity,j} = P_{scenario,j}\, P_{speed,j}\, P_{fire/scenario,j}\, P_{severe\ fire,k} \tag{6}$$

For Category 6 accidents that involve collisions sufficiently severe to fail the cask shell by puncture or shear and its seal by warping of the seal seat,

$$F_{severity,j} = P_{scenario,j}\, P_{speed,jm}\, P_{fire/scenario,j}\, P_{severe\ fire,k}\, P_{puncture/shear} \tag{7}$$

And for Category Fire-only accidents that don't involve collisions,

$$F_{severity,j} = P_{scenario,j}\, P_{severe\ fire,k} \tag{8}$$

because by definition $P_{fire/scenario,j} = 1.0$ for fire-only accidents.

7.2.8.2 Accident Velocity Probabilities

In Section 7.2.5.1, four ranges for the cask impact speed v were defined, $v_{30} \le v < v_{60}$, $v_{60} \le v < v_{90}$, $v_{90} \le v < v_{120}$, and $v_{120} \le v$, where v_{30}, v_{60}, v_{90}, and v_{120} are the impact speeds for end, corner, or side impact orientations onto real yielding surfaces that cause the same damage to the cask and its contents (spent fuel) as is caused respectively by end, corner, and side impacts at speeds of 30, 60, 90, and 120 mph onto an unyielding surface. Thus, $P_{speed,j}$, the probability that the cask impact speed v for collision accident scenario j is large enough to cause consequences of magnitude M has four values, one for each speed range. Specifically,

$$P_{speed,j}(v_{30}, v_{60}) = \sum_{m=1}^{3} P_{orientation,m}\left[P_{speed,jm}(v_{60}) - P_{speed,jm}(v_{30})\right]$$

$$P_{speed,j}(v_{60}, v_{90}) = \sum_{m=1}^{3} P_{orientation,m}\left[P_{speed,jm}(v_{90}) - P_{speed,jm}(v_{60})\right]$$

$$P_{speed,j}(v_{90}, v_{120}) = \sum_{m=1}^{3} P_{orientation,m}\left[P_{speed,jm}(v_{120}) - P_{speed,jm}(v_{90})\right]$$

$$P_{speed,j}(\geq v_{120}) = \sum_{m=1}^{3} P_{orientation,m}\left[1.0 - P_{speed,jm}(v_{120})\right]$$

where v_{30}, v_{60}, v_{90}, and v_{120} have different values for each cask/surface combination, $P_{orientation,m}$ is the probability that the cask impact is an end, corner, or side impact and $P_{speed,jm}(v_{30})$, $P_{speed,jm}(v_{60})$, $P_{speed,jm}(v_{90})$, and $P_{speed,jm}(v_{120})$ are respectively the cumulative probabilities for impact orientation m and accident scenario j that the cask impact speed v is $\leq v_{30}$, $\leq v_{60}$, $\leq v_{90}$, and $\leq v_{120}$.

7.2.8.3 Accident Fire Probabilities

In Section 7.2.5.2, the internal temperature of the cask under ambient conditions T_a, the cask seal leakage temperature T_s, the rod burst rupture temperature T_b, and the average temperature of hydrocarbon fueled fires T_f were used to define three temperature ranges: $T_a \leq T_{cask} \leq T_s$, $T_s < T_{cask} < T_b$, and $T_b \leq T_{cask} \leq T_f$. Now, for fire-only accidents or collisions that initiate fires, let $P_{co\text{-}located}$ be the probability that the cask and the fire are co-located (i.e., that the cask is not significantly offset from the fire), $P_{optically\ dense}$ be the probability that the fire diameter is large enough to make the fire optically dense to loss of energy from the cask (i.e., the fire diameter is about 3 m larger than the fire diameter that just engulfs the cask), $P_{flame\ temp}$ be the probability that the flame temperature of the fire is high enough to raise the temperature of the cask internals to a temperature that falls within one of the three temperature ranges, and $P_{duration}$ be the probability that the fire burns long enough so that the cask internals actually reach a temperature in that temperature range. Finally, for collisions that initiate fires, let $P_{fire/scenario,j}$ be the conditional probability that scenario j initiates a fire.

Given these definitions

$$P_{severe\ fire,k} = P_{co\text{-}located}\, P_{optically\ dense}\, P_{flame\ temp}\, P_{duration,k} \tag{9}$$

where $P_{co\text{-}located}$, $P_{optically\ dense}$, $P_{engulfing}$, $P_{flame\ temp}$, and $P_{duration,k}$ will have different cask-specific values for each of the three temperature ranges, $T_a \leq T_{cask} \leq T_s$, $T_s < T_{cask} < T_b$, and $T_b \leq T_{cask} \leq T_f$.

7.3 Values for Release Fraction Parameters

7.3.1 Fission Product Release from Failed Rods to the Cask Interior

When a spent fuel rod is failed during a transportation accident, depressurization of the rod causes particles (fuel fines) and fission product gases, for example, noble gases and condensible vapors such as Cs atoms, gasborne at the time of rod failure, to be carried into the cask by the flow of He out of the failed rod. Release of fuel fines may be increased if fines on pellet surfaces are entrained into the depressurization flow of rod gases and might be decreased if these fines must flow through and thus be filtered by a bed of larger fines before they reach the location of the rod failure. Release of vapors may be increased if exposure of fuel pellets to the cask atmosphere upon rod failure leads to changes that increase the rate of release of fission product species from the pellets (e.g., oxidation of UO_2 or RuO_2).

7.3.2 Noble Gases

Because spent fuel rods are usually pressurized with He to about 30 atm, when a rod fails, depressurization to 1 atm causes 29/30 of the He in the rod to flow into the cask. Thus, the rod-to-cask release fraction F_{RC} for noble gases is $29/30 = 0.97 \approx 1.0$.

7.3.3 Particles

When first removed from a reactor, spent fuel rods contain particles of UO_2 called fuel fines. If during a transportation accident a spent fuel rod is subjected to large impact forces, fracturing of fuel pellets will generate additional particles of UO_2. If these impact forces or heating of the rod by a fire cause the rod to fail, the rush of rod gases over pellet surfaces during rod depressurization will cause some of the UO_2 particles to be entrained into the depressurization flow of gases which may then transport them to and through the rod failure into the cask interior. Transport of particles through the gap to the rod failure will be inefficient for particles with diameters similar to the gap width. In addition, if the large fuel fines in the gap act as a granular bed, then transport of particles with diameters smaller than the gap width may also be inefficient if these particles are efficiently captured by the bed of larger fuel fines.

Significant transport of particles from failed rods to the cask interior will occur only during rod depressurization. Once rod depressurization has occurred, deposition of particles still gasborne within the failed rod onto cladding and pellet surfaces will be much more rapid than transport by diffusion out of the rod to the cask interior, and entrainment of particles off of fuel pellet and cladding surfaces into diffusive gas flows will not occur as the velocities of diffusive flows are much to small to cause particle entrainment.

Release of particles (fuel fines) from H. B. Robinson one-foot-long spent fuel rod sections upon rod failure due to burst rupture was examined experimentally by Lorenz, et al. [7-26] during high temperature tests. Most of the particles released from the rod were found to be of sizes that deposited very rapidly onto surfaces inside of the furnace tube used to heat the test sections to burst rupture temperatures. Examination of five radioactive particles by scanning electron microscopy indicated that the particles deposited in the furnace tube were large (range of diameters, 140 to 210 μm) while the particles that escaped from the furnace tube had diameters

≤ 10 μm. Lorenz, et al. calculated release fractions for fuel fines (particles of UO_2) for release into the furnace and for escape from the furnace. Table 7.12 summarizes these experimental release fractions and shows that the fraction of respirable particles (particles with diameters ≤ 10 μm) that escaped from H. B. Robinson spent fuel rod test sections during the burst rupture tests of Lorenz, et al. was about $3.1 \times 10^{-6} = (2.4 \times 10^{-4})(0.013)$.

Table 7.12 Experimental Release Fractions for Fuel Fines

Test	Fraction UO_2 Released from the Test Section to the Furnace Tube	Fraction of UO_2 Mass Released to the Furnace Tube that Escapes from Furnace Tube
HBU-7	1.6×10^{-4}	~ 0.02
HBU-8	4.1×10^{-4}	< 0.01
HBU-9	1.8×10^{-4}	~ 0.01
HBU-10	2.2×10^{-4}	~ 0.02
Average	2.4×10^{-4}	~ 0.013

Release of particles (fuel fines) from one-foot-long sections of Turkey Point spent fuel rods upon rod failure due to burst rupture was examined experimentally by Burian, et al. [7-31, 7-32] during high temperature tests. In a typical test, the fraction of UO_2 mass released upon rod rupture was 4.2×10^{-5} and about 90 percent of this particle mass deposited onto surfaces inside of the furnace used to heat the test sections to burst rupture temperatures. The particles that constituted the remaining 10 percent of the particle mass escaped from the furnace and were collected on the stages of a bank of downstream impactors. These particles had aerodynamic diameters of 4 μm or less. Thus, the fraction of respirable particles that escaped from Turkey Point spent fuel rod test sections during the burst rupture tests of Burian, et al. was about $4.2 \times 10^{-6} = (4.2 \times 10^{-5})(0.1)$, which is quite similar to the results obtained by Lorenz, et al. and suggests the use of this value to estimate release from the one-foot portion of a real spent fuel rod that contains the rod rupture.

During collision accidents, the impact forces should lead to the production of additional fuel fines due to fracturing of fuel pellets. In 1994, DOE published a Handbook of airborne release fractions for nuclear materials [7-33]. The handbook presents the following relationship between the fraction $F_{respirable}$ of a brittle material that is converted to respirable particles upon impact onto a hard surface.

$$F_{respirable} = A\rho gh$$

where $A = 2 \times 10^{-11}$ $cm^3/g\ cm^2 sec^{-2}$ is an empirical constant determined by impact tests on glass and ceramic specimens, ρ is the material (specimen) density, g is the acceleration due to gravity, and h is the fall-height. But $mgh = 0.5m(v_{impact})^2$ where v_{impact} is the impact velocity of the specimen onto the hard surface. So $F_{respirable} = 0.5A\rho(v_{impact})^2$. Therefore, because fuel pellet densities are about 10 g/cm^3, for 30, 60, 90, and 120 mph pellet impacts onto cladding surfaces, one might expect the following fractions of the pellet mass to be converted to respirable particles, 1.8×10^{-4} at 30 mph, 7.2×10^{-4} at 60 mph, 1.6×10^{-3} at 90 mph, and 2.9×10^{-3}, at 120 mph.

The distribution of particle sizes produced by impact fracturing of depleted UO_2 pellets has been determined experimentally [7-34]. Figure 7.5 presents the experimental cumulative distribution of particle sizes. The figure shows that almost 99.99 percent of the particles produced by impact fracturing of depleted UO_2 pellets have diameters ≥ 10 µm. This data suggests that, during impact accidents, pellet fracturing would be expected to generate a bed of particles with diameters ≥ 10 µm that fills the pellet cladding gap in the spent fuel rod and any internal crack network in the fuel pellets.

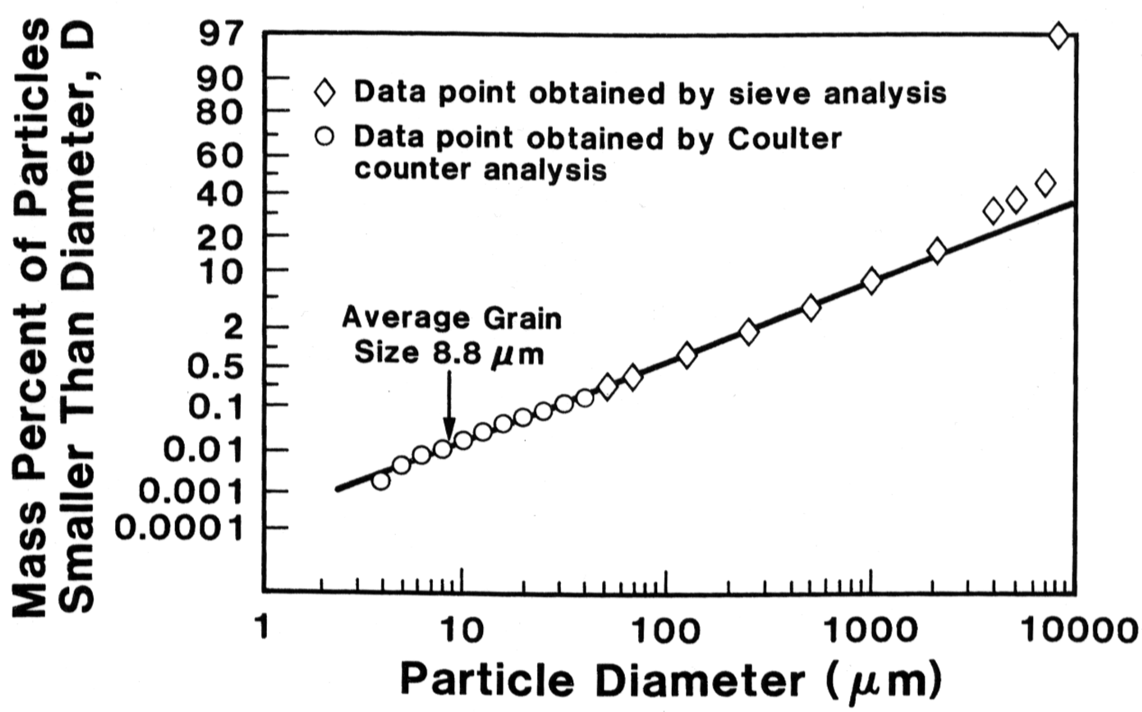

Figure 7.5 Fracture particle size distribution for depleted UO_2.

Capture of particles by a granular bed has been examined by Otani, et al. [7-35] who find that interception is the dominant removal mechanism for particles that are somewhat smaller than the average diameter of the bed particles. For such particles, Otani, et al. state that the single particle interception removal efficiency η_R is

$$\eta_R = 16R^{2-[\mathrm{Re}/(\mathrm{Re}^{1/3}+1)^3]}$$

and the total bed removal efficiency E is

$$\eta = -\frac{2}{3}\left[\frac{1-\alpha}{\alpha}\right]\frac{d_g}{L}\ln(1-E)$$

where $R = d_p/d_g$, d_p is the diameter of the particles entrained in the gases flowing through the granular bed, d_g is the diameter of the particles that comprise the granular bed; $Re = \rho_f d_g u_i/\mu$ is the Reynolds number of the gas flowing through the bed (He for spent fuel rods); $u_i = u_s/\alpha$; ρ_f, u_i, u_s, and μ are the density, interstitial velocity, superficial velocity, and dynamic viscosity of the gas flowing through the bed; α is the particle volumetric packing density, and L is the bed length.

Now, if η is equated to η_R (i.e., all removal mechanisms other than interception are neglected), then for a fixed value of E, for example 0.99, L increases as η_R decreases. Thus, use of larger values for d_g and Re will generate larger values for L. Accordingly, since the experiments of Lorenz, et al. show that the largest particles that escaped from the spent fuel rod sections upon burst rupture had diameters of about 200 μm, let d_g = 200 μm. A CONTAIN calculation described below indicates that $u_s = 6 \times 10^2$ cm s^{-1} for He flow through a one-foot section of a spent fuel rod that has a 20 μm gap and is pressurized to 18.6 atm. Because u_s should be increased by higher pressures and decreased by longer flow lengths, this value is reasonable for a full length rod pressurized to 30 atm. Thus, $u_i = 1.2 \times 10^3$ cm s^{-1}. Because a bed of 200 μm particles formed in the 20 μm pellet cladding gap must look something like a single layer of spheres, $\alpha = (4/3)\pi r^3/(2r)^3 = 0.5$. For He at 750 C, the likely burst rupture temperature for spent fuel rods pressurized to 30 atm, Re = 77 and thus $\eta_R = 16R^{1.47}$. For He at 350°C, the approximate temperature of spent fuel rods during normal transport and thus the rod depressurization temperature when failure is caused by collision impact rather than burst rupture, Re = 311 and $\eta_R = 16R^{1.34}$.

Now, let the bed efficiency E = 0.99, whereupon $L = 6.14 \times 10^{-2}/\eta_R$. Table 7.13 presents, for several particle diameters d_p of interest, values of η_R and L for a single layer bed of 200 μm particles with He Reynolds numbers of Re = 77 or 311. The table shows that this bed will remove particles with diameters ≥ 1 μm with an efficiency of 0.99. Thus, respirable fines with diameters of 1 to 10 μm should also be removed with similar efficiencies from the depressurization flow of He through the gap of a full length spent fuel rod that occurs when the rod fails due to impact loads or thermal burst rupture.

Table 7.13 Granular Bed Lengths that Provide 99 Percent Filtering Efficiencies

	Re = 77		**Re = 310**	
d_p(μm)	η_R	**L(cm)**	η_R	**L(cm)**
30	1.00	0.06	1.00	0.06
10	0.20	0.31	0.29	0.21
1	6.6×10^{-3}	9.3	1.3×10^{-2}	4.7
0.1	8.4×10^{-5}	728	6.0×10^{-4}	102

Table 7.13 indicates that beds with lengths of 0.06, 0.31, and 9.26 cm would be expected to provide 99 percent filtering efficiency respectively for particles with diameters ≥ 30, ≥ 10, and ≥ 1 μm. Thus, it seems reasonable to conclude that only about one percent of the respirable fuel fines in a spent fuel rod will be able to be transported by depressurization gas flows through a rod gap filled with fuel fines with diameters of order 50 to 200 μm.

Based on the preceding discussion, a rod not subject to impact (no particle production by fracturing of UO_2) might be expected to generate during depressurization a plug (bed) of fuel fines in the rod gap that would cause fines not in the one-foot section of the rod that contains the rod rupture to be filtered while the fines in the one-foot section would escape with negligible diminution due to filtering. Therefore, a reasonable estimate for F_{RC}, the rod to cask release fraction for respirable fuel fines (particulates), for a rod not subjected to impact (no particle production by fracturing of UO_2) is

$$F_{RC} = \left(4.2\times10^{-6}\right)\left[\frac{1}{12}+\frac{11}{12}(0.01)\right] = 3.9\times10^{-7}$$

and because an 0.3 cm long bed of 200 μ particles will capture 99 percent of the respirable fuel fines that enter the bed, reasonable estimates for rods subject to impact fracturing are

$$F_{RC} = \left(4.2\times10^{-6}+2.9\times10^{-3}\right)\left[\frac{0.25}{144}+\frac{143.75}{144}(0.01)\right] = 3.4\times10^{-5} \quad \text{for 120 mph impacts,}$$

$$F_{RC} = \left(4.2\times10^{-6}+1.6\times10^{-3}\right)\left[\frac{0.25}{144}+\frac{143.75}{144}(0.01)\right] = 1.9\times10^{-5} \quad \text{for 90 mph impacts,}$$

$$F_{RC} = \left(4.2\times10^{-6}+7.2\times10^{-4}\right)\left[\frac{0.25}{144}+\frac{143.75}{144}(0.01)\right] = 8.5\times10^{-6} \quad \text{for 60 mph impacts,}$$

$$F_{RC} = \left(4.2\times10^{-6}+1.8\times10^{-4}\right)\left[\frac{0.25}{144}+\frac{143.75}{144}(0.01)\right] = 2.2\times10^{-6} \quad \text{for 30 mph impacts,}$$

where the first term in the brackets in these expressions represents particle release from the 0.25 inch (0.25 inch = 2 x 0.3 cm) portion of the rod that contains the rupture and the second term represents particle release from the other 143.75 inches of the rod, 0.01 represents the fraction of respirable fines that will pass through a plug or a bed of larger fuel fines, the release fraction value of 4.2×10^{-6} reflects the experimental release fractions for respirable fuel fines measured for the one-foot-long experimental test sections of Lorenz, et al. [7-26] and Burian, et al. [7-31], and 2.9×10^{-3}, 1.6×10^{-3}, 7.2×10^{-4}, and 1.8×10^{-4} are estimates of the fractions of UO_2 mass in fuel pellets converted to respirable fuel fines by impact fracturing as a result of 120, 90, 60, and 30 mph impacts. Finally, given the precision of this analysis, use of values of 4×10^{-7} and 3×10^{-5} respectively for F_{RC} for release of particles during non-impact and impact accidents seems appropriate.

7.3.4 Cesium

The amount of a condensible vapor (e.g., Cs atoms) carried from a failed rod to the cask interior should be determined by the free volume of the rod (the sum of the rod plenum volumes, the cladding gap volume, and the volume of the internal network of cracks in the fuel pellets contained in the rod) and by the partial pressure of the condensible vapor at the rod temperature at the time of rod failure. If rod depressurization leads to the adiabatic expansion of rod gases, significant cooling of those gases and of the cladding and pellet surfaces that they contact could take place. If this happens and if the condensible vapors in the rod helium encounter a cooled surface before they are carried out of the rod into the cask, significant condensation onto fuel pellet and rod internal cladding surfaces may take place which would significantly decrease the amounts of condensible vapors released to the cask. Thus, one might expect release fractions for condensible vapors to reflect the partial pressure of the vapor at either the burst rupture temperature of the rod or the temperature of pellet and/or cladding surfaces that have been substantially cooled by adiabatic expansion of gases during rod depressurization.

After a failed rod has depressurized, if the cask and rods are heated by a fire to elevated temperatures, fission products volatile at fire temperatures may vaporize from pellet surfaces and then diffuse out of the rod into the cask interior. Thus, condensible vapors could be released both by transport in rod depressurization gas flows and, after rod depressurization, by diffusion from the rod free volume through the rod failure into the cask.

7.3.4.1 Cs Release Fractions for Burst Rupture and Diffusion

Lorenz, et al. examined release of Cs from heated sections of simulated [7-36] and real [7-26] spent fuel rods by diffusion and during depressurization following rod failure due to burst rupture. By fitting their experimental results, Lorenz, et al. developed empirical models for the release of volatile fission products due to burst rupture of pressurized spent fuel rods and diffusion subsequent to burst rupture [7-37, 7-38]. For burst rupture, the following model applies,

$$F_{burst} = \frac{M_{burst}}{M_{inventory}} = \alpha V_{burst} M_{inventory}^{-0.2} \left(\frac{F_{gap}}{A_{clad}} \right)^{0.8} \exp\left[-\left(C/T \right) \right] \qquad (10)$$

where M_{burst} is the mass (g) of the volatile fission product released due to rupture of the fuel rod while pressurized, $M_{inventory}$ is the mass (g) of the total inventory of the fission product in the rod, V_{burst} is the volume (cm^3) of rod gases released from the rod due to rod rupture calculated at 0°C and system pressure (0.3 MPa in the experiments of Lorenz, et al.), F_{gap} is the fraction of the total inventory of the fission product that was in the fuel-clad gap at the time the rod ruptured, A_{clad} is the area (cm^2) of the clad with which the fission products in the fuel-clad gap are associated (the surface area of the active length of the fuel rod), T is the temperature (K) of the gap gases at the time of rod rupture, and α and C are adjustable constants determined experimentally for each fission product.

For release by diffusion after rod failure, the following model applies,

$$F_{diffusion} = \frac{M_{diffusion}}{M_{inventory}} = F_{gap}\left\{1 - \exp[-R_o t / F_{gap} M_{inventory}]\right\}$$

(11)

$$R_o = \delta(W/P)\left(F_{gap} M_{inventory} / A_{clad}\right)^{0.8} \exp[-(\gamma/T)]$$

where R_0 is the initial rate of diffusive release (g/hr), T is the diffusion temperature (K), t is the time at the diffusion temperature (hr), W is the width of the fuel-cladding gap (μm), P is the system pressure (MPa), and δ and γ are adjustable constants determined experimentally for each fission product.

Table 7.14 presents the values determined experimentally for Cs by Lorenz, et al. for the adjustable constants in Equations 10 and 11.

Table 7.14 Parameter Values for Lorenz Release Expressions for Cs

Parameter	Cesium
α $(g/cm^3)(g/cm^2)^{-0.8}$	3.49
C K^{-1}	7420
δ (g MPa/μm hr)$(g/cm^2)^{-0.8}$	1.90×10^3
γ K^{-1}	1.98×10^4

7.3.4.2 Relative Importance of Cs Release by Burst Rupture and Diffusion

Table 7.15 presents release fractions for Cs from spent fuel for several temperatures of interest for release due to burst rupture and for 24 hours of release by diffusion. These release fractions were calculated by Sanders et al. [7-39] using Equations 10 and 11 and the values of the adjustable constants presented in Table 7.14.

Table shows (1) that, relative to burst release, release by diffusion is not significant at or below 600°C and (2) that, during a long duration (24 hours) engulfing hydrocarbon fuel fire, diffusion increases total release by a factor of about three over release by burst rupture:

$$(\text{burst rupture} + \text{diffusion})/(\text{burst rupture}) = (5.7 \times 10^{-4} + 9.8 \times 10^{-4})/(5.7 \times 10^{-4}) = 2.7$$

The thermal analyses presented in Section 6 showed that it takes about six hours for an engulfing hydrocarbon fire to heat a spent fuel cask to the average temperature of the fire (1000°C) and the fire statistics presented in Section 7.4.4.1 show that hydrocarbon fires with durations of 6 hours or more are quite rare. Therefore, only a highly improbable fire will be able to heat a cask to average hydrocarbon fire temperatures for more than a few hours. Now, because the exponent in Equation 11 is small, diffusive release for 2 hours at 1000°C will be about 1/12 of the diffusive release produced by 24 hours at 1000°C. Therefore, the diffusive release fraction for a 6-hour fire during which the cask is at 1000°C for 2 hours will be about 0.8×10^{-4} or about 1/7 of the burst rupture release fraction. So for almost all fires, diffusive release will not be important compared to burst release. Consequently, release of Cs by diffusion is neglected.

Table 7.15 Comparison of Cs Release Fractions for Rod Burst Rupture and Diffusive Release

Temperature		Release Fraction	
Value (C)	Condition	Burst Rupture	Diffusion (for 24 hours)
300	Normal Transport	4.6×10^{-7}	1.3×10^{-11}
530	Regulatory Maximum	1.9×10^{-5}	1.7×10^{-7}
600		3.9×10^{-5}	1.1×10^{-6}
800	Regulatory Fire	1.9×10^{-4}	6.4×10^{-5}
1000	Hydrocarbon Fuel Fire	5.7×10^{-4}	9.8×10^{-4}

7.3.4.3 Rod Cooling During Burst Rupture

The influence of adiabatic expansion of rod gases during rod depressurization on the temperature of those gases was examined by performing CONTAIN code [7-40] calculations that modeled the temperatures of the rod gases during depressurization upon burst rupture of the HBU-7 spent fuel test section examined by Lorenz, et al. [7-41]. The analysis focused on the thermal-hydraulic conditions of the helium fill gas in the test section during the blowdown from the initial test section pressure, after rod failure caused by induction heating.

7.3.4.3.1 HBU-7 Test Section Model

The six-cell model used to represent the HBU-7 rod test section during these calculations is depicted in Figure 7.6. Table 7.16 presents the identities, volumes, and initial conditions of these six cells just prior to rod failure. As Figure 7.6 and Table 7.16 show, the helium reservoir attached to the 30.48-cm-long HBU-7 test segment was modeled by one cell, the rod test segment by four cells, and the bulge formed in the test segment cladding just prior to segment failure by one cell. Upon failure of the bulge by burst rupture, gases in the test section were vented through the failure to the environment, which was thus in effect a seventh cell. Three of the six cells described in Figure 7.6 and Table 7.16, Cells 3, 4, and 5, represent those sections of the rod test section that were directly heated by induction during the burst rupture experiment. Because they were not directly heated, the temperatures in Cells 1, 2, and 6 were much lower than the temperatures in Cells 3, 4, and 5. The volumes assigned in Table 7.16 to the cells include an estimate of the effects of clad swelling, as described in Reference 1. The volumes are several times larger than the volumes implied by the hydraulic diameter, $D_H = 43.2$ μm, of the annular gap in the rod test segment, a value that was deduced from the steady-state rod blowdown measurements [7-42].

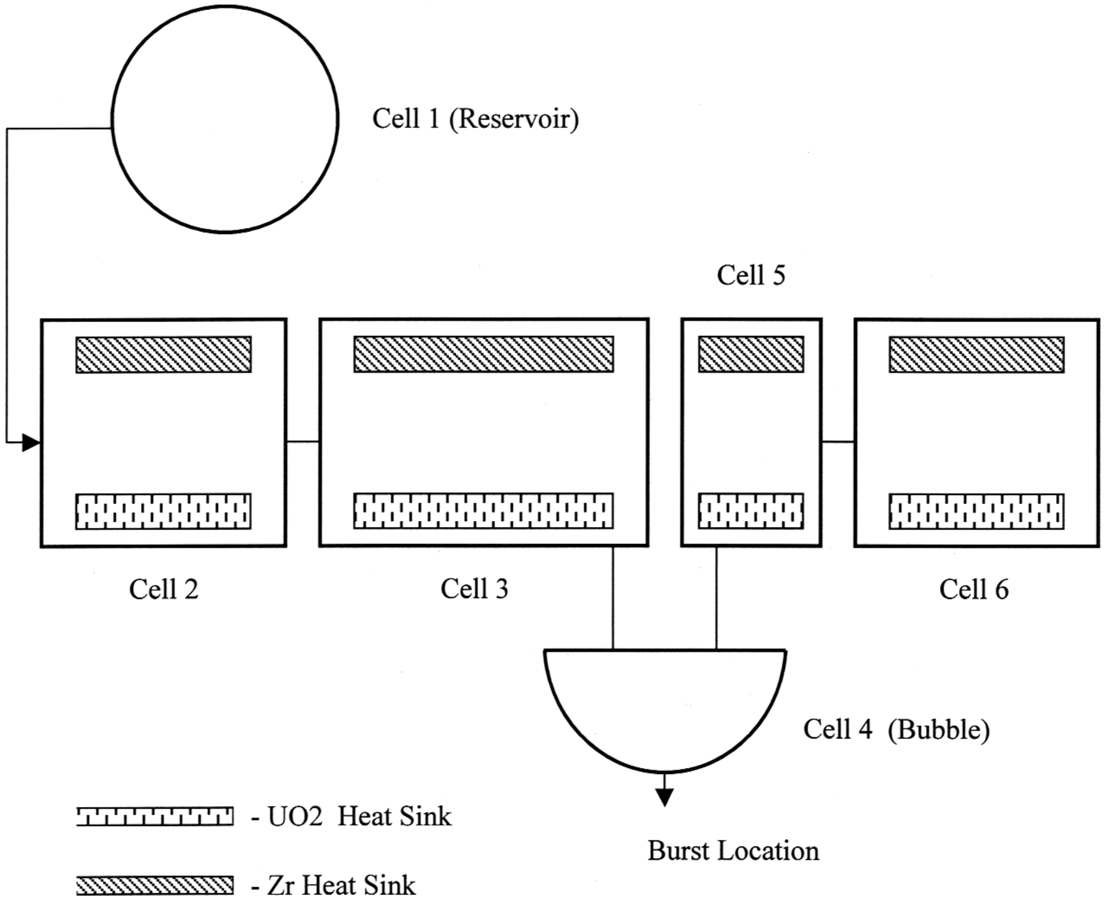

Figure 7.6 Schematic of the CONTAIN Model for the HBU-7 rod blowdown test.

Table 7.16 Initial Conditions and Volumes for the CONTAIN Model Cells

		Test Section Cells				
Cell Name	**Reservoir**	**Left End**	**Left Middle**	**Bulge**	**Right Middle**	**Right End**
Cell No.	1	2	3	4	5	6
Rod Length in Cell (cm)	0	8	12	2*	4	6.48
Initial Pressure (bars)	18.66	18.66	18.66	18.66	18.66	18.66
Initial Temperature (K)	303	742	1181	1181	1181	742
Cell Volume (cm^3)	4.33	0.44	0.45	1.9	0.15	0.36

*Heat sinks were not modeled in the bulge.

As indicated in Figure 7.16, Zr and UO_2 heat sinks were modeled in Cells 2, 3, 5, and 6. Each of the Zr and UO_2 sinks in a cell were assumed to have an effective heat transfer area πDL, where D is the fuel pellet diameter (0.932 cm), and L is the length of the rod section represented by the cell. These heat sinks are expected to be important during the blowdown of the test segment, because they tend to offset the cooling effects caused by gas expansion. Note that the heat transfer areas of the UO_2 heat sinks were calculated assuming that the gas in the rod test section is confined to the rod's annular gap. Because this assumption neglects the surface area of any internal crack network in the fuel pellets, the UO_2 heat sink areas are minimums.

The time constant t_h for heating of gas within the annular gap can be estimated by

$$t_h = \frac{C_p \rho D_H{}^2}{4 \mathrm{Nu}\, k}$$

where C_p is the specific heat of the gas, ρ is the gas density, k is the gas conductivity, and Nu is the heat transfer Nusselt number. Here, Nu is taken to be Nu = 8.32, the Nusselt number appropriate for fully developed laminar flow in an annular gap [7-43]. This value corresponds to the case with equal heat flux from the inner and outer walls into the gap. As discussed below, an order of magnitude result, not a precise value, is of interest here. For this Nusselt number, the above equation gives very small values for the time constant, e.g., $t_h = 5.5 \times 10^{-7}$ s at 1180°K. This value for t_h implies nearly instantaneous equilibration between the heat sinks and the gas passing through the annular gap. However, it also indicates that the timesteps required for stability in the CONTAIN calculation would be much less than the code was designed for. Therefore in the CONTAIN results discussed below, Nu was taken to be 1,000 times smaller (Nu = 0.00832), a value that allows reasonable calculation times but still demonstrates the isothermal nature of the blowdown at late time.

Along with the heating time constant, the time constant t_m for equilibration of volatile fission product concentrations in the gap is also needed. From the heat and mass transfer analogy [7-44], this time constant is given by

$$t_m = \frac{D_H{}^2}{4 \mathrm{Nu}\, D_f}$$

where D_f is the diffusivity of the fission product in helium. One can estimate this time constant from kinetic theory. For I_2, for example, at 1180°K and a total pressure of 20 atm, one obtains $t_m = 2.9 \times 10^{-6}$ s, which is also a very short time.

In the CONTAIN calculation, flow between cells was assumed to be governed by a combination of laminar and turbulent losses of the form

$$\Delta P = K \upsilon W + C_{FC} \frac{W^2}{\rho A^2}$$

where ν is the gas kinematic viscosity, K is the laminar loss coefficient (m^{-3}), W is the mass flow rate, C_{FC} is the CONTAIN turbulent loss coefficient, and A is the flow area. To determine K, the effective hydraulic diameter D_H for the annular gap was used. From the standard expression for laminar flow, this corresponds to a coefficient K equal to 4.07×10^{16} L, where L is in meters. In the CONTAIN model, the laminar loss along the rod was allocated to the flow junctions so that one-half of the laminar loss within a cell was assigned to each junction involving that cell. The flow junction characteristics are summarized in Table 7.17.

Table 7.17 Flow Junction Characteristics in the CONTAIN Model

Junction	Cells 1-2	Cells 2-3	Cells 3-4	Cells 4-5	Cells 5-6	Cells 4-7
Flow Area (cm^2)	0.0198	0.00632	0.00632	0.00632	0.00632	0.02
K (m^{-3})	1.63 $\times 10^{15}$	4.07×10^{15}	2.44×10^{15}	8.14×10^{14}	2.13×10^{15}	0
C_{FC}	1.35	0	0	0	0	1.35

7.3.4.3.2 CONTAIN Calculation Results

Figures 7.7 and 7.8 present the CONTAIN predictions for the HBU-7 rod burst rupture test. Figure 7.7 gives the pressures in the cells along the principal blowdown path, starting with Cell 1 (the reservoir) and ending with the bulge region (Cell 4) where the rod failure occurred. This figure indicates that the bulge region depressurizes on a very short time scale. The reservoir, on the other hand, blows down on a much longer time scale. There is reasonable agreement between the measured depressurization rate and the CONTAIN prediction. Note that somewhat higher experimental depressurization rate may be the result of clad swelling effects, which would lead to a larger D_H than was deduced from the steady-state experiments. Figure 7.8 indicates that gas initially in the bulge cools rapidly due to adiabatic expansions. However, as gas from the rest of the system refills the bulge, there is a rapid temperature rise, and after the initial transient, the blowdown is essentially isothermal. The gas velocity in the flow junction between Cells 3 and 4, based on the gap flow area from the steady-state experiments, is also shown in Figure 7.8. The indicated velocities are consistent with an isothermal process, given the time constant for gas equilibration in the annular gap as discussed above.

Since the temperature behavior shown in Figure 7.8 corresponds to a Nusselt number that is three orders of magnitude smaller than it should be, there is ample margin to accommodate factors such as clad swelling that were ignored in this analysis. The discrepancy between the measured and calculated depressurization rates indicates that clad swelling could have been important. Because the laminar loss coefficient (which depends on D_H to the third power) is somewhat more sensitive to D_H than the time constant for equilibration (which depends on D_H squared), one can conclude that the effect on gap heat transfer would be at most comparable to that in the depressurization rate. The clad swelling would therefore not be large enough to change the essentially isothermal nature of the blowdown at late time.

These results suggest that the work done expanding the gases in the plenum region of the rod causes the gases in the plenum region to cool significantly. However, during transport of plenum gases through the gap region of the rod to the burst rupture location, heat transfer from cladding and fuel pellets to the gases flowing through the gap region heats these gases back to the temperatures near to the rod burst rupture temperature. Therefore, since the characteristic time

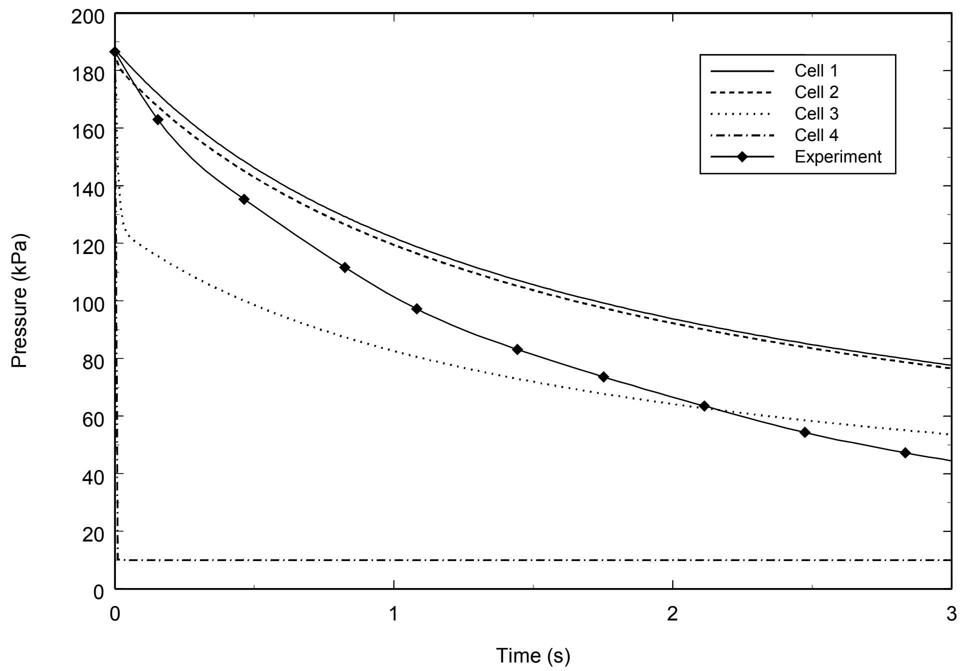

Figure 7.7 CONTAIN predictions for the pressures in the HBU-7 experiment.

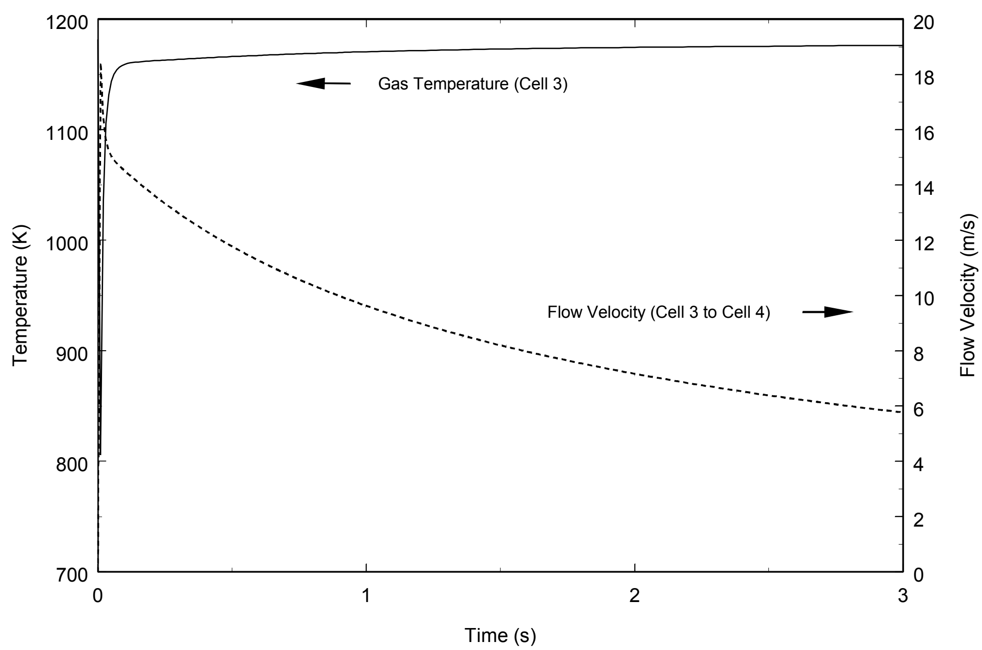

Figure 7.8 CONTAIN predictions for the temperature in Cell 3 and the flow velocity from Cell 3 to Cell 4.

for heat transfer to these gases during flow through the gap region is significantly shorter than the time required to flow through the gap region, when these gases reach the burst rupture location, they will again be saturated with Cs vapor species at the burst rupture temperature of the rod.

7.3.4.4 Burst Rupture Release Expressions for Vapors that Contain Cs

Release of a vapors that contain Cs from a failed spent fuel rod, when depressurization does not lead to significant cooling of the gases escaping from the rupture, should be determined by the vapor pressure of the Cs containing vapor at the temperature (T_b) of the rod at the time burst rupture occurs. For this case, the mass of elemental Cs released (M_R) is given by combining an experimental or theoretical expression for the vapor pressure of the Cs species (Log P = −a/T+b) with the ideal gas equation (PV = nRT) to obtain the following expression:

$$M_R = n_R MW = MW \frac{PV}{RT_b} = MW \frac{V_{rod}}{RT_b} 10^{-a/T_b + b} \tag{12}$$

where n_R is the moles of Cs vapors released, MW is the molecular weight of Cs (133 g mole^{-1}), P is the saturation vapor pressure of the Cs vapor at the rod burst rupture temperature T_b, V_{rod} is the free volume of the spent fuel rod, and R is the gas constant.

7.3.4.4.1 Cs Vapor Species

Condensible Cs vapors likely to exist in the free volume of a spent fuel rod (or rod section) at burst rupture temperatures were identified using the VICTORIA equilibrium thermodynamics code [7-45], which models chemical equilibrium between 288 chemical species. Of these 288 species, 27 were active during these VICTORIA calculations.

The initial molar abundances for active species were taken from the output of the ORIGEN calculation described in Section 7.2.3.2. In addition, all of the calculations assumed that:

- The spent fuel rod (or rod section) is moisture free.

  This assumption is consistent with manufacturing specifications which limit moisture in fuel pellets to 1 ppm by mass and moisture in rod gases to 115 ppm by volume[1].

- All cesium and iodine had migrated to the surfaces of the fuel pellets.

  This is a conservative assumption, because only a few percent of the cesium and iodine in a fuel pellet would be present on or would migrate to the surface of the pellet under transportation accident conditions. Moreover, the calculation of equilibrium is insensitive to the abundances of species on fuel surfaces as long as there are sufficient amounts of the equilibrating species to establish an equilibrium between species that exist in both the condensed and vapor phases.

1. Personal Communication, J. Clauss, 1998.

- All iodine is initially present as cesium iodide (CsI).
- Excess cesium not initially present as CsI is initially present as Cs_2UO_4.
- CsI and Cs_2UO_4 form an ideal solution.
- The gas phase (free volume of the rod) is initially pure helium.

Figure 7.9 shows the variation with temperature of the concentrations of Cs vapor species predicted by the VICTORIA code to exist in the rod free volume. The figure shows that the important cesium species are predicted to be Cs_2I_2, CsI, Cs, and Cs_2O. The figure also shows that at 750°C (1023°K), the likely burst rupture temperature of intact spent fuel rods, CsI(g) is the dominant Cs vapor.

Finally, to test the importance of the assumptions that the rod was dry and that Cs not initially present CsI is present as Cs_2UO_4, calculations were performed with $Cs_2U_2O_7$ as the initial dominant cesium species and with about 0.01 mole-percent steam in the gas phase. The net effect of these changes was to reduce the vapor pressures of Cs species.

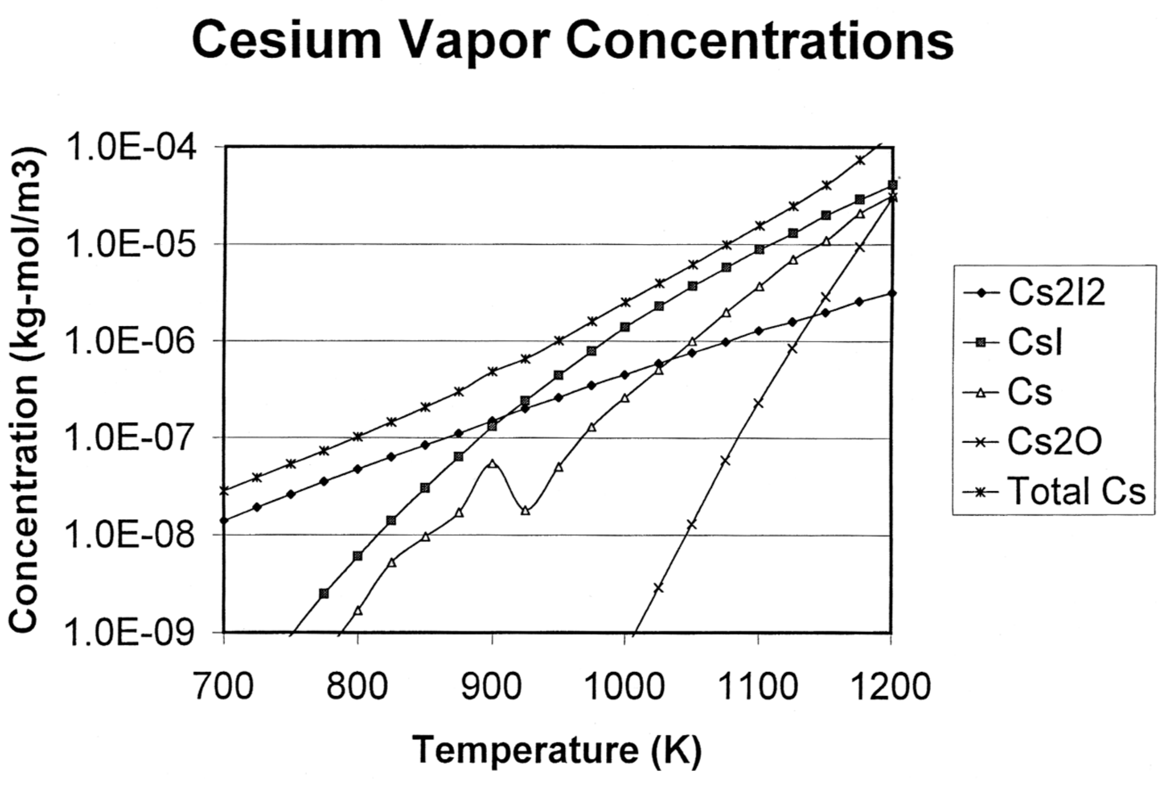

Figure 7.9 Variation with temperature of the concentrations of Cs vapor species predicted by the VICTORIA code.

7.3.4.4.2 Exponential Terms in Release Expressions

Because

$$F_{gap} M_{inventory} = M_{gap}$$

where M_{gap} is the mass of a radionuclide, for example Cs, on surfaces in the gap of the spent fuel rod or rod test section, Equation 10 can be rearranged to yield

$$M_{burst} = \alpha V_{burst} \left(\frac{M_{gap}}{A_{clad}} \right)^{0.8} \exp\left[-\left(C/T \right) \right] \tag{13}$$

The experiments of Lorenz, et al. yielded a value of 7240 K^{-1} for C. Now, if the exponential term in this equation expresses the dependence of Cs vapors on temperature, then one might expect that C/2.303 = 7240/2.303 = 3144 K^{-1} to be similar in magnitude to the value of a for CsI(g) in Equation 12. But for CsI(g), a = 7960 K^{-1}. Thus, the value of C determined by Lorenz, et al. does not seem to be consistent with release of Cs principally as CsI(g). However, as the following derivation shows, the Lorenz value of C is quite consistent with the release of vapor forms of Cs that are comprised principally of CsI(g), provided release of Cs in particles is also considered.

As was stated above, Cs should be released both as a constituent of Cs containing vapors and also as a constituent of fuel fines blown out of the failed rod or rod section upon burst rupture. If Equation 13 is equated to the sum of a vapor release term and a particle release term, then the following equation results

$$\alpha V_{burst} \left(\frac{M_{gap}}{A_{clad}} \right)^{0.8} \exp\left[-\left(C/T_b \right) \right] = MW \frac{V_{rod}}{RT_b} 10^{-a/T_b + b} + M_{inventory} F_{particles} \tag{14}$$

where $F_{particles}$ is the fraction of the mass of the fuel pellets in the rod or rod section that is released as fuel fines. But for the 900°C burst rupture tests conducted by Lorenz, et al. using sections of spent fuel rods, α = 3.49, V_{burst} = 97 cm^3, $V_{rod} = V_{test\,section}$ = 2.5 cm^3, M_{gap}/A_{clad} = 12.4 x 10^{-6} g, T_b = 1173°K, $M_{inventory}$ = 0.456 g Cs, and $F_{particles}$ = 2.4 x 10^{-4}; and for Cs, MW = 133 g, and, when P is expressed in MPa, R = 8.2 cm^3 MPa K^{-1} $mole^{-1}$, a = 7960 K^{-1}, and b = 4.18. Substitution of these values into Equation 14 followed by solving for C now yields a value of 6250 K^{-1} for C, which agrees quite well with the value determined experimentally by Lorenz, et al., which suggests that Cs release at temperatures like those examined by Lorenz, et al. (700 to 900°C) can be treated as the sum of a term for release of vapors that contain Cs, principally CsI(g), and a term for release of fuel fines that contain Cs atoms. Accordingly, division of the right hand side of Equation 14 by $M_{inventory}$ yields a phenomenologically reasonable expression for the rod-to-cask release fraction for Cs that is consistent with the experimental results of Lorenz, et al. Therefore, for Cs

$$F_{RC} = \frac{MW}{M_{inventory}} \frac{V_{rod}}{RT_b} 10^{-a/T_b+b} + F_{particles} \tag{15}$$

A maximum value for F_{RC} for Cs can be calculated by substituting values of a and b for CsI(g) into this expression and using the values for $F_{particles}$ calculated above for impact and non-impact events. Accordingly, because MW_{Cs} = 133 g mole^{-1}, V_{rod} = 30 cm^3, $M_{Cs,rod}$ = 8.0 g, T_b = 1023°K, $F_{particles} = 4 \times 10^{-7}$ and 3×10^{-5} respectively, for non-impact and impact events, and for CsI(g) a = 7960 K^{-1} and b = 4.18 when P is in MPa, $F_{RC} = 1.5 \times 10^{-5} + 4 \times 10^{-7} = 1.5 \times 10^{-5}$ for fire-only events and $1.5 \times 10^{-5} + 3 \times 10^{-5} = 4.5 \times 10^{-5}$ for impact events that initiate fires. As a check, if the CONTAIN result for the molar concentration of Cs in Cs vapors (e.g., CsI, Cs, Cs_2O, and Cs_2I_2) in the free volume of a PWR fuel rod at T = 1025°K is used to calculate F_{RC}, then for non-impact and impact events, respectively, $F_{RC} = 1.3 \times 10^{-5}$ and 4.3×10^{-5}. Therefore, to be slightly conservative, use of $F_{RC} = 2 \times 10^{-5}$ for fire-only events and 5×10^{-5} for impact events that initiate hot, engulfing, optically dense, long-duration fires seems appropriate. Finally, to ensure that these release fractions for cesium vapors are somewhat conservative, for fire scenarios that heat the cask to rod burst rupture temperatures, no credit is taken for deposition of cesium vapors onto cool cask surfaces (say at the ends of the cask), and for collision scenarios that initiate fires, revaporization of cesium from particles that deposited onto cask interior surfaces following release to the cask due to impact failure of rods is modeled whenever cask internal temperatures equal or exceed rod burst rupture temperatures.

7.3.5 Release Following Fuel Oxidation

Lorenz, et al. found [7-46] that the diffusive release of Cs, I, and Ru at 700°C was increased respectively by factors of 54.6, 22.4, and 2.02×10^4 during tests that lasted 5 hours, when the experimental atmosphere was dry air (test HBU-6) rather than steam (test HBU-1). Increased release of Cs and I was attributed to the substantial increase in UO_2 surface area that accompanies the oxidation of UO_2 to UO_{2+x} when UO_2 is exposed to air while at elevated temperatures. Increased release of Ru was attributed to the oxidation of non-volatile asymmetric RuO_2 to volatile symmetric RuO_4.

Assume that release of Cs and Ru from the test segment is complete (release fraction = 1.0) for that region of the test segment that is subject to extensive fuel oxidation. Let $F_{diffusion}$ be the release fraction per hour for Cs or Ru caused by diffusive release in a steam atmosphere, $F_{oxidized}$ be the release fraction per hour for Cs or Ru caused by extensive oxidation of a portion of the test segment, and $R_{air/steam}$ be the ratio of the total release fraction from the test segment per hour in air to that in steam. Then,

$$\frac{F_{oxidized} + F_{diffusion}}{F_{diffusion}} = \frac{F_{oxidized}}{F_{diffusion}} + 1 = R_{air/steam} \tag{16}$$

The diffusive release fractions for Cs and Ru in steam were found by Lorenz, et al. [7-47] to have the following experimental values for test HBU-1: 2.62×10^{-7} for Cs and 3.6×10^{-10} for Ru. Substitution of values for $F_{diffusion}$ and $R_{air/steam}$ into Equation 16 allows the following values to be calculated for $F_{oxidized}$: 1.40×10^{-5} for Cs and 7.27×10^{-6} for Ru. Now, given the precision of the experimental data, these two values are essentially the same, which suggests that the enhanced release of Cs and Ru does occur from the same volume, the volume of the fuel which is extensively oxidized as a result of the exposure to air while at elevated temperatures, and that release of volatile species from this small volume of fuel that becomes extensively oxidized is essentially complete. Now, because $F_{oxidized}$ is referenced to the total volume of the test segment (V_T) rather than to the portion of the test segment that is extensively oxidized due to exposure to air while at elevated temperatures ($V_{oxidized}$),

$$F_{oxidized} V_T = 1.0\, V_{oxidized} \quad (17)$$

Because the test segment has a length of 12 inches and the fuel pellets that occupy that length have a diameter of 9.32 mm, the total volume of the test segment (V_T) is 2.08×10^4 mm^3. Therefore, use of the larger value for $F_{oxidized}$, the value for Cs, yields $V_{oxidized} = 0.29$ mm^3. Now, assume that the enhanced release of Cs and Ru occurs from a disc of oxidized fuel that lies just under the hole predrilled in the cladding of the test segment used in test HBU-6, the test that measured diffusive release in air at 700°C through a predrilled hole with a diameter of 1.6 mm. Thus, if the diameter of the disc is $2d_{oxidized} + d_{hole}$, then

$$V_{oxidized} = \pi\left[\left(2d_{oxidized} + d_{hole}\right)/2\right]^2 d_{oxidized} \quad (18)$$

whereupon substitution of 1.6 mm for d_{hole} and 0.29 mm^3 for $V_{oxidized}$ gives $d_{oxidized} = 0.11$ mm and $d_{oxidized} + d_{hole} = d_{disc} = 1.71$ mm. Since the rate of weight gain by UO_2 powder, when oxidized by exposure to low partial pressures of oxygen ($p_{O_2} = 1\,\mathrm{mm}$) at 500 or 1000°C, is 0.3 mg min^{-1} [7-48], oxidation of the amount of UO_2 in a disc of sintered UO_2 powder having a diameter of 1.61 mm and thickness of 0.11 mm should occur in less than a minute, provided that diffusion of oxygen into the surface layer of a sintered UO_2 pellet isn't extremely slow. Accordingly, oxidation of a disc of sintered UO_2 with dimensions similar to those considered here, and also of all of the Ru in that disc, seems quite reasonable if the disc is exposed to oxygen for several hours while at elevated temperatures (500 to 1000°C).

Fuel pellet surfaces can be exposed to an oxidizing agent (oxygen or carbon dioxide) while at elevated temperatures only during accidents that involve fires. For Category 5 and Fire-only accidents, air can enter the cask through the single cask leakage path only after the fire dies out and cask cooling causes air to flow into the cask. Because cooling will cause any fission product vapors (e.g., CsI or RuO_4) to condense onto cask interior surfaces before they can diffuse out of the cask to the atmosphere, oxidation of fuel during accidents that fall into either of these fire accident categories is not of concern. However, fuel oxidation during Category 6 accidents is of concern because these accidents by definition lead to double failures of the cask. Because of the double failure, differential heating of the cask could induce a buoyant flow of gases through the cask. While the fire is burning, the gases flowing through the cask would be combustion gases, which should contain little molecular oxygen. After the fire dies out, the gas flow would be air. Because fuel cladding is a getter and UO_2 is more easily oxidized the RuO_2, oxidation of Ru and RuO_2 to RuO_4 will not be significant until all of the cladding and all of the UO_2 near the burst rupture hole in the cladding has been oxidized. Nevertheless, because hydrocarbon fuel fires with durations of several hours may occur, if the collision that initiates these fires also causes a double failure of the cask, then any sizeable buoyancy driven flow of combustion gases or air through the cask would be expected to significantly oxidize exposed spent fuel surfaces, which would substantially increase the release of fission products from these oxidized fuel regions. Finally, if combustion gases or air is flowing through the cask, any fission products released to the cask interior would be transported to the environment by the gases that are flowing through the cask with little deposition onto cask interior surfaces.

By definition, Category 6 accidents fail all of the rods in the cask. The finite element cask impact calculations described in Section 5.1.4 show (see Figure 5.6) that severe impacts onto hard surfaces cause substantial slumping of the materials carried in the cask, that is, slumping of the fuel baskets and the rods they contain. Severe slumping means that most of the rods in the cask will be subjected to significant bending. Rod failure mechanisms due to rod bending have been discussed by Sanders, et al., who identified three failure modes, transverse tearing, longitudinal tearing, and rod breakage [7-49]. Assume that tearing of clad produces a crack with a width (w_{crack}) of 1 mm and a length equal to half the circumference of the rod. Then, since typical PWR and BWR rods have inside diameters respectively of about 0.9 and 1.2 cm [7-50], typical cladding tears will expose about 15 mm^2 of pellet surface area to the cask atmosphere, where 15 mm^2 = $\pi d_{pellet} w_{crack}/2 = \pi(10\text{ mm})(1\text{ mm})/2$. By comparison, a full rod break will expose at least the ends of two fuel pellets to the cask atmosphere (more if pellets spill from the broken rod) and thus at least 160 mm^2 = $2\pi(d_{pellet}/2)^2$ of pellet surface area. So, rod breakage will expose much more pellet surface area to the cask atmosphere than will be exposed by a single cladding tear.

In typical spent fuel baskets, the PWR and BWR rods carried in the baskets are supported by six or seven spacers. Thus, the rods will have seven or eight regions between spacers that might undergo bending during a severe accident. Since all of the unsupported portions of a single rod will not undergo the same amount of bending and different rods will be bent in different ways, most rods will fail by cracking or tearing, usually at a single location, some rods may fail by cracking or tearing at more than one location, and a few rods may experience full circumferential breaks. Here, it is assumed that the average set of failures per rod exposes an amount of pellet surface equal to three times the cross-sectional area of a fuel pellet, which is equivalent to assuming that each rod suffers three full rod breaks. But Equation 17 shows that $F_{oxidized} = V_{oxidized}/V_T$. So if rod failure exposes on average an amount of pellet surface equal to six pellet ends, then $V_{oxidized} = 6\pi(d_{pellet}/2)^2 d_{oxidized}$ and $V_T = \pi(d_{pellet}/2)^2 L_{active}$, where L_{active} is the total length of the all of the pellets in the fuel rod (the active length of the rod), typical values of L_{active} for PWRs and BWRs are 3.6 and 3.0 m, respectively [7-50], and $d_{oxidized} = 0.11(2/5) = 0.044$ mm when fuel oxidation occurs over a two-hour rather than a five-hour time period. Therefore, a maximum value for $F_{oxidized}$ for a full spent fuel rod subject to multiple breaks and exposed to air for about two hours is

$$F_{oxidized} = \frac{V_{oxidized}}{V_T} = \frac{6\pi(d_{pellet}/2)^2 d_{oxidized}}{\pi(d_{pellet}/2)^2 L_{active}} = \frac{6d_{oxidized}}{L_{active}} = \frac{6(0.044\,\text{mm})}{3\times10^3\,\text{mm}} = 8.8\times10^{-5}$$

and, given the approximate nature of this analysis, rounding up to the next order of magnitude is appropriate. Therefore, $F_{oxidized} = 10^{-4}$ and thus for Category 6 accidents $F_{RC,6} = F_{RC,5} + F_{oxidized}$

which means that for Cs $F_{RC,6} = 5 \times 10^{-5} + 10^{-4} = 1.5 \times 10^{-4}$, and for particles $F_{RC,6} = 3 \times 10^{-5} + 10^{-4} = 1.3 \times 10^{-4}$.

7.3.6 CRUD

The formation of radioactive deposits called CRUD on the surfaces of spent fuel rods and the release to the cask interior by spallation of these materials during transportation in a spent fuel cask has been critically reviewed by Sandoval, et al. [7-17]. Sandoval, et al. state that "CRUD is a mixture of reactor primary cooling system corrosion products that have deposited on fuel rod surfaces," that the "deposits contain neutron-activated nuclides," and that during transport in a spent fuel cask portions of the deposits "may spall from the rods, become airborne in the cask cavity, and be released to the environment should a leak develop in the cask…." During routine (accident free) transportation of spent fuel, CRUD spallation from rod surfaces is principally caused by vibration of the rods. However, should an accident occur during the course of the trip, the mechanical loads experienced by the rods during the accident might cause large fractions of the CRUD on the rods to spall from the rod surfaces forming flakes and particles, some of which would become gasborne in the cask interior. To develop an expression for $ST_{CRUD,i}$, the contribution of radionuclide i in CRUD to a transportation accident source term, let $I_{CRUD,i}$ be the inventory of radionuclide i in all of the CRUD on all of the spent fuel rods in the spent fuel transportation cask, $F_{CRUD,RCi}$ be the fraction of the CRUD on an average rod that spalls from the rod surface during an accident to form particles that become gasborne in the cask interior, and F_{CEi} be the fraction of the gasborne CRUD particles that is transported from the cask interior to the environment through the cask leak. Then, $ST_{CRUD,i} = I_{CRUD,i}F_{CRUD,RCi}F_{CEi}$.

Sandoval, et al. measured surface concentrations of radionuclides in CRUD on rod surfaces upon discharge from the reactor [7-51]. They found that the following radionuclides accounted for most of the radioactivity at the time of fuel discharge: ^{58}Co, ^{60}Co, ^{54}Mn, ^{51}Cr, ^{59}Fe, ^{95}Zr, ^{125}Sb and ^{65}Zn. However, because all of these radionuclides except ^{60}Co decay rapidly, after storage for 5 years, ^{60}Co accounts for 92 percent of the radioactivity in CRUD on PWR rods and 98 percent on BWR rods. The measurements also showed that maximum ^{60}Co activity densities at discharge ranged from 2 to 140 μCi/cm^2 on rods from U.S. PWRs and from 11 to 595 μCi/cm^2 on rods from U.S. BWRs. Now given that PWR and BWR spent fuel rods have total surfaces areas of approximately 1200 and 1600 cm^2, respectively [7-50], maximum ^{60}Co CRUD inventories per rod are respectively about 2×10^5 μCi = (1200 cm^2)(140 μCi/cm^2) for PWRs and 1×10^6 μCi = (1600 cm^2)(595 μCi/cm^2) for BWRs. Finally, multiplication of these maximum ^{60}Co inventories per rod by the number of rods per cask will yield maximum values for ^{60}Co for $I_{CRUD,i}$.

Scanning Electron Microscopic examination of CRUD shows [7-52] that CRUD deposits are not solid films but instead consist of agglomerates comprised of irregularly shaped particles with diameters that range from approximately 0.1 to 10 μm. The agglomerates have a log-normal size distribution that has a number geometric mean diameter of 3.0 μm and a geometric standard deviation of 1.87. The CRUD layer has a density of 1.1 g cm^{-3} and a void fraction of 0.8. Thus, the density of the CRUD particles is about 5.5 g cm^{-3}, which means that the aerodynamic equivalent Geometric Mass Median Diameter of the particles is about 22.8 μm and the fraction of the mass of the CRUD layer that is in particles with sizes ≤ 10 μm is about 0.094.

Spallation of CRUD from spent fuel rods was reviewed by Sandoval, et al. [7-53]. That review found data for CRUD spallation (a) from rods exposed to flowing gases (air, nitrogen, argon) for long periods of time at ambient or moderately elevated temperatures (230°C), (b) from rods heated to elevated temperatures (300 to 450°C) for short time periods (0.5 to 2.0 hours), but no data for spallation of CRUD from rods subjected to impact loads. Heating of PWR and BWR rods to 230°C for 0.5 hours caused at least 5 to 6 percent of the CRUD on the rods to be removed by spallation and possibly 8 percent when experimental uncertainties are considered. Heating to 300°C for 0.5 hours, then to 400°C for 1.0 hour, and finally to 450°C for 2.0 hours was estimated to cause 12 to 15 percent of the CRUD on the rods to be removed by spallation.

The following equation gives the fraction $F_{respirable}$ of a brittle material that is converted to respirable particles upon impact onto a hard surface,

$$F_{respirable} = A\rho gh$$

where $A = 2 \times 10^{-11}$ cm^3/g cm^{2}sec^{-2} is an empirical constant determined by impact tests on glass and ceramic specimens, ρ is the material (specimen) density, g is the acceleration due to gravity, and h is the fall-height [7-33]. But $mgh = 0.5m(v_{impact})^2$ where v_{impact} is the impact velocity of the specimen onto the hard surface. So $F_{respirable} = 0.5A\rho(v_{impact})^2$. Therefore, because the density of CRUD is 5.5 g/cm^3, if CRUD behaved like a brittle solid, it would have a spallation fraction for respirable particles of about 1.6×10^{-3} for a 120 mph impact onto a hard surface. Because CRUD spallation fractions when subjected to thermal loads are so much larger than this value, it seems likely that CRUD spallation fractions during collisions will also be much larger than 10^{-3}, probably similar to the values found for spallation due to thermal loads, and thus of order 10^{-1}. Therefore, since citation and key-word searches identified no additional CRUD spallation data other than that presented by Sandoval, et al., the following values were used for $F_{CRUD,RC}$, the CRUD spallation fraction: for fires not initiated by collisions, $F_{CRUD,RC} = 0.15$; for collisions that don't initiate fires, $F_{CRUD,RC} = 0.1$; and for collisions that lead to fires, $F_{CRUD,RC,impact} = 0.1$ and $F_{CRUD,RC,fire} = 0.05$.

7.3.7 Impact Failure of Spent Fuel Rods

In Section 5.4, estimates of the fraction of rods failed by end, corner, and side impacts onto an unyielding surface at four speeds, 30, 60, 90, and 120 mph, were developed for each of the four generic casks being examined by this study when each cask is carrying PWR or BWR fuel assemblies. Table 7.18 presents these fractions (expressed as percents), the average result for each impact orientation, and a weighted summation of these average results using as weights the expected frequencies of end (0.056), corner (0.722), and side (0.222) impacts that are defined below in Section 7.4.3.2.

Inspection of Table 7.18 shows that failure of all of the rods in a PWR assembly is predicted for 60 mph corner impacts onto an unyielding surface by steel-DU-steel truck casks and 60 mph end impacts onto an unyielding surface by monolithic steel rail casks. For BWR assemblies, failure of all of the rods is not predicted at 60 mph for any cask or impact orientation but is predicted for corner impacts at 90 mph onto an unyielding surface by steel-DU-steel truck casks. Nevertheless, because the finite element calculations show that slumping of cask internal structures (i.e., the fuel assemblies being carried in the cask) is substantial for 90 mph impacts onto an unyielding surface, failure of all of the rods in PWR or BWR assemblies is assumed for any impact onto an unyielding surface by any cask at any orientation whenever the impact speed is ≥ 90 mph, and thus failure of all rods is also assumed for any impact onto a real yielding surface at a speed that is equivalent to a 90 mph impact onto an unyielding surface (i.e., for impacts onto any real yielding surface, $f_{rod,impact} = 1.0$ whenever $v_{cask} \geq v_{90}$ where v_{90} is the impact speed onto the real surface that is equivalent to a 90 mph impact onto an unyielding surface). For the speed ranges, v_{30} to v_{60} and v_{60} to v_{90}, $f_{rod,impact}$ is assumed to equal the midpoint value of the range of values given in Table 7.18. Thus, for PWR assemblies, $f_{rod,impact} = 0.25$ when $v_{30} \leq v_{cask} < v_{60}$, 0.59 when $v_{60} \leq v_{cask} < v_{90}$, and 1.0 when $v_{90} \leq v_{cask} < v_{120}$ or whenever $v_{cask} \geq v_{120}$. And for BWR assemblies, $f_{rod,impact} = 0.03$ when $v_{30} \leq v_{cask} < v_{60}$, 0.20 when $v_{60} \leq v_{cask} < v_{90}$, and 1.0 when $v_{90} \leq v_{cask} < v_{120}$ or whenever $v_{cask} \geq v_{120}$.

Table 7.18 PWR and BWR Rod Failure Fractions (percent) for Four Generic Casks

a. PWR Fuel Assembly

Cask	Impact Orientation	Impact Speed (mph)			
		30	**60**	**90**	**120**
Steel-Lead-Steel Truck	end	27	60	100	100
	corner	7	73	100	100
	side	0	0	13	27
Steel-DU-Steel Truck	end	27	33	60	87
	corner	13	100	100	100
	side	7	27	60	87
Steel-Lead-Steel Rail	end	13	60	100	100
	corner	0	13	33	100
	side	0	0	13	87
Monolithic Steel Rail	end	13	100	100	100
	corner	0	33	100	100
	side	0	13	33	73
All	end	20.0	63.3	90.0	96.8
	corner	5.0	54.8	83.3	100.0
	side	1.8	10.0	29.8	68.5
All	All	5.1	45.3	71.8	92.8

Table 7.18 PWR and BWR Rod Failure Fractions (percent) for Four Generic Casks (continued)

b. BWR Fuel Assembly

Cask	Impact Orientation	Impact Speed (mph)			
		30	60	90	120
Steel-Lead-Steel Truck	end	0	0	14	29
	corner	0	0	57	100
	side	0	0	0	0
Steel-DU-Steel Truck	end	0	0	0	0
	corner	0	29	100	100
	side	0	0	0	0
Steel-Lead-Steel Rail	end	0	0	14	43
	corner	0	0	0	43
	side	0	0	0	0
Monolithic Steel Rail	end	0	29	57	71
	corner	0	0	29	57
	side	0	0	0	0
All	end	0	7.3	21.3	35.8
	corner	0	7.3	46.5	75.0
	side	0	0.0	0.0	0.0
All	All	0	5.6	34.8	56.2

7.3.8 Fission Product Transport from the Cask Interior to the Environment

Transport of aerosols and fission product vapors, released to the interior of a Type B TN-125 cask, from the cask interior to the environment was modeled by Shaffer using the MELCOR code [7-30]. Figures 7.10 and 7.11 present results from this study for a collision scenario that does not initiate a fire.

Figure 7.10 compares the size distribution of the particles sourced into the cask from the spent fuel rods upon failure due to impact to the distribution of the particles that escape from the cask. The figure shows that for leak paths with cross-sectional areas of 4 and 100 mm^2, deposition processes largely deplete the source distribution of particles with diameters larger than 10 μm.

Figure 7.11 displays the dependence of cask-to-environment release fractions (F_{CE}) on the cross-sectional area of the seal leakage path that was calculated for a TN-125 cask, when the cask is pressurized to 5 atm by the failure of all of the rods in the cask during a high-speed collision and then depressurizes to atmospheric pressure (p_{atm}) at a rate determined by the seal leak area. Figure 7.11 shows that cask-to-environment release fractions (F_{CE}) increase as cask leak areas increase. This is to be expected since, after pressurization due to the failure of the fuel rods, cask depressurization times decrease as cask leak areas increase. Thus, a large leak area means a short depressurization time, little time for fission product deposition to cask interior surfaces, and

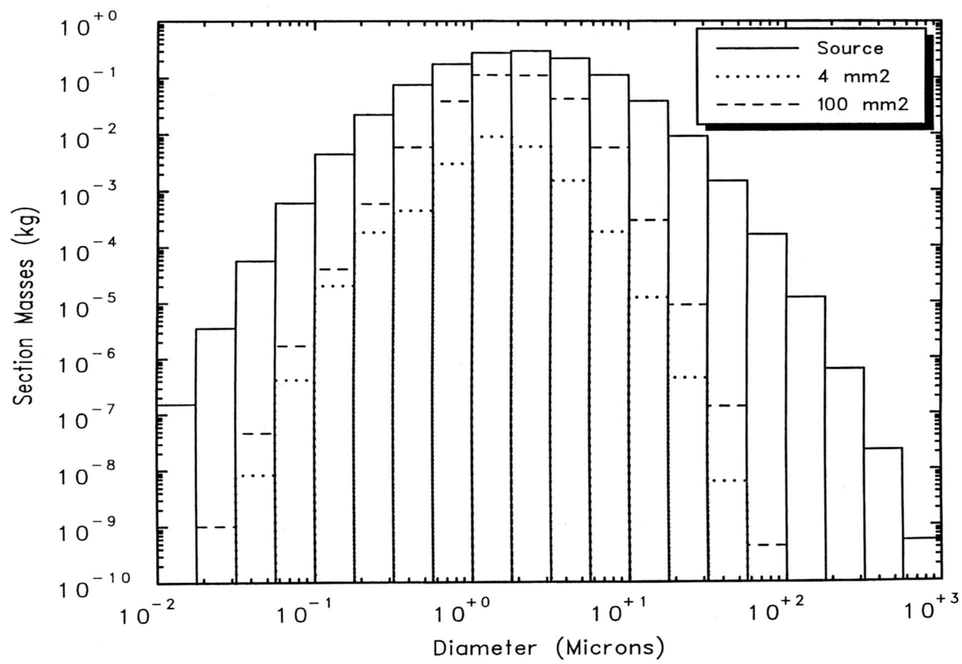

Figure 7.10 Size distributions of the particles sourced into the TN-12 cask from failed spent fuel rods, and of the particles that escaped from the cask through 4 and 100 mm^2 cask failures.

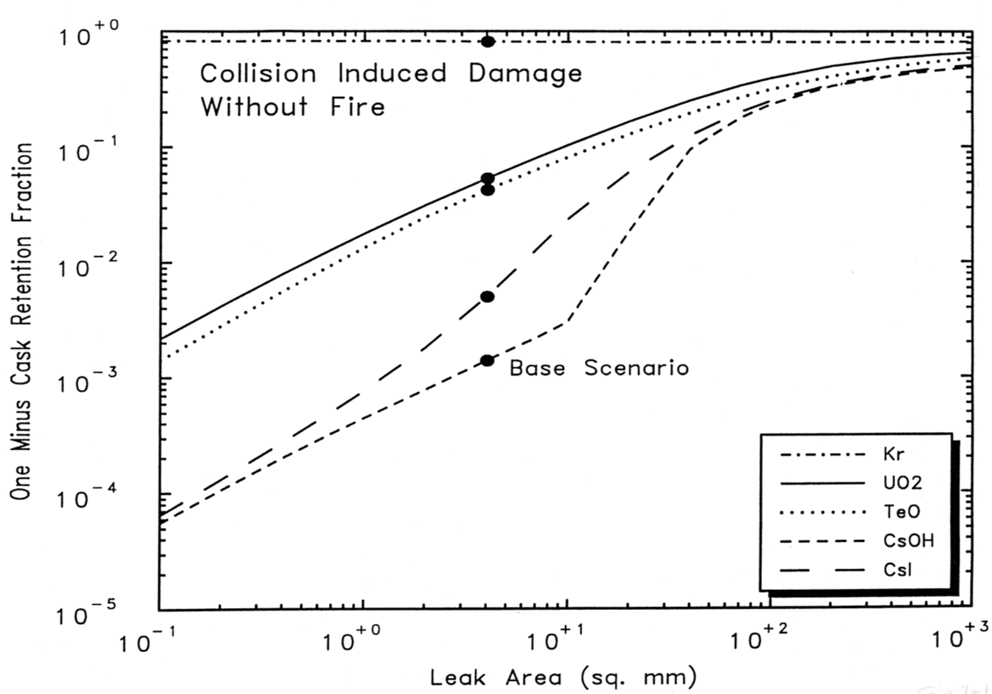

Figure 7.11 Dependence of Cask-to-Environment Release Fractions (1.0 – Retention Fraction) on the Size of the Cask Failure (leak area).

consequently large cask-to-environment release fractions. In Figure 7.11, the curve for TeO closely tracks the curve for fuel fines (i.e., UO_2), while the curves for CsI and CsOH, which exist partly as vapors at cask internal temperatures, diverge from the UO_2 curve as hole sizes decrease. The TeO curve tracks the UO_2 curve because TeO is released and transports as a constituent of particles. The CsI and CsOH curves diverge from the UO_2 curve as hole sizes decrease because, when hole sizes are small and there is significant time for deposition to occur, deposition onto cool interior cask surfaces of the small fraction of CsI and CsOH that is initially released as vapors is significantly more efficient than is deposition of CsI and CsOH that is released as a constituent of particles.

As was stated in Sections 7.2.5.1 and 7.2.5.2, leakage of elastomeric truck and train cask seals due to heating by fires to 350ºC and of elastomeric rail and truck cask seals due to cask impacts onto yielding surfaces at speeds equivalent respectively to 60 and 120 mph impacts onto an unyielding surface are assumed to produce 1 mm^2 leak areas. In Section 7.2.5.2, it was concluded that, when heated above 450ºC, elastomeric seals will fail catastrophically causing seal leak areas to be set by the space between the contacting surfaces of the cask lid and the cask lid well. In Section 5.1.4, the closure region distortions in rail casks produced by impacts onto an unyielding surface at speeds of 60, 90, and 120 mph were used to estimate the seal leak areas that these impacts would cause. Table 7.19 presents the estimates of rail cask seal leak areas developed by this analysis, the values selected for use in developing release fractions, and the values of the cask-to-environment release fractions for particles and CsI(g) that Figure 7.11 shows correspond to these leak areas.

Table 7.19 Seal Leak Areas and Values of F_{CE} for Rail Casks

Cask Impact		Leak Area (mm^2)			F_{CE}	
		Calculated Values		Analysis Values		
Speed	Orientation	Steel-Lead-Steel Cask	Monolithic Steel Cask	All Rail Casks	Particles	CsI(g)
60	Corner		0.18	1[a,b]	0.02	0.0008
90	Corner	346	256	300[c]	0.6	0.4
120	Corner	2046	1616	1800[d]	0.8	0.8
120	Side		9	10	0.2	0.06

a. Rounded to 1 mm^2 so as to be consistent with treatment of truck cask leak areas.
b. The oblong nature of seal leak cross sections and the log-normal character of particle size distributions means that leaks with areas significantly smaller than 1 mm^2 need not be considered. For example, an 0.1 mm^2 leak that is one bolt spacing (35 to 60 mm) long is only 1.5 to 3 μm wide and thus will not transmit significant quantities (by mass) of respirable particles (particles with diameters ≤ 10 μm).
c. Average of steel-lead-steel and monolithic steel rail cask results.
d. Scaled by a factor of six, the average of the ratios of calculated 120 and 90 mph results.

Let $f_{deposition}$ be the fraction of the particles or vapors, released to the interior of a RAM transport cask upon rod failure, that deposit onto cask interior surfaces before they can escape from the cask to the environment. This fraction is related to F_{CE} by the following equation:

$$F_{CE} = (1 - f_{deposition})(1 - p_{atm}/p_{Imp})$$

Since p_{atm} =1.0 and p_{Imp} = 5.0 for the TN-125 cask calculation, values for $f_{deposition}$ can be calculated for the rail cask leak areas presented in Table 7.19 by substitution of the values for F_{CE} that correspond to these leak areas. Then weighted summation of the resulting orientation-dependent leak areas using as weights the expected frequencies of end (0.056), corner (0.722), and side (0.222) impacts that are defined below in Section 7.4.3.2 yields the values for $f_{deposition}$ for the indicated speed ranges listed in Table 7.20.

Table 7.20 Values of $f_{deposition}$ for Rail Casks

Speed Range (mph)	$f_{deposition}$	
	Particles	CsI(g)
60 to 90	0.98	0.999
90 to 120	0.45	0.64
≥ 120	0.2	0.26

Finally, because elastomeric cask seal leakage caused by heating by a fire to 350ºC and elastomeric truck cask seal leakage caused by cask impacts at 120 mph and any orientation onto an unyielding surface are assumed to produce 1 mm^2 seal leak areas, for these seal leak, $f_{deposition}$ equals 0.98 for particles and 0.999 for CsI(g). However, no credit is taken for deposition of Cs vapor species during scenarios that involve fires that heat the cask to temperatures ≥ 750ºC. Thus, whenever release of Cs as a vapor (e.g., CsI) is significant, deposition of that vapor species onto cool cask interior surfaces is neglected (e.g., $f_{deposition,CsI} = 0.0$). Thus, Cs vapor deposition is treated when rod failure is caused by impact but not when it is caused by burst rupture.

7.3.9 Expansion Factor Values

Transport of radioactive species from the cask to the environment during depressurization of the cask or due to heating of cask gases by a fire was discussed in Sections 7.2.5.4 and 7.2.5.5. In Section 7.2.5.6, expansion factor expressions were derived that allowed the fraction of the cask gases that escape from the cask to the environment during cask depressurization or heating by a fire to be calculated. Table 7.21 presents the values of the parameters that enter each expansion factor and the value of the expansion factor produced by these parameter values. Values of p_{Imp} and p_b, which are respectively the pressure of the cask after some fraction of the rods in the cask are failed by impact and by burst rupture, are calculated using the following equations:

$$p_{Imp} = 1.0\,\text{atm} + 4.0\,\text{atm}\,(F_{rod,impact}) \quad \text{and} \quad p_b = 1.0\,\text{atm} + 4.0\,\text{atm}\,(1.0 - F_{rod,impact})$$

where 1.0 atm is the internal pressure of the cask during normal transport and 4.0 atm is the pressure rise produced by the failure of all of the rods in the cask. Thus, for example, p_{imp} = 3.36 atm = 1.0 + 4.0(0.59), when 59 percent of the rods in the cask fail upon impact and p_b = 4.20 atm = 1.0 + 4.0(1.0 – 0.20), when the 80 percent of the rods not failed by collision impact are later failed by burst rupture due to heating by an ensuing fire.

Table 7.21 Expansion Factor Values

Expansion Factor	$F_{rod,impact}$		Temperatures (K)				Pressures (atm)			Value
	PWR	BWR	T_a	T_s	T_b	T_f	p_{atm}	p_{Imp}	p_b	
$f_{e1} = (p_{atm}/p_{Imp})(T_a/T_s)$	1.00	1.00	573	623			1.0	5.00		0.184
	0.59		573	623			1.0	3.36		0.274
	0.25		573	623			1.0	2.00		0.460
		0.20	573	623			1.0	1.80		0.511
		0.03	573	623			1.0	1.12		0.821
$f_{e2} = (T_s/T_b)$		all		623	1023					0.609
$f_{e3} = (p_{atm}/p_{imp})(T_a/T_b)$	1.00	1.00	573		1023		1.0	5.00		0.112
	0.59		573		1023		1.0	3.36		0.167
	0.25		573		1023		1.0	2.00		0.280
		0.20	573		1023		1.0	1.80		0.311
		0.03	573		1023		1.0	1.12		0.500
$f_{e4} = (p_{atm}/p_b)(T_b/T_f)$	1.00	1.00			1023	1273	1.0		1.0	0.804
	0.59				1023	1273	1.0		2.64	0.304
	0.25				1023	1273	1.0		4.00	0.201
		0.20			1023	1273	1.0		4.20	0.191
		0.03			1023	1273	1.0		4.88	0.165
	0.0	0.0			1023	1273	1.0		5.00	0.161
$f_{e5} = (p_{atm}/p_{imp})$	1.00	1.00					1.0	5.00		0.200
	0.59						1.0	3.36		0.298
	0.25						1.0	2.00		0.500
		0.20					1.0	1.80		0.556
		0.03					1.0	1.12		0.893

7.4 Values for Severity Fraction Parameters

7.4.1 Introduction

Severity fraction expressions were formulated in Section 7.2.8. In this section, values are developed first for the parameters that enter those expressions and then for the severity fractions themselves by substitution of the parameter values into the individual severity fraction expressions.

7.4.2 Cask Involvement

When a spent fuel cask is transported by truck, the truck is always a tractor semi-trailer. Trucks that haul more than one trailer are never used. Therefore, for truck accidents, $P_{cask} = 1.0$, because the vehicle that is carrying the cask, the tractor semi-trailer, is always involved in the accident.

Train accident data for 1972 were reviewed by Clarke, et al. [7-54] who found that freight trains typically contain about 66 cars, that on average 10 cars are involved in side or raking collisions, and that the number of cars involved in derailment accidents is speed dependent. For derailment accidents, Clarke, et al. determined the average number of cars derailed during derailment accidents that had derailment speeds that fell into the following four speed ranges: 0 to 10, 10 to 30, 30 to 60, and 60 to 80 mph. Now because the Modal Study [7-55] developed a cumulative distribution of derailment accident speeds, the chance that a derailment accident occurs at a speed that falls within each of these four speed ranges can be calculated. Table 7.22 presents, for each derailment accident speed range, the probability of occurrence of derailment accidents with derailment speeds that fall in each speed range and the average number of cars derailed during those accidents.

Table 7.22 Probability of Occurrence and Average Number of Cars Derailed for Train Derailment Accidents by Accident Speed Range

Speed Range (mph)	0 to 10	10 to 30	30 to 60	30 to 60
Probability of Occurrence	0.402	0.4079	0.1829	0.0050
Average Number of Cars Derailed	5	6	11	17

If the derailment data of Clarke, et al. is weighted using the cumulative speed distribution data for derailment accidents presented in the Modal Study [7-55], the following weighted summation results:

$$N_{cars/derailment} = \sum_i W_i N_i = 5(0.402) + 6(0.4079) + 11(0.1829) + 17(0.0050) = 6.6$$

where the four speed ranges are respectively 0 to 10, 10 to 30, 30 to 60, and 60 to 80 mph. Thus, about six or seven cars will derail during a typical derailment accident. But derailment accidents that occur at speeds < 30 mph will fail neither the cask seal nor any of the spent fuel rods being carried in the cask. So if these accidents are ignored, construction of a weighted sum for the speed ranges 30 to 60 and 60 to 80 mph shows that the average number of cars involved in derailment accidents of concern is

$$N_{cars/derailment} = \sum_i W_i N_i = 11(0.9734) + 17(0.0266) = 11.2$$

Therefore, because the average number of cars involved in side and raking collisions is usually about ten and the average number of cars involved in derailment accidents that occur with speeds ≥ 30 mph is about 11, 0.17 = 11/66 is a reasonable estimate for P_{cask} for train accidents.

7.4.3 Values for Collision Conditional Probabilities

Truck and train accident scenarios were discussed in Section 7.1. That section presented event trees that depicted possible accident scenarios, where a specific scenario is a unique path on the tree. Inspection of the truck and rail event trees depicted in Figures 7.3 and 7.4 shows that each tree lists the conditional probabilities of occurrence of each scenario (path) on the tree, identifies the scenarios that may lead to cask failure (the paths marked with an asterisk), and for collision scenarios specifies an associated accident speed distribution and an impact surface. Accordingly, the value of the conditional probability of truck or train accident scenario j, $P_{scenario,j}$ is read from the appropriate event tree.

7.4.3.1 Accident Velocity Probabilities

For collision accidents, $P_{speed,j}(v_{30},v_{60})$, $P_{speed,j}(v_{60},v_{90})$, $P_{speed,j}(v_{90},v_{120})$, and $P_{speed,j}(\geq v_{120})$ are calculated using the following equations:

$$P_{speed,j}\left(v_{30},v_{60}\right) = \sum_{m=1}^{3} P_{orientation,m}\left[P_{speed,jm}\left(v_{60}\right) - P_{speed,jm}\left(v_{30}\right)\right]$$

$$P_{speed,j}\left(v_{60},v_{90}\right) = \sum_{m=1}^{3} P_{orientation,m}\left[P_{speed,jm}\left(v_{90}\right) - P_{speed,jm}\left(v_{60}\right)\right]$$

$$P_{speed,j}\left(v_{90},v_{120}\right) = \sum_{m=1}^{3} P_{orientation,m}\left[P_{speed,jm}\left(v_{120}\right) - P_{speed,jm}\left(v_{90}\right)\right]$$

$$P_{speed,j}\left(\geq v_{120}\right) = \sum_{m=1}^{3} P_{orientation,m}\left[1.0 - P_{speed,jm}\left(v_{120}\right)\right]$$

where v_{30}, v_{60}, v_{90}, and v_{120} are the impact speeds for end, corner, or side impact orientations onto real yielding surfaces that would cause the same damage to the cask and its contents (spent fuel) as is predicted respectively for end, corner, and side impacts at speeds of 30, 60, 90, and 120 mph onto an unyielding surface; v_{30}, v_{60}, v_{90}, and v_{120} have different values for each cask/surface combination; $P_{orientation,m}$ is the probability that the cask impact is an end, corner, or side impact; and $P_{speed,jm}(v_{30})$, $P_{speed,jm}(v_{60})$, $P_{speed,jm}(v_{90})$, and $P_{speed,jm}(v_{120})$ are respectively the cumulative probabilities for impact orientation m and accident scenario j that the cask impact speed v is $\leq v_{30}$, $\leq v_{60}$, $\leq v_{90}$, and $\leq v_{120}$.

In Section 5.1, cask-specific values for the impact velocities, v_{30}, v_{60}, v_{90}, and v_{120}, were determined by finite element analyses for impacts onto an unyielding surface for each of the four generic casks being examined by this study. In Section 5.2, these unyielding surface impact velocities were extrapolated to yielding surfaces by partitioning the impact energy between the cask and the yielding surface. Table 7.23 presents the cask specific real surface impact velocities determined by those analyses.

7.4.3.2 Cask Impact Orientation Probabilities

The finite element cask impact calculations described in Section 5 examined three cask impact orientations, side, corner, and end, where the cask impact orientation is specified by the angle between the cask axis and the plane of the impact surface. By definition, side impacts have impact angles between 0 and 20 degrees, corner impacts have impact angles between 20 and 85 degrees, and end impacts have angles between 85 and 90 degrees. Thus, for example, a cask must strike an impact surface nearly end-on for the impact orientation to be classed as an end impact. Now, although the probability of occurrence of each of these impact orientations is

Table 7.23 Impact Speeds (mph) onto Real Yielding Surfaces that are Equivalent to 30, 60, 90, and 120 mph Impacts onto an Unyielding Surface

a. Type B Steel-Lead-Steel Spent Fuel Truck Cask

Impact Surface	Impact Orientation	Impact Speed			
		v_{30}	v_{60}	v_{90}	v_{120}
Hard Rock	End	30	60	90	120
	Corner	30	60	90	120
	Side	30	60	90	120
Soft Rock/Hard Soil/Concrete (slab, column, abutment)	End	38*	177	232	273
	Corner	35*	123	172	245
	Side	32*	86	135	209
Clay/Silt	End	84*	>277	>367	>448
	Corner	58*	>135	>195	>279
	Side	32*	>170	>273	>426
Railbed/Roadbed	End	38*	277	367	448
	Corner	35*	135	195	279
	Side	32*	170	273	426
Water	End	78*	∞	∞	∞
	Corner	150*	∞	∞	∞
	Side	42*	∞	∞	∞

* From the Modal Study, driven by impact limiter response, rather than cask response.

b. Type B Steel-DU-Steel Spent Fuel Truck Cask

Impact Surface	Impact Orientation	Impact Speed			
		v_{30}	v_{60}	v_{90}	v_{120}
Hard Rock	End	30	60	90	120
	Corner	30	60	90	120
	Side	30	60	90	120
Soft Rock/Hard Soil/Concrete (slab, column, abutment)	End	38*	167	196	228
	Corner	35*	204	266	316
	Side	32*	142	210	303
Clay/Silt	End	84*	>253	>303	>360
	Corner	58*	>223	>298	>360
	Side	32*	>263	>394	>575
Railbed/Roadbed	End	38*	253	303	360
	Corner	35*	223	298	360
	Side	32*	263	394	575
Water	End	78*	∞	∞	∞
	Corner	150*	∞	∞	∞
	Side	42*	∞	∞	∞

* From the Modal Study, driven by impact limiter response, rather than cask response.

Table 7.23 Impact Speeds (mph) onto Real Yielding Surfaces that are Equivalent to 30, 60, 90, and 120 mph Impacts onto an Unyielding Surface (continued)

c. Type B Monolithic Spent Fuel Rail Cask

Impact Surface	Impact Orientation	Impact Speed			
		v_{30}	v_{60}	v_{90}	v_{120}
Hard Rock	End	30	60	90	120
	Corner	30	60	90	120
	Side	30	60	90	120
Soft Rock/Hard Soil/Concrete (slab, column, abutment)	End	38*	419	507	573
	Corner	35*	1129	1679	2171
	Side	32*	256	451	522
Clay/Silt	End	84*	>521	>632	>750
	Corner	58*	>218	>321	>418
	Side	32*	>230	>394	>505
Railbed/Roadbed	End	38*	521	632	750
	Corner	35*	218	321	418
	Side	32*	230	394	505
Water	End	78*	∞	∞	∞
	Corner	150*	∞	∞	∞
	Side	42*	∞	∞	∞

* From the Modal Study, driven by impact limiter response, rather than cask response.

Table 7.23 Impact Speeds (mph) onto Real Yielding Surfaces that are Equivalent to 30, 60, 90, and 120 mph Impacts onto an Unyielding Surface (continued)

d. Type B Steel-lead-steel Spent Fuel Rail Cask

Impact Surface	Impact Orientation	Impact Speed			
		v_{30}	v_{60}	v_{90}	v_{120}
Hard Rock	End	30	60	90	120
	Corner	30	60	90	120
	Side	30	60	90	120
Soft Rock/Hard Soil/Concrete (slab, column, abutment)	End	38*	319	391	509
	Corner	35*	640	990	>990
	Side	32*	207	289	>289
Clay/Silt	End	84*	>386	>480	>635
	Corner	58*	>133	>208	>223
	Side	32*	>180	>256	>262
Railbed/Roadbed	End	38*	386	480	635
	Corner	35*	133	208	>223
	Side	32*	180	256	>262
Water	End	78*	∞	∞	∞
	Corner	150*	∞	∞	∞
	Side	42*	∞	∞	∞

* From the Modal Study, driven by impact limiter response, rather than cask response.

likely to depend on accident scenario, because such scenario dependencies cannot be easily estimated, it is assumed that impacts at any angle are equally probable. Therefore, the probabilities of side, corner, and end impacts (values of $P_{orientation,m}$) are $P_{side} = 20/90 = 0.222$, $P_{corner} = 65/90 = 0.722$ and $P_{end} = 5/90 = 0.056$.

7.4.3.3 Modal Study Accident Velocity Distributions

The Modal Study developed eight cumulative velocity distributions for truck and train accidents, four truck accident and four train accident distributions. These distributions are presented in Tables 7.24 and 7.25. Values of $P_{speed,jm}$ were calculated by linear interpolation using the data presented in these tables.

The cumulative velocity distributions presented in Tables 7.24 and 7.25 are of three types: (1) a velocity distribution for accidents that occur on level ground, which means that the velocity at accident initiation of the cask and the truck or train is assumed to be the cask impact velocity, (2) a velocity distribution for accidents where the cask and the truck or train plunge off of a bridge and fall to the ground below and thus have an impact velocity that depends on the height of the bridge, and (3) a velocity distribution for accidents where the cask and the truck or train plunge down an embankment and then strike an object or a surface. As stated in the Modal Study, the velocity distributions for truck accidents on level ground (velocity distribution v1) reflect a reduction in velocity due to braking, the velocity distribution for train accidents that occur on level ground (velocity distribution Tv1) take no credit for braking, and the velocity distributions for accidents where the cask and the truck or train plunge down an embankment were developed by constructing the vector sum of the level ground and bridge height velocity distributions [7-56].

7.4.3.4 Puncture/Shear Probability

Collision accidents may generate sharp objects that could fail a cask by puncture or shearing of the cask shell. Puncture and shear failure data for rail tank cars was reviewed in Section 5.3. The review developed an estimate for the probability that a probe capable of causing puncture or shear failures of a Type B spent fuel cask will be both formed during a collision accident, will strike the cask in an orientation that might allow it to cause a cask failure, and will not break before it causes the failure. The review concluded that a sharp probe capable of failing a cask by puncture or shear might be formed during any collision accident, that probe formation would be possible at any accident speed, and that formation was most unlikely at any speed. Accordingly, although there are no data on the frequency of formation of very sharp very robust puncture/shear probes during truck or train accidents, because spent fuel casks have two 1 inch steel shells and only about 4 tank car puncture accidents in 100 lead to puncture of tank cars with 1 inch shells, it is assumed that $P_{puncture/shear} = 0.001 = (0.04)^2$ for all truck accidents and also for all train accidents except train pileup accidents during which the cask is struck by a train car coupler. For train pileup accidents, where the cask is struck by a coupler and therefore puncture or shear is more likely to occur, it is assumed that $P_{puncture/shear} = 0.01$.

Table 7.24 Truck Accident Velocity Distributions

v1 Initial Truck Velocity Adjusted for Braking		v2 Impact Velocity Based on Bridge Heights		v3 Vector Sum of First and Second Distributions		v4 Train Grade Crossing Accident Velocities	
Velocity (mph)	Cumulative Probability[a]	Velocity (mph)	Cumulative Probability[a]	Velocity (mph)	Cumulative Probability[a]	Velocity (mph)	Cumulative Probability[a]
0.0	0.0	0.0	0.0	0.0	0.0	0.0	0.0
2.0	0.03834	7.74	0.00621	5.0	0.0	2.0	0.06014
6.0	0.12916	10.94	0.01550	10.0	0.00141	6.0	0.17906
10.0	0.23508	15.48	0.04754	15.0	0.00821	10.0	0.29398
14.0	0.34886	18.95	0.1051	20.0	0.03387	14.0	0.40255
18.0	0.46237	21.89	0.1952	25.0	0.11129	18.0	0.50280
22.0	0.56877	24.47	0.3178	30.0	0.28292	22.0	0.59331
26.0	0.66345	26.81	0.4629	35.0	0.51279	26.0	0.67319
30.0	0.74353	28.95	0.6124	40.0	0.70110	30.0	0.74210
34.0	0.80877	30.95	0.7464	45.0	0.81951	34.0	0.80022
38.0	0.86020	32.83	0.8508	50.0	0.89168	38.0	0.84814
42.0	0.89961	34.61	0.9217	55.0	0.93543	42.0	0.88676
46.0	0.92881	36.29	0.9635	60.0	0.96178	46.0	0.91718
50.0	0.95009	37.91	0.9849	65.0	0.97751	50.0	0.94062
54.0	0.96547	39.46	0.9945	70.0	0.98680	54.0	0.95826
58.0	0.97634	41.67	0.9991	75.0	0.99227	58.0	0.97125
62.0	0.98383	43.08	0.9998	80.0	0.99547	62.0	0.98060
66.0	0.98908	44.45	0.9999	85.0	0.99766	66.0	0.98717
70.0	0.99261	56.86	1.0	90.0	0.99901	70.0	0.99169
74.0	0.99503			95.0	0.99961	74.0	0.99473
78.0	0.99670			100.0	0.99985	78.0	0.99672
82.0	0.99825			105.0	0.99995	82.0	0.99800
86.0	0.99910			110.0	0.99998	86.0	0.99881
90.0	0.99956			115.0	0.99999	90.0	0.99930
94.0	0.99979			150.0	1.0	94.0	0.99960
98.0	0.99990					98.0	0.99977
102.0	0.99995					102.0	0.99987
106.0	0.99998					106.0	0.99993
110.0	0.99999					110.0	0.99996
150.0	1.0					114.0	0.99998
						118.0	0.99999
						150.0	1.0

a. Probability that the accident or impact velocity is less than or equal to the listed velocity.

Table 7.25 Train Accident Velocity Distributions

Tv1 Collision Accident Train Velocities without Braking		Tv2 Derailment Accident Train Velocities without Braking		Tv3 Impact Velocity Based on Bridge Heights		Tv4 Vector Sum of Second and Third Distributions	
Velocity (mph)	Cumulative Probability[a]	Velocity (mph)	Cumulative Probability[a]	Velocity (mph)	Cumulative Probability[a]	Velocity (mph)	Cumulative Probability[a]
0.0	0.0	0.0	0.0	0.0	0.0	0.0	0.0
2.0	0.09385	2.0	0.07543	7.74	0.00621	5.0	0.0
6.0	0.26286	6.0	0.22036	10.94	0.01550	10.0	0.00232
10.0	0.40788	10.0	0.35480	15.48	0.04754	15.0	0.01244
14.0	0.53042	14.0	0.47634	18.95	0.1051	20.0	0.04814
18.0	0.63240	18.0	0.58341	21.89	0.1952	25.0	0.14919
22.0	0.71598	22.0	0.67534	24.47	0.3178	30.0	0.35837
26.0	0.78345	26.0	0.75225	26.81	0.4629	35.0	0.60624
30.0	0.83709	30.0	0.81495	28.95	0.6124	40.0	0.77834
34.0	0.87908	34.0	0.86477	30.95	0.7464	45.0	0.87230
38.0	0.91147	38.0	0.90385	32.83	0.8508	50.0	0.92649
42.0	0.93606	42.0	0.93246	34.61	0.9217	55.0	0.95855
46.0	0.95446	46.0	0.95386	36.29	0.9635	60.0	0.97727
50.0	0.96801	50.0	0.96920	37.91	0.9849	65.0	0.98792
54.0	0.97784	54.0	0.97991	39.46	0.9945	70.0	0.99379
58.0	0.98486	58.0	0.98720	41.67	0.9991	75.0	0.99692
62.0	0.98980	62.0	0.99204	43.08	0.9998	80.0	0.99852
66.0	0.99323	66.0	0.99516	44.45	0.9999	85.0	0.99932
70.0	0.99557	70.0	0.99713	56.86	1.0	90.0	0.99970
74.0	0.99714	74.0	0.99834			95.0	0.99987
78.0	0.99818	78.0	0.99906			100.0	0.99995
82.0	0.99886	82.0	0.99948			105.0	0.99998
86.0	0.99929	86.0	0.99972			110.0	0.99999
90.0	0.99957	90.0	0.99985			150.0	1.0
94.0	0.99974	94.0	0.99992				
98.0	0.99985	98.0	0.99996				
102.0	0.99991	102.0	0.99998				
106.0	0.99995	106.0	0.99999				
110.0	0.99997	150.0	1.0				
114.0	0.99998						
118.0	0.99999						
150.0	1.0						

a. Probability that the accident or impact velocity is less than or equal to the listed velocity.

7.4.4 Values for Fire Probabilities

For fires that are initiated by collisions, the probability that a fire of concern occurs is the product of the conditional probability that the collision scenario j initiates a fire, $P_{fire/scenario,j}$, and the fraction of these fires, $P_{severe\ fire,k}$, that are severe enough to cause the cask seal to leak and/or the spent fuel rods being transported in the cask k to fail. Of course, if the accident in question is a fire not initiated by a collision (a fire-only accident), then $P_{fire/scenario,j} = 1.0$.

Because of the large mass of Type B spent fuel transportation casks, only a hot, co-located, fully engulfing, optically dense, long-duration fire can heat one of these casks to temperatures where spent fuel rods being transported in the cask will fail by burst rupture. Therefore, the fraction of all fires that can cause thermal burst rupture of spent fuel rods (heat a cask to temperatures in the temperature range $T_b \leq T_{cask} \leq T_f$) is given by

$$P_{severe\ fire,k} = P_{co\text{-}located}\, P_{optically\ dense}\, P_{flame\ temp}\, P_{duration,k} \tag{9}$$

where $P_{co\text{-}located}$ is the probability that the cask and the fire are co-located (i.e., that the cask is not significantly offset from the fire), $P_{optically\ dense}$ is the probability that the fire diameter is large enough to make the fire optically dense to loss of energy from the cask to the atmosphere (i.e., the fire diameter is about 3 m larger than the fire diameter that just engulfs the cask), $P_{flame\ temp}$ is the probability that the average temperature of the fire is high enough to heat the cask to a temperature $\geq T_b$, the temperature at which intact spent fuel rods fail by thermal burst rupture, $P_{duration,k}$ is the probability that the fire will burn long enough to heat generic cask k to that temperature, T_{cask} is the temperature of the cask internals, and T_f is the average flame temperature of a hydrocarbon fuel fire.

It is important to note that the four probabilities that enter the preceding expression for $P_{severe\ fire,k}$ should usually be largely independent. For example, large truck fires can occur only if more than one vehicle is involved in the accident and train fires always involve more that one rail car as the car carrying the spent fuel cask carries no fuel. So fire size and fire location should not be correlated for large fires. Similarly, fuel character and thus fire temperature should not depend on fire location or fire size or fire duration (smoldering smoky fires are probably optically dense but are not likely to be large enough or hot enough to be of concern). And although fire duration might be expected to be inversely proportional to fire size, runoff or soaking of fuel into the ground will cause the seeming correlation to be greatly weakened. So, although some of these four probabilities may be weakly correlated, for this analysis they are treated as though they are uncorrelated.

Although only an unusually severe long-duration fire can heat the internals of a spent fuel cask to rod burst rupture temperatures, less severe fires should be easily able to heat a spent fuel cask to lower temperatures. To capture the lessened fire severity needed to heat a cask to lower temperatures, some of the probabilities in the preceding formula can be relaxed by assuming that all fires meet the requirement represented by that probability. For example, because elastomeric cask seals begin to leak at about 350ºC, a temperature only 50 to 100ºC above normal cask internal temperatures, it would seem that most fires that burn hot enough and long enough to heat a spent fuel cask to 350ºC would be able to do so even if they were somewhat offset (not co-located) and weren't optically dense (smoldering fires, very small collocated fires, and large offset fires located far from the cask are exceptions to this statement). Accordingly, the fraction of all fires that can heat a spent fuel cask to a temperature in the temperature range $T_a \le T_{cask} \le T_s$, where T_a is the cask internal temperature under ambient (normal transport) conditions and T_s is the cask seal leakage temperature, is here taken to be

$$P_{\text{severe fire,k}} = P_{\text{co-located}}\, P_{\text{optically dense}}\, P_{\text{flame temp}}\, P_{\text{duration,k}} = P_{\text{flame temp}}\, P_{\text{duration,k}}$$

since for this temperature range it is assumed that $P_{\text{co-located}} = P_{\text{optically dense}} = 1.0$.

Similarly, any moderately large fire not well-separated from the cask that burns hot enough and long enough should be able to heat the cask to a temperature greater than the temperature that cause the cask seal to leak but not to the temperature where rods fail by burst rupture, that is, to some temperature in the temperature range $T_s<T_{cask}<T_b$. Thus, the fraction of all fires that can heat a spent fuel cask to a temperature in the temperature range $T_s<T_{cask}<T_b$ is taken to be

$$P_{\text{severe fire,k}} = P_{\text{co-located}}\, P_{\text{optically dense}}\, P_{\text{flame temp}}\, P_{\text{duration,k}} = P_{\text{co-located}}\, P_{\text{flame temp}}\, P_{\text{duration,k}}$$

or

$$P_{\text{severe fire,k}} = P_{\text{co-located}}\, P_{\text{optically dense}}\, P_{\text{flame temp}}\, P_{\text{duration,k}} = P_{\text{optically dense}}\, P_{\text{flame temp}}\, P_{\text{duration,k}}$$

since, for a fire to heat a cask to temperature in this temperature range, the fire must either be fairly large (i.e., $P_{\text{optically dense}} = 1.0$) but not colocated (i.e., $P_{\text{co-located}} < 1.0$) or it must be co-located (i.e., $P_{\text{co-located}} = 1.0$) but not optically dense ($P_{\text{optically dense}} < 1.0$).

Finally, the conditional probability, $P_{\text{duration,k}}$, that the fire burns long enough so that generic cask k is heated to a temperature that falls within one of the three temperature ranges, $T_a \le T_{cask} \le T_s$, $T_s < T_{cask} < T_b$, and $T_b \le T_{cask} \le T_f$, is calculated using the following expressions:

$$\begin{aligned}
P_{\text{duration,k}}(T_a \le T_{\text{cask}} \le T_s) &= P_{\text{duration,k}}(t_{k,T_s}) \\
P_{\text{duration,k}}(T_s < T_{\text{cask}} < T_b) &= P_{\text{duration,k}}(t_{k,T_b}) - P_{\text{duration,k}}(t_{k,T_s}) \\
P_{\text{duration,k}}(T_b \le T_{\text{cask}} \le T_f) &= 1.0 - P_{\text{duration,k}}(t_{k,T_b})
\end{aligned}$$

where for example t_{k,T_s} is the time that it takes an optically dense, co-located, hydrocarbon fueled fire to heat generic cask k to its seal leakage temperature T_s given that the normal internal temperature of the cask is T_a, and $P_{\text{duration,k}}(t_{k,T_s})$ and $P_{\text{duration,k}}(t_{k,T_b})$ are respectively the cumulative probabilities that the fire duration is $\le t_{k,T_s}$ and $\le t_{k,T_b}$.

Cask-specific values for the heating times, t_{k,T_s}, t_{k,T_b}, and t_{k,T_f}, were determined by 1-D thermal calculations for each of the four generic casks being examined by this study. Those calculations were described in Section 6. Table 7.26 presents the cask specific heating times determined by those calculations.

Table 7.26 Durations (hr) of Co-Located, Fully Engulfing, Optically Dense, Hydrocarbon Fuel Fires that Raise the Temperature of Each Generic Cask to T_s, T_b, and T_f

Cask	Temperature (°C)		
	T_s = 350	T_b = 750	T_f = 1000
Steel-Lead-Steel Truck	1.04	2.09	5.55
Steel-DU-Steel Truck	0.59	1.96	5.32
Steel-Lead-Steel Rail	1.06	2.91	6.43
Monolithic Steel Rail	1.37	6.57	11

7.4.4.1 Modal Study Fire Duration Distributions

The Modal Study developed eight cumulative fire duration distributions for truck and train fires, five truck fire distributions and three train fire distributions. Tables 7.27 and 7.28 present these cumulative fire duration distributions. Values of $P_{\text{duration},k}(t_{k,T_s})$, $P_{\text{duration},k}(t_{k,T_b})$, and $P_{\text{duration},k}(t_{k,T_f})$ were determined by linear interpolation using the data in these tables.

7.4.4.2 Optically Dense Fire Size

The four generic casks being examined by this study all have lengths of about 5 m (200 inches). Therefore, if engulfed by a fire, the fire must have a diameter of about 8 m (26.7 ft) if it is to be optically dense with respect to the engulfed cask (large enough so that the cask doesn't lose heat by radiation through the fire plume to the atmosphere) [7-57,7-58].

7.4.4.3 Truck Collision Fire Statistics

Cumulative distributions of fire temperatures, diameters, stand-off distances, and durations for fires initiated by collisions of trucks with other vehicles, with trains, or with fixed and non-fixed objects have been developed by Clauss, et al. [7-5]. Clauss, et al. find that

- essentially all fires have average fire temperatures greater than 650ºC, which agrees well with the results of Lopez, et al. who found [7-59] that essentially all fires have average flame temperatures greater than 725ºC,
- only one fire in two reaches average fire temperatures of 1000ºC,
- no more than one fire in two is an engulfing fire,
- 80 percent of all fires not caused by train collisions have diameters < 25 ft,
- all fires caused by train collisions have diameters > 25 ft,
- fires with diameters ≥ 25 ft initiated by truck collisions with other trucks, with cars, and with fixed or non-fixed objects all have fire durations < 60 minutes (i.e., there is not enough fuel available to support fires of longer durations),

- 85 percent of all fires initiated by truck collisions with tankers have durations longer than 60 minutes, and

- only 25 percent of all fires initiated by the collision of a train with a truck have durations longer than 60 minutes (this is because most train fires are so large, i.e., have such large diameters, that they do not burn very long).

Table 7.27 Truck Accident Fire Durations

Duration (hr)	Non-Collision Accidents	Off-Road Accidents and Collisions with Fixed Objects	Truck/Truck Collisions	Truck/Car Collisions	Train Grade Crossing Accidents
0.	0.	0.	0.	0.	0.
0.083	0.3311	0.0321	0.0035	0.0131	0.00238
0.167	0.6596	0.2821	0.0451	0.1653	0.07222
0.250	0.8551	0.5860	0.1572	0.4179	0.16427
0.333	0.9625	0.7754	0.3488	0.6516	0.31099
0.417	0.9801	0.8769	0.5001	0.7878	0.43757
0.500	0.9897	0.9358	0.6034	0.8725	0.54957
0.583	0.9944	0.9643	0.6771	0.9161	0.64690
0.667	0.9970	0.9800	0.7322	0.9456	0.73075
0.750	0.9985	0.9902	0.7750	0.9662	0.80265
0.833	0.9992	0.9949	0.7960	0.9761	0.86416
0.917	0.9996	0.9973	0.8123	0.9838	0.87612
1.0	0.9998	0.9989	0.8257	0.9898	0.88589
1.083	0.99991	0.9995	0.8367	0.9936	
1.167	0.99996	0.9998	0.8459	0.9964	0.89828
1.250	0.99999	0.99995	0.8535	0.9984	
1.333	1.0	0.99998	0.8596	0.9993	0.90934
1.417		0.99999	0.8652	0.9997	
1.500		1.0	0.8696	0.9999	0.91874
1.583			0.8737	0.99996	
1.667			0.8779	0.99997	0.92730
1.750			0.8812	0.99999	
1.833			0.8847	1.0	0.93452
1.917			0.8882		
2.0			0.8917		0.94126
3.0			0.9287		0.96792
4.0			0.9503		0.98247
5.0			0.9641		0.99056
6.0			0.9773		0.99643
7.0			0.9905		1.0
8.0			1.0		

Table 7.28 Train Accident Fire Durations

Duration (hr)	Collision Accidents	Derailment Accidents	Fire-Only Accidents
0.083	0.00238	0.01009	0.00943
0.167	0.07222	0.09213	0.09180
0.250	0.16427	0.17603	0.17574
0.330	0.31099	0.29164	0.29183
0.417	0.43757	0.39717	0.39789
0.500	0.54957	0.49517	0.49648
0.583	0.64690	0.58120	0.58291
0.667	0.73075	0.65917	0.66075
0.750	0.80265	0.72958	0.73139
0.833	0.86416	0.79154	0.79373
0.917	0.87612	0.80544	0.80765
1.0	0.88589	0.81870	0.82036
1.167	0.89828	0.83308	0.83454
1.333	0.90934	0.84752	0.91874
1.500	0.91874	0.86071	0.86292
1.667	0.92730	0.87388	0.87564
1.833	0.93452	0.88537	0.88704
2.0	0.94126	0.89665	0.89792
3.0	0.96792	0.94290	0.94342
4.0	0.98247	0.96790	0.96821
5.0	0.99056	0.98166	0.98239
6.0	0.99643	0.98868	0.98941
7.0	1.0	0.99380	0.99403
8.0		0.99702	0.99754
9.0		0.99910	0.99928
10.0		0.99978	0.99985
11.0		1.0	1.0

Now because only hydrocarbon fuel (or liquid chemical) fires will have average fire temperatures ≥ 1000ºC, while essentially all fires will have average fire temperatures > 650ºC, for trucks, $P_{flame\ temp}(T_a \leq T_{cask} \leq T_b) = 1.0$ and $P_{flame\ temp}(T_b \leq T_{cask} \leq T_f) = 0.5$. Since only fully engulfing fires with diameters > 25 ft will be optically dense and all truck/train accident fires have diameters > 25 ft, $P_{optically\ dense/train} = 1.0$. Because 80 percent of all other truck accidents lead to fires with diameters < 25 ft, $P_{optically\ dense/not\ train} = 0.2$. Because one truck fire in two is an engulfing fire, $P_{co\text{-}located} = 0.5$. Substitution of these values into Equation 9 yields the following expressions for the probability of fires sufficiently severe to heat a truck spent fuel cask to a temperature in the indicated temperature range.

$$P_{severe\ fire,k}(T_b \le T_{cask} \le T_f = P_{optically\ dense}\ P_{co\text{-}located}\ P_{flame\ temp}(T_b \le T_{cask} \le T_f)\ P_{duration,k}(T_b \le T_{cask} \le T_f)$$

$$= (0.2)(0.5)(0.5)\ P_{duration,k} = 0.05\ P_{duration,k}(T_b \le T_{cask} \le T_f)$$

for truck accidents that don't involve trains

$$= (1.0)(0.5)(0.5)\ P_{duration,k} = 0.25\ P_{duration,k}(T_b \le T_{cask} \le T_f)$$

for train collisions with trucks

$$P_{severe\ fire,k}(T_s \le T_{cask} \le T_b) = P_{optically\ dense}\ P_{co\text{-}located}\ P_{flame\ temp}(T_s \le T_{cask} \le T_b)\ P_{duration,k}(T_s \le T_{cask} \le T_b)$$

$$= (0.2)(1.0)(1.0)\ P_{duration,k} = 0.2\ P_{duration,\ k}(T_s \le T_{cask} \le T_b)$$

for truck accidents that don't involve trains

$$= (1.0)(1.0)(1.0)\ P_{duration,k} = P_{duration,k}(T_s \le T_{cask} \le T_b)$$

for train collisions with trucks at grade crossings

since, for fires in this temperature range, it is assumed that $P_{co\text{-}located} = 1.0$.

$$P_{severe\ fire,k}(T_a \le T_{cask} \le T_s) = P_{optically\ dense}\ P_{co\text{-}located}\ P_{flame\ temp}(T_a \le T_{cask} \le T_s)\ P_{duration,k}(T_a \le T_{cask} \le T_s)$$

$$= (1.0)(1.0)(1.0)\ P_{duration,k} = P_{duration,k}(T_a \le T_{cask} \le T_s)$$

for all truck accidents

since, for fires in this temperature range, it is assumed that $P_{optically\ dense} = P_{co\text{-}located} = 1.0$.

Finally, Clauss et al. developed cumulative distributions of fire diameters for truck collisions with cars, trucks, trains, and off-road objects. In addition, for each of these classes of collisions, they also developed cumulative distributions of fire duration for fires of different sizes (ranges of fire diameters). Now, if P_{di} is the probability that a truck collision with another truck leads to a fire with a diameter d that lies in the diameter range d_i to d_{i+1}, and P_i is the probability that fires in this size range have durations ≤ 1 hour, then the chance P_T that a truck collision will produce a fire of any size that has a duration ≤ 1 hour is

$$P_T = \sum_i P_{di} P_i$$

Table 7.29 compares the values of cumulative fire duration probabilities for fires of any size with durations ≤ 1.0 hour for various truck collisions developed using this summation and the data of Clauss, et al. to the values developed by the Modal Study.

Table 7.29 Comparison of Modal Study Cumulative Fire Durations for Various Truck Accidents to Those Developed by Weighted Summation of Data from Clauss, et al. [7-5]

Collision	With Car	With Truck	With Train	Off-Road
Clauss, et al.	0.99	0.80	0.94	0.995
Modal Study	0.9898	0.8257	0.8859	0.9989

Inspection of the table suggests that the results of Clauss, et al. are quite consistent with those presented in the Modal Study. Accordingly, use of values of $P_{optically\ dense}$, $P_{co\text{-}located}$, and $P_{flame\ temp}$ developed from the data of Clauss, et al. with Modal Study fire duration data and truck accident event tree probabilities seems appropriate.

7.4.4.4 Train Collision Fire Statistics

Because a modern study of train collision fire statistics was not identified, estimates of $P_{optically\ dense}$, $P_{co\text{-}located}$, and $P_{flame\ temp}$ for fires initiated by train collisions had to be developed by considering other data. The results of Clauss, et al. show that fires initiated by the collision of a train with a truck almost always have diameters ≥ 25 ft and that half of these fires have diameters ≥ 30 ft. Because these collisions are unlikely to lead to train derailments, the fires they initiate may involve the fuel that powers the diesel engine that was hauling the train but are not likely to involve liquid chemicals in tank cars further back in the train's consist (the set of cars that make up the train). Accordingly, because train accidents that lead to derailments that also initiate fires frequently involve more than one car in the consist, the cumulative probability distribution of the sizes of fires initiated by train derailments should lie higher than the distribution found for fires initiated by train collisions with trucks. Therefore, because (a) fires with diameters ≥ 25 ft will be optically dense to a cask that is engulfed by the fire, (b) fires initiated by train derailments are likely to be larger than fires initiated by the collision of a train with a truck, and (c) essentially all fires initiated by train collisions with a truck have diameters ≥ 25 ft, for all train fires it is assumed that $P_{optically\ dense} = 1.0$.

Data on truck and train cargoes, specifically commodity flow statistics, has been compiled by the Department of Transportation for the year 1993. Table 7.30 presents the ton-miles and ton-mile fractions of highly combustible cargoes (commodities) that were transported over long distances by trucks and by trains during 1993.

Table 7.30 Truck and Train Commodity Flow Statistics for 1993

Highly Combustible Cargo	**Train**			**Truck**		
	Ton-miles (millions)	**Fraction**		**Ton-miles (millions)**	**Fraction**	
		w Coal	**w/o Coal**		**w Coal**	**w/o Coal**
Coal	3.93×10^5	0.417		7.24×10^3	0.012	
Petroleum	na	na	na	na	na	na
Chemicals	1.13×10^5	0.120	0.205	5.73×10^4	0.091	0.092
Petroleum Products	4.76×10^4	0.050	0.087	3.00×10^4	0.048	0.048
Rubber, Plastics	1.11×10^3	0.001	0.002	1.94×10^4	0.031	0.031
Lumber, Wood Products	3.04×10^4	0.032	0.055	2.29×10^4	0.036	0.037
Pulp, Paper	3.77×10^4	0.040	0.069	4.74×10^4	0.075	0.076
All Highly Combustible – w Coal	6.23×10^5	0.661		4.28×10^5	0.680	
All Highly Combustible – w/o Coal	2.30×10^5		0.418	4.21×10^5		0.677
All – w Coal	9.43×10^5			6.29×10^5		
All – w/o Coal	5.50×10^5			6.22×10^5		

Table 7.30 shows that, when coal is excluded from consideration, the number of ton-miles of highly combustible cargoes transported by truck is about twice that transported by train, and that the relative amounts of the types of combustibles carried by the two transport modes are quite similar, differing principally in that trains carry more chemicals and petroleum products than trucks while trucks carry more rubber and plastics than trains. Because, when shipped by train, most coal is hauled in unit trains, and because little petroleum is transported by train (long distance transport of gaseous and liquid hydrocarbons is almost always done by pipeline), while petroleum fuels (diesel, gasoline) are almost always transported from tank farms to gasoline stations by truck, it is clear that large quantities of petroleum are transported by truck but little by train. Therefore, derailments of regular trains which haul little coal or petroleum should be less likely to initiate fires fueled by highly combustible fuels than are fires initiated by truck collisions. Accordingly, the chance that a train derailment will initiate a fire that has an average temperature ≥ 1000°C should be smaller than the chance that a fire initiated by truck collision initiates such a fire. But $P_{\text{flame temp}}(T_b \le T_{\text{cask}} \le T_f) = 0.5$ for fires initiated by truck collisions. Therefore, for fires initiated by train derailments, use of $P_{\text{flame temp}}(T_b \le T_{\text{cask}} \le T_f) = 0.5$ should be conservative.

The discussion presented in Section 7.4.2 above suggests that side and raking collisions and train derailments typically involve about ten rail cars. Inspection of Table 7.30 shows that about 42 percent of all cargo in regular trains (not unit trains such as coal trains) is highly combustible. So a typical train accident will involve four cars that are carrying highly combustible cargo. Now, given that the train accident has led to a fire and that the car carrying the spent fuel cask is one of the cars involved in the accident, an upper bound on the chance that the ensuing fire engulfs the cask can be calculated as the ratio of the 50 percentile fire area to the minimum area occupied by the ten cars. Thus,

$$P_{\text{engulfing}} = \frac{\pi\left(r_{\text{fire}}\right)^2}{10\left(w_{\text{car}}\, l_{\text{car}}\right)} = \frac{\pi(15\,\text{ft})^2}{10(10\text{ft} \times 21\text{ft})} = 0.3$$

where 10 ft and 21 ft are the width and length of a typical flat bed rail car.

Substitution of the values developed for $P_{\text{optically dense}}$, $P_{\text{flame temp}}$, and $P_{\text{co-located}}$ for train fires into Equation 9 yields the following expressions for the probability of train fires sufficiently severe to heat a rail spent fuel cask to a temperature in the indicated temperature range.

$$\begin{aligned} P_{\text{severe fire},k}(T_b \le T_{\text{cask}} \le T_f) &= P_{\text{optically dense}}\, P_{\text{co-located}}\, P_{\text{flame temp}}(T_b \le T_{\text{cask}} \le T_f)\, P_{\text{duration},k}(T_b \le T_{\text{cask}} \le T_f) \\ &= (1.0)(0.3)(0.5)\, P_{\text{duration},k} = 0.15\, P_{\text{duration},k}(T_b \le T_{\text{cask}} \le T_f) \end{aligned}$$

$$\begin{aligned} P_{\text{severe fire},k}(T_s \le T_{\text{cask}} \le T_b) &= P_{\text{optically dense}}\, P_{\text{co-located}}\, P_{\text{flame temp}}(T_s \le T_{\text{cask}} \le T_b)\, P_{\text{duration},k}(T_s \le T_{\text{cask}} \le T_b) \\ &= (1.0)(0.3)(1.0)\, P_{\text{duration},k} = 0.2\, P_{\text{duration},k}(T_s \le T_{\text{cask}} \le T_b) \end{aligned}$$

since, for fires in this temperature range, it is assumed that $P_{\text{flame temp}} = 1.0$.

$$\begin{aligned} P_{\text{severe fire},k}(T_a \le T_{\text{cask}} \le T_s) &= P_{\text{optically dense}}\, P_{\text{co-located}}\, P_{\text{flame temp}}(T_a \le T_{\text{cask}} \le T_s)\, P_{\text{duration},k}(T_a \le T_{\text{cask}} \le T_s) \\ &= (1.0)(1.0)(1.0)\, P_{\text{duration},k} = P_{\text{duration},k}(T_a \le T_{\text{cask}} \le T_s) \end{aligned}$$

since, for fires in this temperature range, it is assumed that $P_{\text{flame temp}} = P_{\text{co-located}} = 1.0$.

7.5 Values for Release Fractions and Severity Fractions

7.5.1 Introduction

Severity fraction values can now be calculated by substituting the severity fraction parameter values developed in Section 7.4 into the severity fraction expressions developed in Section 7.2. When this is done, four sets of severity fractions are obtained, one for each of the four generic casks, the steel-lead-steel and steel-DU-steel truck casks, and the steel-lead-steel and monolithic steel rail casks, for which specifications were developed in Section 4.

Similarly, release fraction values can now be calculated by substituting the release fraction parameter values developed in Section 7.3 into the release fraction expressions developed in Section 7.2. When this is done, because low to moderate impact loads are estimated to fail more PWR rods than BWR rods, two sets of release fractions are obtained for each generic cask, one for PWR spent fuel and another for BWR spent fuel. Thus, eight sets of release fractions are constructed, four sets of PWR release fractions (one set for each generic cask) and four sets of BWR release fractions (again one set for each generic cask).

7.5.2 Calculational Method

Release fractions and severity fractions were calculated using spreadsheets. Copies of these spreadsheets are presented in the Appendix D. Calculation of release fraction values was done using a single spreadsheet. Four linked spreadsheets were used to calculate the severity fraction values for each generic cask.

The first of the four severity fraction spreadsheets is the truck or train accident event tree that gives constructs values for individual accident scenarios, $P_{scenario,j}$ values. The second severity fraction spreadsheet calculates values for $P_{speed,j}$ (v_{30},v_{60}), $P_{speed,j}$ (v_{60},v_{90}), $P_{speed,j}$ (v_{90},v_{120}), and $P_{speed,j}$ ($\geq v_{120}$), where v_{30}, v_{60}, v_{90}, and v_{120} are the cask impact speeds for accident scenario and accident surface j that are equivalent to 30, 60, 90, and 120 mph impacts onto an unyielding surface, and for example $P_{speed,j}$ (v_{30},v_{60}) is the chance that the cask impact velocity onto that surface falls within the speed range (v_{30},v_{60}). These speed range probabilities are calculated by linear interpolation using the appropriate Modal Study cumulative accident velocity distribution and the real-surface values of v_{30}, v_{60}, v_{90}, and v_{120} developed from the finite element cask impact results for unyielding surfaces described in Section 5.1 by partitioning of the impact energy between the cask and the real yielding surface as described in Section 5.2.

The third severity fraction spreadsheet calculate values for $P_{duration,k}$ (T_a,T_s), $P_{duration,k}$ (T_s,T_b), and $P_{duration,k}$ (T_b,T_f), where T_a, T_s, and T_f are respectively the normal internal temperature of the spent fuel cask, the temperature at which cask elastomeric seals begin to leak due to thermal loads, and the average temperature of a hydrocarbon fuel fire, and for example $P_{duration,k}$ (T_a,T_s) is the chance that the fire initiated by the accident burns long enough to raise the temperature of cask k into the temperature range (T_a,T_s). As was done for cask impact velocities, these fire duration probabilities are calculated by linear interpolation using the appropriate Modal Study cumulative accident fire duration distribution and the values of T_a, T_s, and T_f that were developed in Section 6 for each of the four generic casks. Finally, the fourth severity fraction spreadsheet calculates individual severity fraction values for each combination of one of the 31 truck accident scenarios with one of the 18 truck accident cases, or one of the 25 train accident scenarios with one of the 20 rail accident cases, and then sums the results for each accident case over all of the accident scenarios that contribute to that accident case thereby producing a set of 18 truck accident severity fractions for each generic truck cask or 20 train accident severity fractions for each generic rail cask.

7.5.3 Source Term Severity Fraction and Release Fraction Values

Finally, Table 7.31 presents the severity fraction and release fraction values developed by the process outlined in the preceding section.

7.6 Conservatisms

Some of the source term models developed in this section use treatments of phenomena or parameter values that are significantly conservative. The more significant of these conservatisms are:

- the use of high burnup, three year cooled cask inventories rather than average burnup, ten year cooled cask inventories that would better represent the average characteristics of the spent fuel generated to date;
- the assumption that during collision accidents all of the pellets in a fuel rod fracture and the calculation of the degree of fracturing assuming that the pellets are subjected to forces equal to those generated by a 120 mph impact onto an unyielding surface;
- the assumption that the particle size distribution produced by spallation of CRUD from rod surfaces due to mechanical or thermal loads is identical to the size distribution of the agglomerated crystalites that comprise the CRUD deposits on the rod surfaces;
- the treatment of particle and vapor deposition onto cask interior surfaces only during the short time period that immediately follows rod failure (e.g., during collisions accidents that lead to fires, particle and vapor deposition is neglected during the long time periods between the failure of some of the rods due to impact and the failure of the rest of the rods due to burst rupture, and the neglect of vapor deposition onto cooler cask interior surfaces following rod failure by burst rupture); and
- the neglect of plugging of small seal leak paths (leaks with cross sectional areas of order 1 mm^2) which are likely to be cracks that are much longer (at least one bolt spacing) than they are wide (< 30 μm) and thus easily subject to plugging by larger particles entrained in the cask's blowdown gas flow.

Table 7.31 Source Term Severity Fractions and Release Fractions

Steel-DU-Steel Truck Cask						
Number of PWR Fuel Assemblies: 3						
Case	Severity Fraction	PWR Release Fractions				
		Kr	Cs	Ru	Particulates	CRUD
1	1.53E-08	8.0E-01	2.4E-08	6.0E-07	6.0E-07	2.0E-03
2	5.88E-05	1.4E-01	4.1E-09	1.0E-07	1.0E-07	1.4E-03
3	1.81E-06	1.8E-01	5.4E-09	1.3E-07	1.3E-07	1.8E-03
4	7.49E-08	8.4E-01	3.6E-05	3.8E-06	3.8E-06	3.2E-03
5	4.65E-07	4.3E-01	1.3E-08	3.2E-07	3.2E-07	1.8E-03
6	3.31E-09	4.9E-01	1.5E-08	3.7E-07	3.7E-07	2.1E-03
7	0.00E+00	8.5E-01	2.7E-05	2.1E-06	2.1E-06	3.1E-03
8	1.13E-08	8.2E-01	2.4E-08	6.1E-07	6.1E-07	2.0E-03
9	8.03E-11	8.9E-01	2.7E-08	6.7E-07	6.7E-07	2.2E-03
10	0.00E+00	9.1E-01	5.9E-06	6.8E-07	6.8E-07	2.5E-03
11	1.44E-10	8.2E-01	2.4E-08	6.1E-07	6.1E-07	2.0E-03
12	1.02E-12	8.9E-01	2.7E-08	6.7E-07	6.7E-07	2.2E-03
13	0.00E+00	9.1E-01	5.9E-06	6.8E-07	6.8E-07	2.5E-03
14	7.49E-11	8.4E-01	9.6E-05	8.4E-05	1.8E-05	6.4E-03
15	0.00E+00	8.5E-01	5.5E-05	5.0E-05	9.0E-06	5.9E-03
16	0.00E+00	9.1E-01	5.9E-06	6.4E-06	6.8E-07	3.3E-03
17	0.00E+00	9.1E-01	5.9E-06	6.4E-06	6.8E-07	3.3E-03
18	5.86E-06	8.4E-01	1.7E-05	6.7E-08	6.7E-08	2.5E-03
19	0.99993	0.0	0.0	0.0	0.0	0.0
	1.00000					

Steel-DU-Steel Truck Cask						
Number of BWR Fuel Assemblies: 7						
Case	Severity Fraction	BWR Release Fractions				
		Kr	Cs	Ru	Particulates	CRUD
1	1.53E-08	8.0E-01	2.4E-08	6.0E-07	6.0E-07	2.0E-03
2	5.88E-05	5.4E-03	1.6E-10	4.0E-09	4.0E-09	4.5E-04
3	1.81E-06	1.5E-02	4.5E-10	1.1E-08	1.1E-08	1.3E-03
4	7.49E-08	8.4E-01	4.1E-05	4.9E-06	4.9E-06	3.1E-03
5	4.65E-07	9.8E-02	2.9E-09	7.3E-08	7.3E-08	1.2E-03
6	3.31E-09	1.4E-01	4.1E-09	1.0E-07	1.0E-07	1.7E-03
7	0.00E+00	8.4E-01	3.7E-05	4.0E-06	4.0E-06	3.2E-03
8	1.13E-08	8.2E-01	2.4E-08	6.1E-07	6.1E-07	2.0E-03
9	8.03E-11	8.9E-01	2.7E-08	6.7E-07	6.7E-07	2.2E-03
10	0.00E+00	9.1E-01	5.9E-06	6.8E-07	6.8E-07	2.5E-03
11	1.44E-10	8.2E-01	2.4E-08	6.1E-07	6.1E-07	2.0E-03
12	1.02E-12	8.9E-01	2.7E-08	6.7E-07	6.7E-07	2.2E-03
13	0.00E+00	9.1E-01	5.9E-06	6.8E-07	6.8E-07	2.5E-03
14	7.49E-11	8.4E-01	1.2E-04	1.1E-04	2.4E-05	6.5E-03
15	0.00E+00	8.4E-01	1.0E-04	8.9E-05	2.0E-05	6.4E-03
16	0.00E+00	9.1E-01	5.9E-06	6.4E-06	6.8E-07	3.3E-03
17	0.00E+00	9.1E-01	5.9E-06	6.4E-06	6.8E-07	3.3E-03
18	5.86E-06	8.4E-01	1.7E-05	6.7E-08	6.7E-08	2.5E-03
19	0.99993	0.0	0.0	0.0	0.0	0.0
	1.00000					

Aerosolized Fraction = 1.0

Respirable Fraction = 1.0

Table 7.31 Source Term Severity Fractions and Release Fractions (continued)

Steel-Lead-Steel Truck Cask						
Number of PWR Fuel Assemblies: 1						
Case	Severity Fraction	PWR Release Fractions				
		Kr	Cs	Ru	Particulates	CRUD
1	1.53E-08	8.0E-01	2.4E-08	6.0E-07	6.0E-07	2.0E-03
2	6.19E-05	1.4E-01	4.1E-09	1.0E-07	1.0E-07	1.4E-03
3	2.81E-07	1.8E-01	5.4E-09	1.3E-07	1.3E-07	1.8E-03
4	6.99E-08	8.4E-01	3.6E-05	3.8E-06	3.8E-06	3.2E-03
5	4.89E-07	4.3E-01	1.3E-08	3.2E-07	3.2E-07	1.8E-03
6	9.22E-11	4.9E-01	1.5E-08	3.7E-07	3.7E-07	2.1E-03
7	3.30E-12	8.5E-01	2.7E-05	2.1E-06	2.1E-06	3.1E-03
8	1.17E-08	8.2E-01	2.4E-08	6.1E-07	6.1E-07	2.0E-03
9	1.90E-12	8.9E-01	2.7E-08	6.7E-07	6.7E-07	2.2E-03
10	0.00E+00	9.1E-01	5.9E-06	6.8E-07	6.8E-07	2.5E-03
11	1.49E-10	8.2E-01	2.4E-08	6.1E-07	6.1E-07	2.0E-03
12	2.41E-14	8.9E-01	2.7E-08	6.7E-07	6.7E-07	2.2E-03
13	0.00E+00	9.1E-01	5.9E-06	6.8E-07	6.8E-07	2.5E-03
14	6.99E-11	8.4E-01	9.6E-05	8.4E-05	1.8E-05	6.4E-03
15	3.30E-15	8.5E-01	5.5E-05	5.0E-05	9.0E-06	5.9E-03
16	0.00E+00	9.1E-01	5.9E-06	6.4E-06	6.8E-07	3.3E-03
17	0.00E+00	9.1E-01	5.9E-06	6.4E-06	6.8E-07	3.3E-03
18	5.59E-06	8.4E-01	1.7E-05	6.7E-08	6.7E-08	2.5E-03
19	0.99993	0.0	0.0	0.0	0.0	0.0
	1.00000					

Steel-Lead-Steel Truck Cask						
Number of BWR Fuel Assemblies: 2						
Case	Severity Fraction	BWR Release Fractions				
		Kr	Cs	Ru	Particulates	CRUD
1	1.53E-08	8.0E-01	2.4E-08	6.0E-07	6.0E-07	2.0E-03
2	6.19E-05	5.4E-03	1.6E-10	4.0E-09	4.0E-09	4.5E-04
3	2.81E-07	1.5E-02	4.5E-10	1.1E-08	1.1E-08	1.3E-03
4	6.99E-08	8.4E-01	4.1E-05	4.9E-06	4.9E-06	3.1E-03
5	4.89E-07	9.8E-02	2.9E-09	7.3E-08	7.3E-08	1.2E-03
6	9.22E-11	1.4E-01	4.1E-09	1.0E-07	1.0E-07	1.7E-03
7	3.30E-12	8.4E-01	3.7E-05	4.0E-06	4.0E-06	3.2E-03
8	1.17E-08	8.2E-01	2.4E-08	6.1E-07	6.1E-07	2.0E-03
9	1.90E-12	8.9E-01	2.7E-08	6.7E-07	6.7E-07	2.2E-03
10	0.00E+00	9.1E-01	5.9E-06	6.8E-07	6.8E-07	2.5E-03
11	1.49E-10	8.2E-01	2.4E-08	6.1E-07	6.1E-07	2.0E-03
12	2.41E-14	8.9E-01	2.7E-08	6.7E-07	6.7E-07	2.2E-03
13	0.00E+00	9.1E-01	5.9E-06	6.8E-07	6.8E-07	2.5E-03
14	6.99E-11	8.4E-01	1.2E-04	1.1E-04	2.4E-05	6.5E-03
15	3.30E-15	8.4E-01	1.0E-04	8.9E-05	2.0E-05	6.4E-03
16	0.00E+00	9.1E-01	5.9E-06	6.4E-06	6.8E-07	3.3E-03
17	0.00E+00	9.1E-01	5.9E-06	6.4E-06	6.8E-07	3.3E-03
18	5.59E-06	8.4E-01	1.7E-05	6.7E-08	6.7E-08	2.5E-03
19	0.99993	0.0	0.0	0.0	0.0	0.0
	1.00000					

Aerosolized Fraction = 1.0
Respirable Fraction = 1.0

Table 7.31 Source Term Severity Fractions and Release Fractions (continued)

Monolithic Rail Cask						
Number of PWR Fuel Assemblies: 24						
Case	Severity Fraction	PWR Release Fractions				
		Kr	Cs	Ru	Particulates	CRUD
1	4.49E-09	4.1E-01	1.2E-08	2.5E-07	2.5E-07	1.4E-03
2	1.17E-07	8.0E-01	8.6E-06	1.3E-05	1.3E-05	4.4E-02
3	4.49E-09	8.0E-01	1.8E-05	1.9E-05	1.9E-05	6.4E-02
4	3.05E-05	1.4E-01	4.1E-09	1.0E-07	1.0E-07	1.4E-03
5	1.01E-06	1.8E-01	5.4E-09	1.3E-07	1.3E-07	1.8E-03
6	1.51E-08	8.4E-01	3.6E-05	1.4E-05	1.4E-05	5.4E-03
7	7.31E-08	4.3E-01	1.3E-08	2.6E-07	2.6E-07	1.5E-03
8	2.43E-09	4.9E-01	1.5E-08	2.9E-07	2.9E-07	1.7E-03
9	3.61E-11	8.5E-01	2.7E-05	6.8E-06	6.8E-06	4.5E-03
10	9.93E-10	8.2E-01	8.8E-06	1.3E-05	1.3E-05	4.5E-02
11	3.30E-11	8.9E-01	9.6E-06	1.5E-05	1.5E-05	4.9E-02
12	4.91E-13	9.1E-01	1.4E-05	1.5E-05	1.5E-05	5.1E-02
13	3.82E-11	8.2E-01	1.8E-05	2.0E-05	2.0E-05	6.5E-02
14	1.27E-12	8.9E-01	2.0E-05	2.1E-05	2.1E-05	7.1E-02
15	1.88E-14	9.1E-01	2.2E-05	2.2E-05	2.2E-05	7.4E-02
16	5.69E-11	8.4E-01	9.6E-05	8.4E-05	1.8E-05	6.4E-03
17	3.61E-14	8.5E-01	5.5E-05	5.0E-05	8.9E-06	5.4E-03
18	4.91E-16	9.1E-01	1.4E-05	1.8E-05	1.5E-05	5.1E-02
19	1.88E-17	9.1E-01	2.2E-05	2.3E-05	2.2E-05	7.4E-02
20	6.32E-06	8.4E-01	1.7E-05	2.5E-07	2.5E-07	9.4E-03
21	0.99996	0.0	0.0	0.0	0.0	0.0
	1.00000					

Monolithic Rail Cask						
Number of BWR Fuel Assemblies: 52						
Case	Severity Fraction	BWR Release Fractions				
		Kr	Cs	Ru	Particulates	CRUD
1	4.49E-09	8.9E-02	2.7E-09	5.3E-08	5.3E-08	8.9E-04
2	1.17E-07	8.0E-01	8.6E-06	1.3E-05	1.3E-05	4.4E-02
3	4.49E-09	8.0E-01	1.8E-05	1.9E-05	1.9E-05	6.4E-02
4	3.05E-05	5.4E-03	1.6E-10	4.0E-09	4.0E-09	4.5E-04
5	1.01E-06	1.5E-02	4.5E-10	1.1E-08	1.1E-08	1.3E-03
6	1.51E-08	8.4E-01	4.1E-05	1.8E-05	1.8E-05	5.4E-03
7	7.31E-08	9.8E-02	2.9E-09	5.9E-08	5.9E-08	9.8E-04
8	2.43E-09	1.4E-01	4.1E-09	8.3E-08	8.3E-08	1.4E-03
9	3.61E-11	8.4E-01	3.7E-05	1.5E-05	1.5E-05	4.9E-03
10	9.93E-10	8.2E-01	8.8E-06	1.3E-05	1.3E-05	4.5E-02
11	3.30E-11	8.9E-01	9.6E-06	1.5E-05	1.5E-05	4.9E-02
12	4.91E-13	9.1E-01	1.4E-05	1.5E-05	1.5E-05	5.1E-02
13	3.82E-11	8.2E-01	1.8E-05	2.0E-05	2.0E-05	6.5E-02
14	1.27E-12	8.9E-01	2.0E-05	2.1E-05	2.1E-05	7.1E-02
15	1.88E-14	9.1E-01	2.2E-05	2.2E-05	2.2E-05	7.4E-02
16	5.69E-11	8.4E-01	1.2E-04	1.1E-04	2.4E-05	6.5E-03
17	3.61E-14	8.4E-01	1.0E-04	8.9E-05	2.0E-05	5.9E-03
18	4.91E-16	9.1E-01	1.4E-05	1.8E-05	1.5E-05	5.1E-02
19	1.88E-17	9.1E-01	2.2E-05	2.3E-05	2.2E-05	7.4E-02
20	6.32E-06	8.4E-01	1.7E-05	2.5E-07	2.5E-07	9.4E-03
19	0.99996	0.0	0.0	0.0	0.0	0.0
21	1.00000					

Aerosolized Fraction = 1.0
Respirable Fraction = 1.0

Table 7.31 Source Term Severity Fractions and Release Fractions (continued)

Steel-Lead-Steel Rail Cask						
Number of PWR Fuel Assemblies: 24						
Case	Severity Fraction	PWR Release Fractions				
		Kr	Cs	Ru	Particulates	CRUD
1	8.20E-06	4.1E-01	1.2E-08	2.5E-07	2.5E-07	1.4E-03
2	5.68E-07	8.0E-01	8.6E-06	1.3E-05	1.3E-05	4.4E-02
3	4.49E-09	8.0E-01	1.8E-05	1.9E-05	1.9E-05	6.4E-02
4	2.96E-05	1.4E-01	4.1E-09	1.0E-07	1.0E-07	1.4E-03
5	8.24E-07	1.8E-01	5.4E-09	1.3E-07	1.3E-07	1.8E-03
6	1.10E-07	8.4E-01	3.6E-05	1.4E-05	1.4E-05	5.4E-03
7	6.76E-08	4.3E-01	1.3E-08	2.6E-07	2.6E-07	1.5E-03
8	1.88E-09	4.9E-01	1.5E-08	2.9E-07	2.9E-07	1.7E-03
9	2.51E-10	8.5E-01	2.7E-05	6.8E-06	6.8E-06	4.5E-03
10	4.68E-09	8.2E-01	8.8E-06	1.3E-05	1.3E-05	4.5E-02
11	1.31E-10	8.9E-01	9.6E-06	1.5E-05	1.5E-05	4.9E-02
12	1.74E-11	9.1E-01	1.4E-05	1.5E-05	1.5E-05	5.1E-02
13	3.70E-11	8.2E-01	1.8E-05	2.0E-05	2.0E-05	6.5E-02
14	1.03E-12	8.9E-01	2.0E-05	2.1E-05	2.1E-05	7.1E-02
15	1.37E-13	9.1E-01	2.2E-05	2.2E-05	2.2E-05	7.4E-02
16	4.15E-10	8.4E-01	9.6E-05	8.4E-05	1.8E-05	6.4E-03
17	2.51E-13	8.5E-01	5.5E-05	5.0E-05	8.9E-06	5.4E-03
18	1.74E-14	9.1E-01	1.4E-05	1.8E-05	1.5E-05	5.1E-02
19	1.37E-16	9.1E-01	2.2E-05	2.3E-05	2.2E-05	7.4E-02
20	4.91E-05	8.4E-01	1.7E-05	2.5E-07	2.5E-07	9.4E-03
21	0.99991	0.0	0.0	0.0	0.0	0.0
	1.00000					

Steel-Lead-Steel Rail Cask						
Number of BWR Fuel Assemblies: 52						
Case	Severity Fraction	BWR Release Fractions				
		Kr	Cs	Ru	Particulates	CRUD
1	8.20E-06	8.9E-02	2.7E-09	5.3E-08	5.3E-08	8.9E-04
2	5.68E-07	8.0E-01	8.6E-06	1.3E-05	1.3E-05	4.4E-02
3	4.49E-09	8.0E-01	1.8E-05	1.9E-05	1.9E-05	6.4E-02
4	2.96E-05	5.4E-03	1.6E-10	4.0E-09	4.0E-09	4.5E-04
5	8.24E-07	1.5E-02	4.5E-10	1.1E-08	1.1E-08	1.3E-03
6	1.10E-07	8.4E-01	4.1E-05	1.8E-05	1.8E-05	5.4E-03
7	6.76E-08	9.8E-02	2.9E-09	5.9E-08	5.9E-08	9.8E-04
8	1.88E-09	1.4E-01	4.1E-09	8.3E-08	8.3E-08	1.4E-03
9	2.51E-10	8.4E-01	3.7E-05	1.5E-05	1.5E-05	4.9E-03
10	4.68E-09	8.2E-01	8.8E-06	1.3E-05	1.3E-05	4.5E-02
11	1.31E-10	8.9E-01	9.6E-06	1.5E-05	1.5E-05	4.9E-02
12	1.74E-11	9.1E-01	1.4E-05	1.5E-05	1.5E-05	5.1E-02
13	3.70E-11	8.2E-01	1.8E-05	2.0E-05	2.0E-05	6.5E-02
14	1.03E-12	8.9E-01	2.0E-05	2.1E-05	2.1E-05	7.1E-02
15	1.37E-13	9.1E-01	2.2E-05	2.2E-05	2.2E-05	7.4E-02
16	4.15E-10	8.4E-01	1.2E-04	1.1E-04	2.4E-05	6.5E-03
17	2.51E-13	8.4E-01	1.0E-04	8.9E-05	2.0E-05	5.9E-03
18	1.74E-14	9.1E-01	1.4E-05	1.8E-05	1.5E-05	5.1E-02
19	1.37E-16	9.1E-01	2.2E-05	2.3E-05	2.2E-05	7.4E-02
20	4.91E-05	8.4E-01	1.7E-05	2.5E-07	2.5E-07	9.4E-03
21	0.99991	0.0	0.0	0.0	0.0	0.0
	1.00000					

Aerosolized Fraction = 1.0

Respirable Fraction = 1.0

7.7 References

[7-1] L. E. Fischer, et al., "Shipping Container Response to Severe Highway and Railway Accident Conditions," NUREG/CR-4829, Lawrence Livermore National Laboratory, Livermore, CA, February 1987.

[7-2] ARC/INFO Coverages and Arc View Project, K. C. Bayer Digital Map of the U.S., purchased from Geologic Data Systems, Inc., 1600 Emerson St., Denver, CO 80218.

[7-3] State Soil Graphics (STATSGO) Data Base, available on the Internet at ftp.ftw.nrcs.usda.gov/pub/statsgo.

[7-4] Accidents of Motor Carriers of Property (for the years 1973 through 1983), Bureau of Motor Carrier Safety, Federal Highway Administration, U.S. Department of Transportation, Washington, DC, 1975-1984.

[7-5] D. B. Clauss, et al., "A Statistical Description of the Types and Severities of Accidents Involving Tractor Semi-Trailers," SAND93-2580, Sandia National Laboratories, Albuquerque, NM, June 1994.

[7-6] Accident/Incident Bulletins Nos. 145 through 151, Office of Safety, Federal Railroad Administration, U.S. Department of Transportation, Washington, DC, 1977-1983.

[7-7] Ref. [7-1], p. 2-30.

[7-8] Comments by meeting attendees at the Rail Accident Event Tree Meeting held at the American Association of Railroads Offices in Washington, DC, November 3, 1997.

[7-9] K. S. Neuhauser and F. L. Kanipe, "RADTRAN 4, Volume II, Technical Manual," SAND89-2370, Sandia National Laboratories, Albuquerque, NM, May 1994.

[7-10] K. S. Neuhauser and F. L. Kanipe, "RADTRAN 4, Volume III, User Guide," SAND89-2370, Sandia National Laboratories, Albuquerque, NM, January 1992.

[7-11] A. G. Croff, "ORIGEN2 - A Revised and Updated Version of the Oak Ridge Isotope Generation and Depletion Code," ORNL-5621, Oak Ridge National Laboratory, Oak Ridge, TN, July 1980.

[7-12] ORIGEN2 Isotope Generation and Depletion Code, CCC-371, Oak Ridge National Laboratory, Oak Ridge, TN, 1991.

[7-13] Spent Nuclear Fuel Discharges from U.S. Reactors, Energy Information Administration, U.S. Department of Energy, SR/CNEAF/96-01, 1994.

[7-14] *International Atomic Energy Agency, Safety Series No. 7, IAEA Safety Guides, Explanatory Material for the IAEA Regulations for the Safe Transport of Radioactive Material* (1985 Edition), 2nd Edition, Vienna, 1987.

[7-15] Code of Federal Regulations, Volume 49, Part 173.435 (49 CFR 173.435).

[7-16] RADSEL, unpublished Sandia code, available upon request.

[7-17] R. P. Sandoval, et al., "Estimate of CRUD Contribution to Shipping Cask Containment Requirements," SAND88-1358, Sandia National Laboratories, Albuquerque, NM, January 1991.

[7-18] "Environmental Assessment of Urgent-Relief Acceptance of Foreign Research Reactor Spent Nuclear Fuel," DOE/EA-0912, U.S. Department of Energy, Washington, DC, April 1994, Table E-7, p. E-12.

[7-19] D. A. Powers, et al., "A Review of the Technical Issues of Air Ingression During Severe Reactor Accidents," NUREG/CR-6218, Sandia National Laboratories, Albuquerque, NM, September 1994.

[7-20] T. L. Sanders, et al., "A Method for Determining the Spent-Fuel Contribution to Transport Cask Containment Requirements, Appendix III, Spent Fuel Response to Transport Environments," SAND90-2406, Sandia National Laboratories, Albuquerque, NM, November 1992.

[7-21] Ref. [7-20], p. III-48.

[7-22] Ref. [7-20], p. II-138.

[7-23] J. J. Gregory, et al., Thermal Measurements in Large Pool Fires, *J. Heat Transfer* **111**, 446 (1989).

[7-24] P. J. Nigrey, "Prediction of Packaging Seal Life Using Thermoanalytical Techniques," Proceedings of the 12th International Conference on the Packaging and Transportation of Radioactive Materials (PATRAM '98), IAEA, Vol. 4, p. 1730, 1998.

[7-25] H.-P. Weise, et al., "Untersuchung der Sicherheitreserven von Dichtsytemen für Umschliessungen zum Transport und zur Lagerung Radioaktiver Stoffe," Research Project BMU/St. Sch. 1081, Final Report, 1992.

[7-26] R. A. Lorenz, et al., "Fission Product Release from Highly Irradiated LWR Fuel," NUREG/CR-0722, Oak Ridge National Laboratory, Oak Ridge, TN, February 1980, pp. 48-80.

[7-27] E. L. Wilmot, "Transportation Accident Scenarios for Commercial Spent Fuel," SAND80-2124, Sandia National Laboratories, Albuquerque, NM, February 1981.

[7-28] Ref. [7-20], p. II-149.

[7-29] L. B. Shappert, et al., "Cask Designers Guide," ORNL-NSIC-68, Oak Ridge National Laboratory, Oak Ridge TN, February 1970, p. 156.

[7-30] J. L. Sprung, et al., "Data and Methods for the Assessment of the Risks Associated with the Maritime Transport of Radioactive Materials: Results of the SeaRAM Program, Vol. 2, Appendix IV, Cask-to-Environment Release Fractions," SAND97-2222, Sandia National Laboratories, Albuquerque, NM, August 1997.

[7-31] R. J. Burian, et al., "Response of Spent LWR Fuel to Extreme Environments," SAND85-7213, Sandia National Laboratories, Albuquerque, NM, August 1985 (unpublished contractor report prepared by Battelle Columbus Laboratories; available on request).

[7-32] R. P. Sandoval, R. J. Burian, et al., "Response of Spent LWR Fuel to Extreme Environments," Proceedings of International Symposium on the Packaging and Transportation of Radioactive Materials (PATRAM '86), IAEA, Vol. 2, p. 695, 1987.

[7-33] Airborne Release Fractions/Rates and Respirable Fractions for Nonreactor Nuclear Facilities, DOE-HDBK-3010-94, U.S. Department of Energy, Washington, DC, Vol. 1, p. 5-23.

[7-34] Ref. [7-20], p. IV-13.

[7-35] Y. Otani, *Aerosol Science Technol.* **10**, 463 (1989).

[7-36] R. A. Lorenz, "Fission Product Release from Simulated LWR Fuel," NUREG/CR-0274, Oak Ridge National Laboratory, Oak Ridge, TN, October 1978.

[7-37] R. A. Lorenz, et al., "Fission Product Source Terms for the Light Water Reactor Loss-of-Coolant Accident, *Nuclear. Technology*. **46**, 404 (1979).

[7-38] R. A. Lorenz, et al., "Fission Product Source Terms for the Light Water Reactor Loss-of-Coolant Accident," NUREG/CR-1288, Oak Ridge National Laboratory, Oak Ridge, TN, July 1980.

[7-39] Ref. [7-20], p. IV-5.

[7-40] K. K. Murata, et al., "Code Manual for CONTAIN 2.0: A Computer Code for Nuclear Reactor Containment Analysis," NUREG/CR-6533, SAND97-1735, Sandia National Laboratories, Albuquerque, NM, December 1977.

[7-41] Ref. [7-26], p. 48.

[7-42] Ref. [7-26], p. 128.

[7-43] F. P. Incropera and D. P. DeWitt, *Fundamentals of Heat and Mass Transfer,* John Wiley & Sons, New York, 1985.

[7-44] R. B. Bird, W. E. Stewart, and E. N. Lightfoot, *Transport Phenomena,* John Wiley & Sons, New York, 1960.

[7-45] N. E. Bixler, "VICTORIA 2.0: A Mechanistic Model for Radionuclide Behavior in a Nuclear Reactor Coolant System Under Severe Accident Conditions," NUREG/CR-6131, Sandia National Laboratories, Albuquerque, NM, 1998.

[7-46] Ref. [7-26], p. 104.

[7-47] Ref. [7-26], pp. 18-22.

[7-48] S. R. Dharwadkar and M. D. Karkhanavala, *Indian J. Chem,* **13**, 685 (1975).

[7-49] Ref. [7-20], p. III-51.

[7-50] Ref. [7-20], Table I-3, p. I-10.

[7-51] Ref. [7-20], Table I-17, p. I-51.

[7-52] Ref. [7-20], Figures I-10 through I-12, p. I-36.

[7-53] Ref. [7-20], p. I-30.

[7-54] R. K. Clarke, et al., "Severities of Transportation Accidents, Vol. IV, Train," SLA-74-0001, Sandia National Laboratories, Albuquerque, NM, July 1976, pp. 15-17.

[7-55] Ref. [7-1], Table 5.2, p. 5-10.

[7-56] Ref. [7-1], Table 5.1, p. 5-8 and Table 5.2, p. 5-10.

[7-57] 10CFR71.73

[7-58] L. A. Gritzo, et al., "Transient Measurements of Radiative Properties, Soot Volume Fraction and Soot Temperature in a Large Pool Fire," *Combust. Sci. and Tech*. 139, 113 (1998).

[7-59] A. R. Lopez, et al., "Risk Assessment Compatible Fire Models (RACFMs)," SAND97-1562, Sandia National Laboratories, Albuquerque, NM, July 1998.